UNIVERSITY OF BIRMINGHAM

Modelling of the combustion parameters of biogenous fuel gases to predict stable combustion conditions in multifuel systems

by

RAPHAEL BALTHASAR LECHNER

A thesis submitted to the University of Birmingham
for the degree of
DOCTOR OF PHILOSOPHY

School of Chemical Engineering
College of Engineering and Physical Sciences
University of Birmingham
September 2019

Abstract

Classical fuel rating methods, such as the methane number or the related propane knock index were found to fail for the variety of biogenous fuel gas compositions encountered in practice. Thus, a novel methodology based on the detonation theory and the characteristic parameters chemical ignition delay, excitation time and laminar flame speed was adopted. The method enables an a priori, simulation-based determination of the knock propensity of fuels and centres on the two dimensionless parameters ξ and ε which characterise the possible regimes of auto-ignition propagation from hot spots.

The methodology was applied to a range of 38 syngas and reference gas blends determined with a statistical mixture plan. To supplement the data, measurements were conducted at an intermediate pyrolysis plant featuring the Thermo-Catalytic Reforming technology developed at Fraunhofer UMSICHT. The required combustion parameters were obtained from detailed chemical kinetic simulations.

Syngas showed to be more prone to knock than methane or biogas, albeit less than propane. Admixtures of higher hydrocarbons were found to increase the knock propensity. Lean equivalence ratios, exhaust gas recirculation and the addition of water vapour were effective measures to mitigate the risk of knock.

Acknowledgments

My warm thanks go to my first supervisor Professor Andreas Hornung for his guidance and support and for giving me the opportunity to carry out my PhD project within the framework of the *University of Birmingham and Fraunhofer UMSICHT Joint Research Platform*. I would also like to express my gratitude to my second supervisor Professor Yulong Ding and to my examiners Professor Joseph Wood and Professor Günter Elsbett.

The research work was conducted in cooperation with the *Centre of Excellence for Co-generation Technologies (CECoGen)* at the *Ostbayerische Technische Hochschule (OTH) Amberg-Weiden – Technical University of Applied Sciences*. I greatly appreciate the support of Professor Markus Brautsch from the OTH, who opened many doors for me. Though not individually funded, this work would not have been possible without the generous financial support from the Free State of Bavaria for the research carried out at CECoGen.

Many thanks to Julia Kast at Fraunhofer UMSICHT in Sulzbach-Rosenberg and to Lynn Draper at the School of Chemical Engineering for support in all administration matters. I also wish to thank Thorsten Hornung from Susteen Technologies for facilitating measurements at a TCR pilot plant and for allowing me to use the data for my work.

Special thanks go to Tom Goßner for implementing and testing reactor and flame models within the scope of his master's thesis. To Michael Hebauer for support with the analysis of fuel gases. To Max Becker for coming up with the idea of design of experiments and for his support in implementing it into my work. To Nicholas O'Connell for backing up the theoretical considerations with real-world data. To Dominik Edenharter, Larissa Köster and Melanie Werner for their support as student assistants. To Felicitas Langowski who did an excellent job of copy editing this thesis for conventions of language, spelling and grammar. To all I have not mentioned here, but who have contributed in many ways to this work. To my family and friends for their support and encouragement throughout the years. Thank you.

Table of contents

List of figures

List of tables

List of symbols and abbreviations

Symbols

A	Kinetic pre-exponential factor	varies
a	Acoustic velocity	m/s
B	Bore	m
C	Symbol for arbitrary constant	varies
C_p	Molar heat capacity at constant pressure	J/(mol K)
C_v	Molar heat capacity at constant volume	J/(mol K)
CR	Compression ratio	-
c_p	Specific heat capacity at constant pressure	J/(kg K)
c_v	Specific heat capacity at constant pressure	J/(kg K)
D	Diffusion coefficient	m²/s
E	Activation energy	J/mol
$\bar{E}$	Dimensionless parameter $\bar{E} = \tau_i/\tau_e \cdot E/(RT)$	-
E/R	Activation temperature	K
G	Gibbs free energy	J/mol
H	Enthalpy	J
h	Specific enthalpy	J/kg
j	Diffusive mass flux	kg/(m² s)
K_p	Equilibrium constant at constant pressure	-
k	Reaction rate constant	varies
L	Stroke	m
Le	Lewis number	-
l	Connecting rod length	m
n	Number of moles	mol
M_j	Symbol for arbitrary chemical species j	-
m	Mass	kg
$\dot{m}''$	Mass flux per unit area	kg/(m² s)
P	Total pressure	Pa
p	Partial pressure	Pa
Q	Heat	J
q_i	Rate of progress of reaction i	mol/(m³ s)
R	Universal gas constant	J/(mol K)
R	Ratio connecting rod length / crank radius	-

r	Radius	m
r_0	Hot spot radius	m
$\bar{r}$	Dimensionless hot spot radius $\bar{r} = r/r_0$	-
r^2	Coefficient of determination	-
S	Entropy	J/K
s	Specific entropy	J(kg K)
T	Temperature	K
T_0	Temperature at centre of hot spot	K
t	Time	s
U	Internal energy	J
u	Specific internal energy	J/kg
u	Velocity	m/s
u_d	Deflagrative wave speed	m/s
u_L	Laminar flame speed	m/s
u_p	Auto-ignitive propagation speed	m/s
V	Volume	m³
V_c	Clearance volume	m³
V_d	Displaced volume	m³
W	Molecular weight	kg/mol
X	Volume fraction	-
Y	Mass fraction	-
z	Axial coordinate	m

Greek symbols

α	Thermal diffusivity	m²/s
β	Dimensionless transition parameter	-
δ_L	Laminar flame thickness	m
ε	Dimensionless parameter $\varepsilon = r_0/(a/\tau_e)$	-
θ	Crank angle	radians
λ	Thermal conductivity	W/(m K)
μ	Dynamic viscosity	kg/(m s)
μ_j	Chemical potential of species j	J
ν	Stoichiometric coefficient	-
ξ	Dimensionless parameter $\xi = a/u_p$	-
π	Archimedes' constant	-

ρ	Density	kg/m³
τ_i	Ignition delay time	s
τ_e	Excitation time	s
ϕ	Fuel/air equivalence ratio	-
ω	Angular velocity	radians/s
$\dot{\omega}_j$	Production rate of species *j*	mol/(m³ s)

Indices

B	Burned
b	Backward
c	Critical
f	Forward
j	Species
l	Lower
U	Unburned
u	Upper

Abbreviations

C	Carbon
CFD	Computational fluid dynamics
CFR	Cooperative Fuel Research
C_xH_y	Generic higher hydrocarbon
CHP	Combined heat and power
CoPa	Combustion Parameters toolbox
DME	Dimethyl ether
DNS	Direct numerical simulation
DoE	Design of Experiments
EGR	Exhaust gas recirculation
GC	Gas chromatograph
GRI	Gas Research Institute
H	Hydrogen
HCCI	Homogenous charge compression ignition
HHV	Higher heating value
IAPWS	International Association for the Properties of Water and Steam

LHV	Lower heating value
MN	Methane number
MNR	Methane number requirement
MON	Motor octane number
N	Nitrogen
NO_x	Nitrogen oxides
NUI	National University of Ireland
O	Oxygen
PKI	Propane knock index
PODE	Polyoxymethylene dimethyl ether
POLIMI	Politecnico di Milano
ppmv	Parts per million volume
PRF	Primary reference fuel
RANS	Reynolds-averaged Navier-Stokes
RCM	Rapid compression machine
RON	Research octane number
S	Sulphur
SI	Spark ignition
TCR	Thermo-Catalytic Reforming
UCSD	University of California at San Diego
USC	University of Southern California
vol%	Volume percent
wt%	Weight percent

Chapter 1 Introduction

1.1 Background

Global warming caused by anthropogenic carbon dioxide (CO_2) emissions and the depletion of fossil energy resources present major challenges to humanity. A first measure to prolong the availability of fossil fuels and at the same time reduce the carbon dioxide emissions is to increase the efficiency of energy conversion processes. This can be accomplished, for example, by decentralised *combined heat and power production (CHP)*. In addition, fossil carbon based energy sources will have to be replaced by carbon-neutral alternatives in order to limit global warming to reasonable values.

Hydrocarbon fuels produced from renewable sources, referred to as *biofuels* commonly, present an ideal, carbon neutral option for many applications due to their high energy density, excellent storability and easy handling. *First generation biofuels*, such as ethanol from sugar or starch crops, fatty acid methyl esters produced from vegetable oil and anaerobic digester gas generated from maize and manure, are already being widely used as an admixture to fossil fuels or as sole fuel. An essential disadvantage of these fuels is the limited feedstock, which often competes directly with agricultural food production.

This drawback is overcome by *second generation biofuels*, which are produced from the residual, non-food parts of crops [1] through a variety of processes developed in recent years, such as *biomass gasification* [2], *Fischer-Tropsch synthesis* [3] and *pyrolysis processes*, such as the *Thermo-Catalytic Reforming* process *(TCR®)* developed by *Fraunhofer UMSICHT*[1] [4].

[1] Fraunhofer Institute for Environmental, Safety, and Energy Technology UMSICHT, Sulzbach-Rosenberg, Germany

Even newer developments are targeted at using surplus electricity from renewable sources to produce synthetic fuels based on C1-chemistry, such as *methanol*, *polyoxymethylene dimethyl ethers (PODE)* and *methyl formate* [5]. These fuels are often denominated *electro-fuels* or *e-fuels* [6, 7]. Recent studies show that PODE could be a feasible option to reduce the harmful exhaust gas emissions from stationary power production due to their favourable combustion characteristics [8, 9].

An alternative option to reduce global carbon dioxide emissions could be the shift towards a *hydrogen economy* as described in [10] and [11]. Hydrogen is an extremely versatile and clean energy carrier since it can be generated from a variety of sources and hence can span the several phases of a transition towards future energy markets [10]. Renewable hydrogen, also known as *green hydrogen* or *bio-hydrogen*, is usually produced by water electrolysis from wind or photovoltaic power [12]. New process routes, for example via the gasification of biomass or the reforming of biochars, could open up ways for low-cost residue biomass into hydrogen production [12].

All of the renewable fuel options presented above can be utilised for power production in stationary internal combustion engines. *Gaseous biofuels* are normally used in *spark ignition (SI) engines*, also known as Otto engines, while *liquid biofuels* are applied in *compression ignition engines*, also known as diesel engines. An alternative concept is the *dual-fuel engine*, in which a homogenous combustible mixture of gas and oxidiser is ignited by injecting a small amount of liquid fuel (diesel-ignited gas-engine [13, 14]). These engines prove to be very flexible in operation since they allow a wide range of combinations and ratios of gaseous and liquid fuel. Different configurations of dual-fuel engines for natural gas, biomethane, wood-gas and different pilot fuels, such as diesel, vegetable oil, biodiesel and PODE have been investigated in the recent years at the *Ostbayerische Technische*

Hochschule Amberg-Weiden – Technical University of Applied Sciences [8, 9, 15, 16]. Gaseous biofuels, for example, biogas, bio-hydrogen and producer gas from gasification or pyrolysis, are the most suitable option with regard to combined heat and power generation in stationary combustion engines.

The combustion characteristics of biogenous fuel gases may differ considerably from today's standard fuels. This implies that either the existing internal combustion engine designs have to be adapted or the fuels have to be processed in order to be compatible with existing engine technologies. Both options require in-depth knowledge of the combustion behaviour at engine operating conditions, which can be gathered through experiments, for example, in rapid compression machines or single-cylinder research engines. However, experimental setups are often complex and expensive and the investigations are time-consuming, so that only a limited number of tests for constrained conditions can be performed. Another problem often encountered in practice is that only a limited amount of fuel might be available for testing and the costs for providing test fuels might be prohibitively high. This applies especially to on-site settings, where the fuel quality may vary according to the feedstock and process and the limited number of envisaged installations does not justify extensive experimental testing and standardisation. This raises the question of whether it is possible with today's modern computational methods to predict the combustion behaviour of new generation fuel gases based solely on a set of characteristic parameters derived from the chemical composition of the fuel.

1.2 Objectives and approaches

The main objective of *this study* is to establish a simulation-based methodology for a priori estimating the combustion behaviour of gaseous biofuels from thermo-chemical conversion based on characteristic parameters derived from the chemical composition of the fuel. The individual objectives are

a) to perform a survey of the typical composition of biogenous fuel gases from different feedstocks and processes with regard to their utilisation as engine fuel paying special attention to intermediate pyrolysis, namely *Thermo-Catalytic Reforming,*

b) to identify a suitable simulation-based methodology for a priori characterising the combustion behaviour of gaseous fuels applying detailed chemical kinetics,

c) to develop a modular software toolkit based on open source chemical kinetics solvers for calculating the required characteristic combustion parameters,

d) to apply the methodology to assess the combustion characteristics of a range of biogenous fuel gas compositions determined on the basis of published data and own measurements.

The investigated characteristic combustion parameters are the *chemical ignition delay time*, the *excitation time*, and the *laminar flame speed*. These are used to calculate dimensionless parameters for assessing the auto-ignition propensity of fuels applying the *detonation theory,* the *ξ-ε diagram* and the *Sankaran criterion*. A *homogenous constant-volume reactor* model is set up in order to determine the ignition delay and excitation times, and a *premixed, one-dimensional, freely propagating flame* is used for calculation of the laminar flame speed. In addition, a *homogenous charge compression ignition reactor* model is applied to determine the *critical compression ratio* at which auto-ignition occurs. The models are implemented in a *Python* package – the *Combustion Parameters (CoPa)* toolbox– based on the open-source chemical kinetics software suite *Cantera*.

1.3 Thesis outline

This thesis is structured into 7 chapters, including the introduction in Chapter 1. Each chapter is summarised at the end.

In Chapter 2, the relevant literature is reviewed, starting with engine combustion processes and engine modelling, followed by a presentation of the characteristic parameters determining the combustion properties of fuels. Subsequently, the relevant conversion routes leading to biogenous fuel gases are presented and fuel gas compositions from different processes are reviewed.

Chapter 3 deals with the experimental methodology for measuring fuel gas compositions and the experimental plant.

In Chapter 4, the modelling methodology is presented. First, the equations for modelling chemically reacting mixtures of fuel, oxidiser and residual gas – the combustion gas – are presented. Then, the zero-dimensional reactor models and the one-dimensional laminar flame model are introduced and the fundamentals of auto-ignitive regimes and the detonation theory are presented.

The computational implementation of the models is described in Chapter 5. The simulation workflow is presented and the models are verified with reference data from literature.

In Chapter 6, the results of the measurements at the experimental plant and the investigated fuel gas blends are presented. The developed simulation methodology is applied to assess the combustion characteristics of the fuel blends. Special attention is paid to the knock propensity and to measures for mitigating the risk of knock.

Finally, the main findings of the thesis are summarised in Chapter 7 and recommendations for further work are provided.

Chapter 2 Literature review

2.1 Engine combustion processes

2.1.1 Spark ignition engines

In conventional *spark ignition engines* (SI engines) fuel and air are mixed together in the intake system, inducted through the intake valves into the cylinder – where mixing with the residual gases takes place – and then compressed and ignited by an electric discharge (spark plug) towards the end of the compression stroke [17]. After inflammation a turbulent flame develops and propagates through the premixed mixture of fuel, oxidiser and burned gas until it reaches the combustion chamber walls and extinguishes [17].

The general idea adopted in many combustion models for SI engines is that of a premixed flame front propagating into the cylinder from the source of ignition with a flame surface that is a portion of the surface of a sphere [17, 18]. The speed at which the flame front travels through the unburned mixture is determined by the *laminar flame speed,* which is an intrinsic property of the combustible mixture [17], and the level of turbulence in the cylinder charge, resulting in a *turbulent flame speed* [18, 19].

A general feature of spark ignition engines is that a substantial variation of the combustion process from cycle-to-cycle can be observed. The cyclic variations are usually expressed in measurable parameters, such as the *coefficient of variation* of the *indicated mean effective pressure* [17] or the *peak pressure* [20]. Cycle-to-cycle variations limit the operating regime of SI engines and can lead to abnormal combustion or misfiring [20, 21]. The most important abnormal combustion phenomenon in spark ignition engines is *knock*, characterised by a spontaneous auto-ignition and rapid energy release of the unburned mixture ahead of the flame front, the *end gas* [17]. The occurrence of knock “reflects the outcome of a race between the advancing flame front and the precombustion reactions in the unburned end gas”

(Heywood [17] p. 375). According to the detonation theory engine knock is linked to the speed of sound and the reaction velocity (cf. [22–26]).

Stoichiometric or lean burn spark ignition engines are often applied for the conversion of gaseous fuels in stationary applications. These engines are in many cases derived from diesel engines which are redesigned for gas operation [27]. Smaller gas engines feature open combustion chambers, while in large bore lean burn engines the spark plug is usually mounted into a pre-chamber in order to maximize ignition energy [27]. For ultra-lean operation with fuel/air equivalence ratios < 0.5, this pre-chamber can be equipped with a separate gas supply in order to achieve a richer mixture inside the chamber, which is easier to ignite [27].

In stoichiometric gas engines, three-way-catalysts are applied for reducing emissions of nitrogen oxides (NO_x), carbon monoxide and unburned hydrocarbons. In lean burn gas engines oxidation catalysts are used for reducing carbon monoxide and unburned hydrocarbons, and the NO_x emissions are controlled by leaning the mixture in order to reduce the combustion temperature [27]. For increasing the power output, especially in lean engines, turbochargers are applied [27].

In order to meet the demands on high efficiency and at the same time low emissions of NO_x, different technologies are conceivable, as presented in Table 2-1. Up to now turbocharged lean burn engines are preferred in practical application due to their higher efficiency, but further emission reduction in these engines is complex, especially with regard to NO_x as well as unburned hydrocarbons and in particular methane [28]. Thus, with stricter emission regulations stoichiometric engines could prove to be advantageous, and new developments aim to overcome their efficiency drawbacks by turbocharging combined with Miller valve timing for knock mitigation [29].

Table 2-1: Comparison of different SI gas engine technologies (adapted from [29])

	Lean burn 500 mg/m³ NO_x*	Ultra-lean-burn 250 mg/m³ NO_x*	Lean-burn with SCR** catalyst 10 - 250 mg/m³ NO_x*	Stoichiometric 50 mg/m³ NO_x*
Complexity	Medium	Medium	High	Low
Electric efficiency	High	Medium	High to very high	Low
Total efficiency in CHP operation	Medium	Medium	High	Very high
Specific maintenance costs	Medium	Medium to high	Medium to high	Medium to high
Hydrocarbon emissions	Medium	High	Medium to low	Low
Cost for exhaust gas after-treatment	Low	Medium	High	Low
Capability for off-grid operation	High	Medium	High	Very high
Sensitivity to methane number	Medium	Low to medium	Medium to high	Low

*all NO_x emission values refer to 5 vol% O_2 in the exhaust gas
** Selective catalytic reduction

2.1.2 Compression ignition engines

In conventional *compression ignition engines* a liquid fuel is injected into the cylinder towards the end of the compression stroke. The fuel atomises into small drops and penetrates into the combustion chamber where it evaporates and mixes with the compressed hot air in the cylinder [17]. The essential difference to a conventional spark ignition engine is that the mixture preparation takes place inside the cylinder, whereas in SI engines, fuel and oxidiser are normally premixed. Diesel engines always operate with lean fuel/air ratios and the power output is controlled by varying the amount of fuel injected per cycle [17] (quantity control instead of quality control like in SI engines).

Combustion in diesel engines is usually characterised by four periods (see [17, 30]): first the injected fuel is atomised into fine droplets, heated and vaporised; during this time no combustion happens, therefore it is called the ignition delay period. The next phase is the premixed burning of the mixture prepared during ignition delay which is characterised by a

sudden, steep increase in the cylinder pressure, causing the typical diesel sound. After the premixed burning until the end of injection, the combustion is controlled by mixing of the fuel jet with the air in the cylinder. After the end of injection the remaining fuel burns in a diffusion flame (late mixing-controlled burning) with decreasing heat release rate due to the temperature of the mixture falling during expansion.

A special type of compression ignition engine is the homogenous charge compression ignition (HCCI) engine, which has the theoretical potential of reducing both NO_x and particulate matter emissions, whilst retaining high efficiency [31]. In this type of engine the fuel is introduced into the cylinder at a very early stage in order to create a premixed, lean, homogenous mixture, which is then auto-ignited by compression [31]. The main challenge in HCCI combustion is the lack of a combustion-initiating device, which implies that ignition must be controlled by other parameters, such as compression ratio, fuel/air equivalence ratio, valve timings and intake manifold temperature [31]. Ignition in HCCI engines is primarily controlled by cool flame kinetics, which also plays an important role in SI engine knock [31].

2.1.3 Dual-fuel engines

Dual-fuel engines are basically conventional compression ignition engines of the diesel type where a liquid fuel injected in to the cylinder provides the source of ignition for a premixed lean mixture of gaseous fuel and air. Thus, they are also referred to as *diesel-ignited gas engine*s [13, 14].

Typically, only relatively small quantities of liquid fuel are injected to provide ignition of the lean mixture of gaseous fuel and air [13]. This type of dual-fuel engine is also denominated pilot injection or micro-pilot injection engine and the injection system is modified accordingly for the injection of small fuel quantities [32, 33]. The flame front propagates

through the lean background mixture after ignition similar to conventional premixed gas engine combustion [14]. In the second type of dual-fuel engines the liquid fuel is supplemented up to the level of a fully functional diesel engine and the gaseous fuel is added to the intake air up to a certain limit, which is mainly determinated by knock [13, 15].

2.1.4 Modelling of engine combustion processes

Nowadays, two complementary approaches for modelling the in-cylinder processes in engines are commonly used:

a) *Thermodynamic* models based predominantly on energy conservation, also labelled as *empiric*, *phenomenological* or *quasi-dimensional models*, depending on the level of detail that is considered in addition to energy conservation [17]

b) *Fluid dynamic* or *multidimensional* modelling based on a full analysis of the fluid motion [17]

Based on these two approaches a variety of different zero- and multidimensional models for engine combustion have been developed. An overview of common modelling approaches can be found in [17, 34, 35].

Zero-dimensional models are usually intended for the fast simulation of full engine processes at many different operating points (engine maps, transients, etc.) at the expense of insight into the detailed physical and chemical processes occurring in the cylinder. Simple empirical thermodynamic models, for example *VIBE* models [36, 37], rely on experimentally calibrated mathematical functions to describe combustion. In the recent years more sophisticated phenomenological and quasi-dimensional models for diesel engines (see Hiroyasu [38]), gas engines (see Auer [39]) and dual-fuel engines (see Walther [40]) have been developed. These models add further detail and geometric features in addition to the energy conservation equation [17] and take into account the relevant physical and chemical phenomena

occurring in the cylinder, such as the propagation of the spark ignition flame or the diesel spray pattern, thus enabling predictive calculations once the model is tuned with reference measurements.

Detailed fluid dynamic modelling is used when in-depth insight into the combustion process is required, for example, during the pre-development of new engines and combustion concepts. Due to computational costs and time requirement, multidimensional modelling is usually limited to the investigation of a few relevant operating points and single cylinders. The essential difference compared to zero- or quasi-dimensional modelling is that in multidimensional modelling the turbulent flow field inside the cylinder is explicitly modelled and solved. Since *direct numerical simulation* (DNS) requires supercomputers (cf. [41]) and is still not feasible today [35], different computational simplification methods like *large eddy simulation* or *Reynold-averaged Navier Stokes* (RANS) are used for this purpose [39].

Depending on the level of detail to be considered regarding specific combustion phenomena such as ignition delay time, engine knock or emission formation, more or less specific knowledge of the combustion behaviour of fuels and the underlying chemical reactions is needed. Two important combustion parameters commonly required in modelling of gas engines are the *ignition delay time* for knock models (see [21, 42]) and the *laminar flame speed* for flame propagation models (see [21, 39]). Both will be illustrated in more detail in section 2.2.2.

2.2 Combustion characteristics of fuels

2.2.1 Chemically reacting systems

The complex chemical processes taking place in combustion can be broken down into a set of multiple elementary reactions interacting with each other according to a defined *reaction mechanism*. This reaction mechanism provides a complete set of species and reactions for a given combustion system together with the required reaction kinetics coefficients. In addition, thermodynamic data, for example, in NASA polynomial parametrisation [43], as well as transport data is usually provided with the mechanism. Reaction mechanisms are usually developed based on experimental data from shock tubes, rapid compression machines, flames, jet-stirred or plug-flow reactors (cf. [44–47]). The complex kinetic schemes can only be solved with computational methods. A non-exhaustive overview of chemical kinetics software is given in Appendix A.

When dealing with reaction mechanisms, one has to carefully consider for which purpose they were developed and against which data they were validated. This applies for the species and reactions involved as well as the range of temperatures, pressures and equivalence ratios. Practical fuels frequently feature a complex composition of several different aliphatic and aromatic hydrocarbon species which is difficult to reproduce in reaction mechanisms. Therefore in chemical kinetics they are often replaced by simplified surrogates consisting of a blend of hydrocarbons for which the reaction mechanisms are known, such as blends of n-heptane, toluene and isooctane which are used as surrogates for diesel and gasoline fuels [48]. Detailed reaction mechanisms can comprise thousands of species and reactions and thus require high computational effort in solving the differential equation sets. Thus a variety of strategies for mechanism reduction has been developed in order to limit species and reactions to those relevant for the specific task (see [49–53]). Subsequently, a non-exhaustive selection of mechanisms considered relevant for this thesis will be briefly presented. The

referenced institutions often provide a variety of mechanisms for different purposes. A compilation of relevant data for the presented mechanisms is given in Table 2-2.

GRI-Mech 3.0 [54] is an optimised detailed chemical reaction mechanism developed for the combustion of methane and natural gas flames and ignition, which was developed in a project financed by the *Gas Research Institute* (GRI). The mechanism considers all steps important for natural gas combustion including NO formation and reduction and was validated extensively with experimental data. Soot formation and the chemistry involved in selective non-catalytic reduction of NO are not described by GRI-Mech 3.0 [54]. GRI-Mech includes reactions of the higher hydrocarbon constituents of natural gas (e.g., propane and butane) but was not designed to model the combustion of such pure fuels. The range of ambient conditions covered by the mechanism is roughly 1 000…2 500 K at 1.3×10^{-3} … 1 MPa and equivalence ratios from 0.1 to 5 for premixed systems.

USC-Mech II [55] is a high-temperature combustion reaction model of H_2, CO and C_1-C_4 compounds developed at the *Combustion Kinetics Laboratory* of the *University of Southern California* (USC). The mechanism is applicable to a variety of combustion scenarios for gaseous fuels. It was developed, among other sources, on the basis of GRI-Mech and validated against reliable experimental data.

A variety of mechanisms is available from the *Combustion Chemistry Centre* at *National University of Ireland, Galway (NUI Galway).* The development has been supported by *Saudi Aramco,* hence the mechanisms are denominated *AramcoMech*, with the newest version *AramcoMech 3.0* [56] and the prior versions *AramcoMech 2.0* [46, 57–62] and *AramcoMech 1.3* [59] respectively. Additionally, NUI Galway provides mechanisms for hydrogen/syngas [58] including NO_x [63], and for alcohols, esters, ethers as well as alkanes and alkenes. AramcoMech was developed in a hierarchical way, starting with a H_2/O_2 submechanism, followed by a C1 sub-mechanism, followed by larger carbon species such as ethane, ethylene,

acetylene, allene, propyne, propene, n-butane, isobutane, isobutene, 1-butene and 2-butene, and oxygenated species including formaldehyde, acetaldehyde, methanol, ethanol, and dimethyl ether [64]. Validations of the mechanism were carried out against a large array of experimental measurements including data from shock tubes, rapid compression machines, flames, jet-stirred and plug-flow reactors [64].

Extensive work on reaction kinetics simulation is carried out at the *Politecnico di Milano (POLIMI)* by the *CRECK* modelling group. Currently the group maintains a set of hierarchically organised reaction mechanisms ranging from hydrogen oxidation with 14 species and 33 reactions to a complete low and high temperature mechanism for hydrocarbon fuels including NO_x formation with 484 species and 19341 reactions [65]. In addition, several reduced mechanisms are provided, for example, for diesel/biodiesel and gasoline/biogasoline surrogates.

The *Combustion Research Group* of the *University of California at San Diego* (UCSD) provides the *San Diego Mechanism*, whose design focuses on the conditions relating to flames, high temperature ignition and detonations [66]. In contrast to other approaches, the San Diego Mechanism aims to keep the number of species and reactions to a minimum in order to reduce uncertainties with regard to the rate parameters. This is justified with the fact that a relatively small number of elementary steps is crucial for the predictions while the cumulative effects of a large number of steps is less significant [66]. The base mechanism can be complemented with reactions for nitrogen chemistry, jet-propellant, heptane and dimethyl ether [66].

Table 2-2: Compilation of reaction mechanisms

Mechanism	Source	Species	Reactions	Scope	Release
AramcoMech 3.0	National University of Ireland (NUI Galway) [56]	581	3 037	C1-C4 hydrocarbon and oxygenated fuels	2018
POLIMI	Politecnico di Milano [65]	484	19 341	Pyrolysis, partial oxidation and combustion of hydrocarbon and oxygenated fuels, high and low temperature including NO_x	2014
GRI-Mech 3.0	Gas Research Institute [54]	53	325	Methane, natural gas	1999
San Diego (base mechanism)	University of California at San Diego (UCSD) [66]	58	270	Flames, high temperature ignition and detonation of fuels	2016
USC Mech II	University of Southern California (USC) [55]	111	784	H_2, CO, C1-C4 Compounds	2007

2.2.2 Laminar flame speed and ignition delay

One of the most important parameters to describe premixed combustion in gas engines is the *laminar flame speed* [67] which is defined as "the velocity at which unburned gases move through the combustion wave in the direction normal to the wave surface" (Glassman et al. [68] p. 153). The laminar flame speed is an intrinsic property of a combustible mixture of fuel, oxidiser and burned gas [17] and can thus be used to characterise the combustion behaviour irrespective of the specific combustion system layout. Other common denominations are *flame velocity*, *burning velocity* or *normal combustion velocity* [68]. Several analytical models have been developed for calculating laminar flame speeds, such as the theories by Mallard and Le Chatelier and Zeldovich, Frank-Kamenetskii and Semenov [68]. With modern computational techniques it is nowadays possible to solve the complete set of steady state mass, species and energy conservation equations with detailed chemical reaction mechanisms [68]. The model of a *freely-propagating, one-dimensional, adiabatic, premixed flame* is normally used for this purpose [21, 68, 69].

A second important parameter is the *auto-ignition delay time* which can be observed under the specific operational conditions in technical devices between the introduction of a combustible mixture and the appearance of the flame [31]. For non-premixed mixtures of air and liquid fuel, as in the case of a diesel engine, the observed ignition delay time is considered the sum of a *physical ignition delay* and a *chemical ignition delay* [31]. The former presents the delay owing to the physical processes involved with mixture preparation, such as atomisation, fuel evaporation and air entrainment into the spray, while the latter corresponds to a period of significant chemical activity, involving the generation of a radical pool and cool flame exothermal reactions, ultimately leading to the onset of a flame [31]. For *premixed homogenous mixtures* of fuel and oxidiser, as they occur in gas engines, only the chemical ignition delay time is relevant. Auto-ignition and chemical ignition delay of fuel/oxidiser mixtures can be numerically determined by simulating a closed homogenous batch reactor with constrained volume and adiabatic walls, as shown in various studies [21, 42, 44, 45, 70–73]. The chemical auto-ignition delay time for a given mixture of fuel and oxidiser is a function of the temperature and the pressure [74] and plays an important role with regard to knock in SI engines, which is caused by uncontrolled auto-ignition in the unburnt zone during the regular combustion [75, 76]. A general overview of knock in SI engines and knock analyses is presented amongst others by Wang [77], Zhen [78] and Kalghatgi [79]. For details on knock modelling one can refer to the numerous publications on the topic (e.g., [20, 42, 80–82]).

The ignition delay time and the laminar flame speed of fuels have been studied extensively both experimentally and numerically by several authors, and relevant data has found its way into textbooks on combustion (e.g., [68]). However, many authors focus merely on the combustion of standard fuels, such as methane, see Bates [71], Hu [70], El Merhubi [45] and Burke [72]. Blends of methane and hydrogen are also often investigated, for example,

by Bougrine [83], Kumar [84] and Zhang [73]. A comprehensive collection of digitised data from combustion experiments is available from *Cloudflame* [85], a platform operated by the Clean Combustion Research Center at the King Abdullah University of Science and Technology in Thuwal, Saudi Arabia.

Pizzuti et al. [86] performed a literature review of published data on laminar flame speed and flammability limits in biogas. They conclude that the presence of CO_2 in biogas leads to a decrease in burning velocity which affects the stability of the flame. A feasible way for increasing the laminar flame speed is the admixture of faster burning fuels, such as H_2 or propane. Although the flammability limits of biogas are narrower than those of methane or natural gas the lean limit is improved due to the radiation absorption by CO_2. The presence of water vapour leads to an increase of the lean flammability limit.

An extensive review of laminar flame and ignition delay times of syngas mixtures is presented by Lee et al. [87]. Lee concludes that although a large number of experimental data is available for the combustion of syngas with various H_2/CO concentrations, data at elevated pressures and studies on syngas mixed with other gases such as CH_4, CO_2 and H_2O are still very limited. The addition of CO_2, CH_4, and H_2O can however dramatically alter the ignition delay time compared to pure H_2/CO mixtures, which strongly implies that a simple syngas mixture is not fully adequate to represent practical syngas chemical kinetics [87]. This is addressed to some extent in newer investigations, for example, by Ouyang et al. [88] who studied auto-ignition of synthesis gas at elevated temperatures and pressures in a shock tube also including CH_4. According to Ouyang both CH_4 and CO act as inhibitor, thus increasing ignition delay, albeit the inhibiting effect of CO is only conspicuous if the concentration is high enough.

Ignition delay in dual fuel engines has been comprehensively studied by Karim and Liu [13, 89]. Detailed chemical kinetics calculations presented by Karim for mixtures of n-heptane and methane show a very rapid reduction in ignition delay and subsequent combustion time with increasing mole fraction of liquid fuel vapour, already at relatively small quantities. According to Karim n-heptane, which can be considered to be a representative of diesel fuel, begins reacting with the oxidiser well ahead of the methane, producing some exothermic energy release and required radicals for the methane oxidation, thus speeding up the ignition processes substantially. This is confirmed by Burke et al. [72] who studied dual-fuel ignition delay of methane in *dimethyl ether* (DME) in a rapid compression machine and developed a detailed chemical kinetic mechanism for methane/DME combustion. The ignition delay time was found to be considerable reduced in the dual-fuel regime even when adding just small amounts of DME, with DME controlling the ignition of blends even if there is a greater concentration of methane, since the radical pool builds at lower temperatures and therefore increases the rate of methane combustion [72].

Since experimental data for laminar flame speed and ignition delay at engine combustion conditions (high pressure and temperature) is hardly available and extrapolation from measured data to unsurveyed ranges is problematic, the required data is often determined by reaction kinetics calculations using detailed chemical reaction mechanisms which are assumed to be essentially valid also under engine related boundary conditions [21, 39, 90–92]. To save computational costs, chemical data for engine modelling is often implemented using correlations, like the *Gülder correlation* for the laminar flame speed ([93] in [21]), rather than by considering the full reaction mechanism in the combustion model. Recent investigations by Hann et al. [21, 90] reveal, however, that the Gülder correlation requires “a high level of revising to account for all influences” (Hann et al. [21] p. 68). Hann developed a new correlation based on detailed reaction kinetics simulations of the laminar flame speed

and expanded its applicability to binary mixtures of ethane, propane, n-butane and hydrogen with methane [21]. The laminar flame speed will be also affected by the residual gas fraction [17], which is taken into account in the correlations by Hann [21] for methane blends and by Verhelst for hydrogen [94]. Doosje et al. [95] present a correlation of laminar flame speed for natural gas with admixture of hydrogen and ethene for stoichiometric and lean conditions based on measurements in constant-volume bomb and chemical kinetics calculations.

Another approach is presented by Chmela et al. [67] who modified a two-zone thermodynamic engine model for simulation of non-standard gases such as flare gas, anaerobic digester gas and producer gas. Ignition delay and laminar flame speed are required as input parameters for the model, which poses the problem that such data is mostly just available for pure gases or for a limited range of temperatures, pressures and equivalence ratios. Instead of using correlations, which according to Chmela would be difficult and would require extensive experimental verification, a polynomial approximation based on regression analyses of 2 150 measured (ignition delay) and simulated (laminar flame speed) values is used.

2.2.3 Auto-ignition propensity of fuels

The resistance of fuels to engine knock has traditionally been rated according to the anti-knock performance of mixtures of *primary reference fuels (PRF)*. These are iso-octane and n-heptane for liquid fuels and methane and hydrogen for gaseous fuels. The associated rating numbers are accordingly denominated the *octane number* and the *methane number*. A specific fuel will be given the octane or methane number that corresponds to the volume fraction of iso-octane and methane, respectively, in the PRF fuel blend exhibiting the same anti-knock performance [74, 96]. Both the octane and methane number are determined experimentally in standardised single cylinder test engines, the *cooperative fuel research engines (CFR)* [97], featuring a variable compression ratio which is increased during the test until

knock is detected [74, 96]. For liquid fuels two different test procedures with different initial temperatures and engine speeds are defined, resulting in the *research octane number (RON)* and the *motor octane number (MON)* [74]. Despite being still widely in use, both the octane number and the methane number have serious drawbacks since they are essentially only indirect methods for measuring the auto-ignition delay time which is the principal underlying combustion parameter for engine auto-ignition [97]. Both methods also exhibit the problem that any fuel less knock-resistant than n-heptane or hydrogen, or more knock-resistant than iso-octane or methane requires extrapolation to PRF mixtures that cannot exist [74]. In case of the methane number, this issue is solved to some extent by adding CO_2 to pure methane allowing for values of MN > 100 [96].

In an effort to improve the characterisation of fuels based on the actual phenomenology of auto-ignition, Bates et al. present a comprehensive methodology for characterising the auto-ignition regimes evolving from hot spots in engines [23, 25, 71, 74] based on the detonation theory developed by the group of Bradley at the University of Leeds (cf. [98, 99]). According to Bates hot spots can arise for a number of reasons, such as fuel inhomogeneities, and local temperature gradients caused by hot surfaces (e.g., exhaust valves) or hot recirculated gases. Such primary hot spots can pre-ignite and initiate a premature flame propagation causing increases in temperature and pressure in the unburned gas. They serve as kernels for the generation of secondary, more reactive hot spots in the reactants which may develop into a detonation [23]. While the mechanisms leading to primary hot spots are not yet fully understood, reaction propagation from secondary hot spots has been extensively studied and developed into a fundamental approach capable of characterising fuel anti-knock properties and engine auto-ignition ranging from mild knock to super-knock [23].

Bates introduced an extended version of the ξ-ε diagram (see Figure 2-1) indicating the possible regimes of deflagration, detonation and transition between the two modes based on

two dimensionless parameters representing the energy transferred into the acoustic wave front moving through a hot spot (ε) and the auto-ignition propagation velocity normalised by the acoustic velocity (ξ). The energy transferred into the acoustic wave is determined by the *excitation time* τ_e defined as the time during which the majority of the heat is released. It accounts for the fact that heat release is not instantaneous, but takes place over a finite amount of time [74]. According to a definition by Lutz et al. ([100] in [71]) the excitation time is the time span between the point where 5 % of the maximum heat release rate is reached and the point at which the maximum is attained. As an alternative definition, Bates suggests the period of time where the heat release is more than 20 % of the maximum, since during this time the most intense heat release occurs [71]. According to Bates the chemical excitation cannot be measured with current methods due to the extremely short timescales involved and because experiments are not able to capture the initial reaction at just a single point, but will rather be limited to the bulk volume [74]. Thus, the only method to obtain the excitation time is through numerical simulations [71].

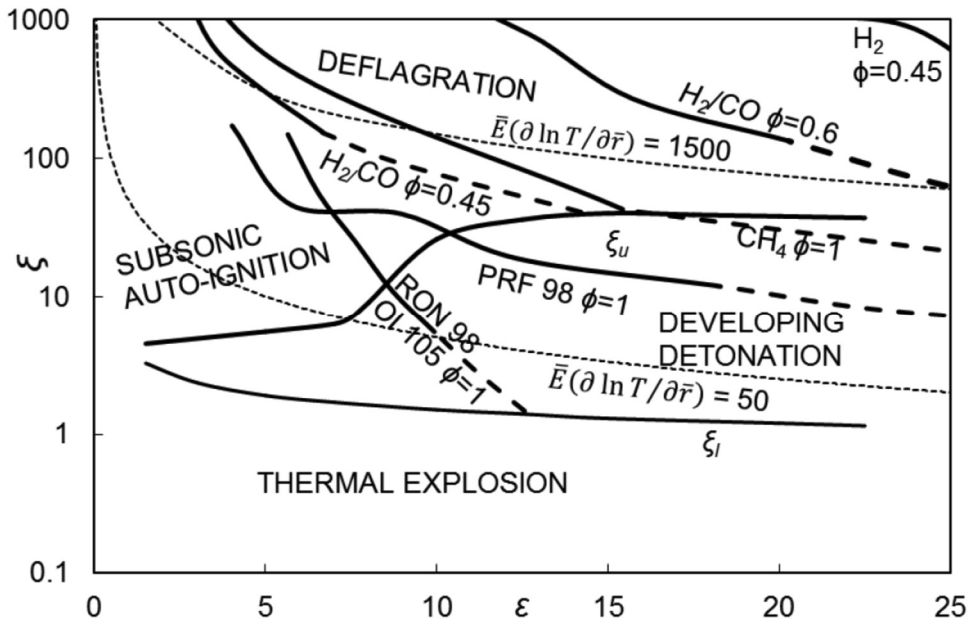

Figure 2-1: ξ-ε diagram with isentropic compression curves for different fuels [74]

The ξ-ε diagram comprises a detonation peninsula marked by the upper and lower boundaries of ξ_u and ξ_l which separate the region of dominating deflagration from the region of strong thermal explosions with the transition regime of developing detonations being in between. The boundaries of the peninsula were obtained from several numerical and experimental studies prior to Bates by mapping the edges of detonative conditions [74] (cf. the DNS study by Gu et al. [98]).

Sankaran [101] performed a high fidelity DNS of the auto-ignition of hydrogen-air mixtures identifying two prominent ignition regimes emanating from thermal hot spots: a wide-range spontaneous explosion and a narrow flame-like deflagration. To distinguish between these two patterns, Sankaran introduced a dimensionless transition parameter $\beta = C_\beta \, u_d/u_p$ which relates the deflagration wave speed u_d (slow) to the auto-ignition propagation speed u_p (fast). If the mixture is highly reactive and the temperature gradient is small β will be < 1 and each local point in the mixture will ignite in a homogenous explosion with an ignition front travelling at a speed much higher than the deflagration speed [101]. In the opposite case of $\beta > 1$, the mixture will feature low reactivity and allow a deflagration front to develop upon ignition [101]. Most cases of $\beta > 1$ were found to be in locations with high temperature gradients, but not all regions with high temperature gradients necessarily lead to deflagration [101]. The transition factor β does in fact not define a strict threshold, but is rather an indicator for the relative dominance of the two ignition regimes [101].

The findings of Sankaran were later experimentally confirmed by Mansfield et al. [102] using the University of Michigan Rapid Compression Facility. A sample of homogenous and inhomogenous ignition recorded with chemiluminescence measurements in this facility is presented in Figure 2-2. Homogeneous ignition is indicated by spatially uniform emission, whereas inhomogeneous ignition features flame-like structures which propagate and merge [102].

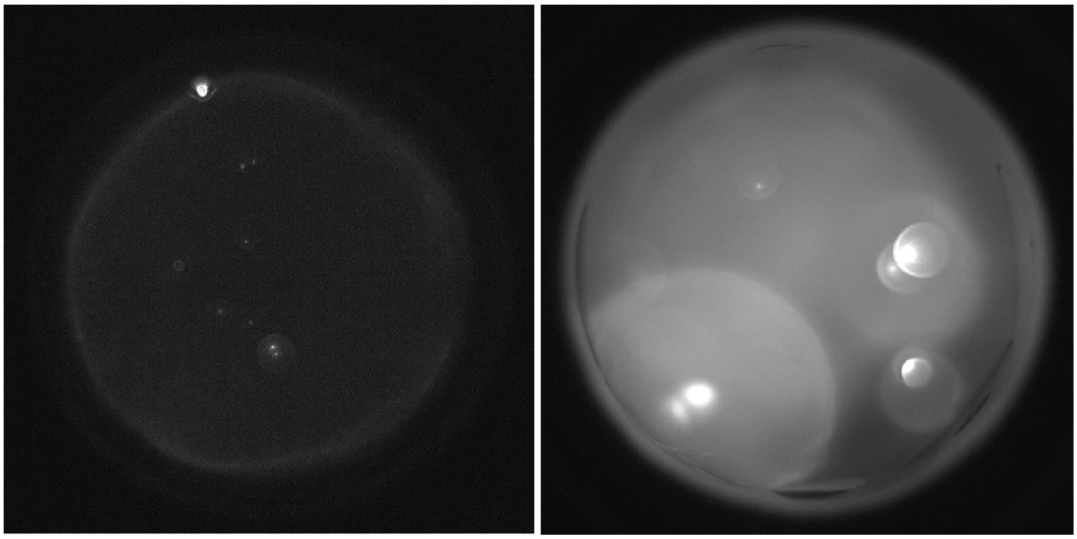

Figure 2-2: Inhomogenous (left) and homogenous ignition behaviour (right): single frame from high-speed chemiluminescence imaging [102]

Sankaran et al. [101] observed that auto-ignition and deflagrative propagations can co-exist. Based on these findings Bates introduced a new tentative threshold defined by constant values of $-\bar{E}(\partial lnT/\partial \bar{r}) = 1\,500$ in the ξ-ε diagram to characterise the auto-ignition behaviour above the upper limit of the peninsula [23, 74] (see Figure 2-1). Below this threshold auto-ignitive propagation dominates, while above the threshold deflagration becomes dominant, although there is no sharp division between the two modes and they can co-exist in a broad regime [23].

The hot spots are assumed to be of spherical shape, although the actual structure may be less ordered [23]. With this simplification and the temperature gradient throughout the hot spot assumed to be constant, it is possible to determine both ξ and ε for a specific fuel solely from the ignition delay τ_i and excitation time τ_e, which can both be simulated using detailed chemical kinetics. The ξ-ε diagram has thus the potential to be used for a priori characterisation of the auto-ignition propensity of fuels without the need for experimentation (cf. studies of Bates for methane/air ignition [71]). Moreover, the detonation theory can also be applied for predicting knock at specific engine operating points, as recently demonstrated by

Netzer et al. [22, 24], who successfully used the ξ-ε diagram with a three-dimensional computational fluid dynamics analysis to predict knocking regimes in a gasoline-fuelled passenger car engine.

2.3 Biogenous fuel gases

2.3.1 Biomass conversion routes

Figure 2-3 presents typical conversion routes for biomass leading to fuels for heat and power production according to Kaltschmitt [103]. Gaseous biofuels can generally be provided either by bio-chemical or by thermo-chemical conversion. In the bio-chemical conversion route gaseous fuels are produced through anaerobic digestion of organic material by bacteria in an oxygen-free atmosphere, releasing a gas which mainly consists of CH_4 > 50 vol% and CO_2 [103]. Anaerobic digestion is well suited for biomass with a high water content in aqueous solution, such as manure or sewage sludge, but can also be applied for energy crops like maize silage, as long as these do not contain high share of lignin (e.g., wood) which cannot be degraded by anaerobic bacteria due to biological reasons [103]. For crops with a high share of lignin the thermo-chemical conversion route is suitable which can be further divided into pyrolysis and gasification processes [103, 104]. The main difference between the two processes is that in gasification a small amount of an oxidising agent is added to the process in order to transfer the maximum possible share of chemical energy into a gas directly usable as a source of energy [103, 105]. By contrast, in pyrolysis biomass is heated up in a basically oxygen-free environment in order to obtain solid, liquid and gaseous products [103].

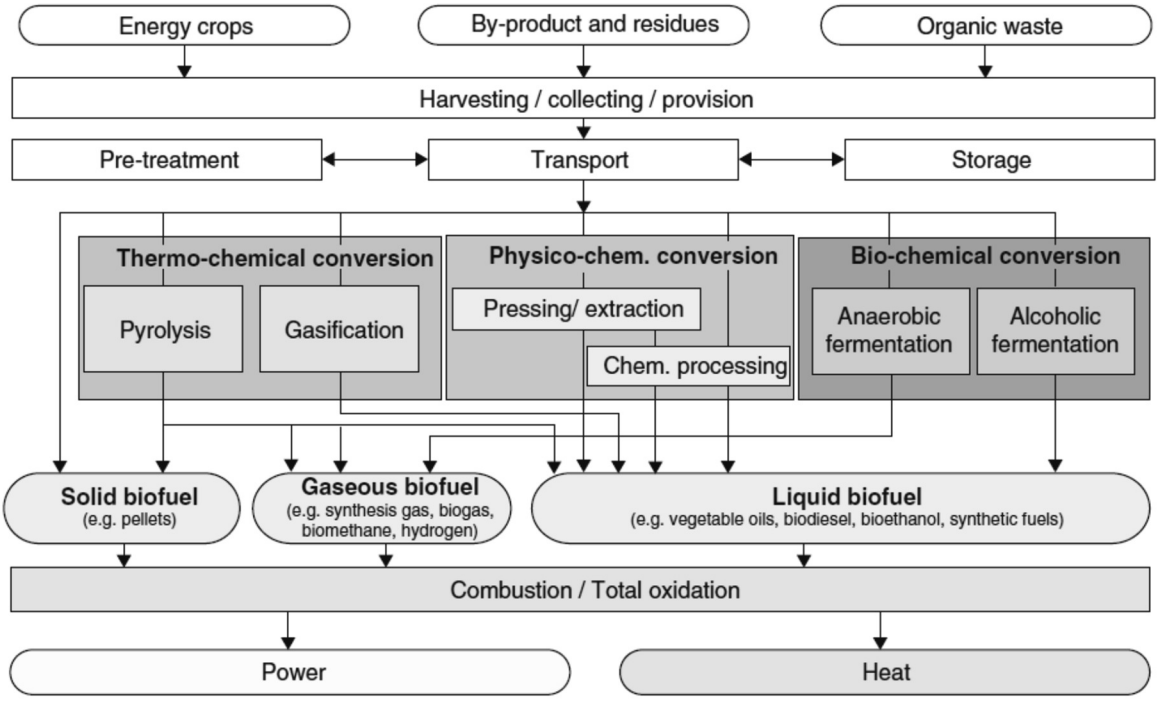

Figure 2-3: Possible conversion routes for biomass as renewable source of energy [103]

2.3.2 Anaerobic digester gas

Anaerobic digester gas is also known as *biogas*, *landfill gas* or *sewage gas* depending on where it is produced [103]. Both the flowrate and the composition depend on the feedstock and type of anaerobic digestion process, that is, closed digester or open landfill [106]. Irrespective of the digestion system the biogas product typically consists of methane, carbon dioxide and trace levels of nitrogen, hydrogen sulphide and water [107] (cf. Table 2-3).

According to Rodero [106] biogas from closed digesters, for example, from the anaerobic digestion of livestock manure, sewage sludge or municipal organic waste, produces biogas containing CH_4 at 50-70 vol%, CO_2 at 30-50 vol%, N_2 at < 3 vol%, O_2 at < 1 vol%, H_20 at 5-10 vol% and traces of higher hydrocarbons < 200 mg/m³, H_2S < 10,000 ppmv, NH_3 < 100 ppmv and siloxanes < 40 mg/m³. Landfill gas contains less combustible CH_4 at 35-65 vol%, but significantly more N_2 at 5-40 vol% and O_2 at < 5 vol%, with CO_2 15-50 vol%,

H_2 < 3 vol% and CO < 3 vol% [106]. Additionally, ammonia, halogenated hydrocarbons, volatile organic contaminants, siloxanes, chlorine and fluorine are reported [106].

Biogas has favourable characteristics for the utilisation in internal combustion engines, since the main combustible constituent is CH_4 which makes it in principle compatible with existing engine designs for natural gas. Due to the dilution with CO_2, biogas is generally more resistant to knock, thus allowing higher compression ratios, which increases efficiency and compensates to some extent the lower heating value as compared to natural gas [86]. For the utilisation in internal combustion engines biogas has to be cleaned from H_2S (< 100 ppmv recommended) and water [108]. Alternatively, it can be upgraded by removing carbon dioxide, for example, by adsorption or absorption or membrane separation, and injected into existing natural gas distribution systems, where it is then usually denominated *biomethane* [108].

Table 2-3: Typical composition of biogas in vol% (adapted from [106])

	Landfill gas	Biogas anaerobic digestion	North sea natural gas	Dutch natural gas
CH_4	45	63	87	81
CH_4 variation	36-65	53-70	-	-
H_2	0-3	0	0	-
Higher hydrocarbons	0	0	12	3.5
CO	0	0	0	0
CO_2	40	47	1.2	1
CO_2 variation	15-50	30-47	-	-
N_2	15	0.2	0.3	14
N_2 variation	5-40	-	-	-
O_2	1	0	0	0
O_2 variation	0-5	-	-	-
H_2S (ppmv)	< 100	< 1 000	1-2	-
NH_3 (ppmv)	5	< 100	0	-
Total chlorine Cl^- (mg/m³)	20-200	0-5	0	-

2.3.3 Syngas from thermo-chemical gasification

Gasification is the thermochemical conversion of solid biomass into combustible fuels in the presence of an oxidant with less than the stoichiometric ratio [2]. The main steps of the gasification process are drying, pyrolysis, partial oxidation and reduction [2, 109, 110]. Different types of gasifiers have been developed, such as fixed bed downdraft, updraft and crossdraft gasifiers, fluidised bed gasifiers, bubbling bed gasifiers and circular bed gasifiers [2]. The main output product of gasification is a combustible gas consisting mainly of H_2, CO, CO_2 CH_4, N_2 and water vapour [2], which is also known as *syngas*.

The fuel gas composition can vary greatly according to the feedstock, the type of gasifier and the process settings. A range of typical fuel gas compositions obtained from different gasifier types is presented by Schulzke [110] in his review of current technologies for the gasification of wood for producing heat, electricity and base chemicals (see Table 2-4).

Table 2-4: Typical composition of fuel gases from biomass gasification (adapted from [110])

	UMSICHT	Güssing	Chrisgas	CUTEC
Gasifying agent	Air	Steam	Oxygen (+steam)	Oxygen (+steam)
Pressure	Atmospheric	Atmospheric	10-15 bar	Atmospheric
H_2 / vol%	14	26	11.8	32
CO / vol%	16	15.6	11.9	27
CO_2 / vol%	13	13.7	27.9	35
CH_4 /vol%	4	6.5	8.2	2
$C2_+$ / vol%	n.a.	1.6	1.6	n.a.
H_2O / vol%	10	35	37.7	3 [a]
N_2 / vol%	43	1.3	< 0.9 [b]	< 0.3

n.a.: not analysed; [a] after water quench (H_2O at reactor exit approx. 30-40 vol%); [b] by difference

Reil [109] presents product gas compositions obtained from stratified downdraft gasification of wood with air as gasification agent. According to Reil, the product gas composition varies with the maximum gasification temperature, the water content of the input material and the superficial flow velocity. The gas composition was measured with infrared detectors for CO, CO_2 and CH_4 and a thermal conductivity detector for H_2. Higher hydrocarbons were measured by gas bag sampling and subsequent laboratory analysis. The main combustible constituents are H_2 at 11-15 vol% and CO at 12-19 vol%, followed by CH_4 at 1.5-3 vol% (approximate values, all on wet basis). The non-combustible components are CO_2 at about 10-12 vol% and H_2O at 12-25 vol% (wet basis). Reil detected higher hydrocarbons C2 to C5 which together with methane peaked at about 3.5 vol%. The individual contributions of C_2H_6, C_2H_2, C_3H_8 and C_3H_6 were all less than 0.1 vol% and C_2H_4 was about 0.5 vol%.

Patuzzi et al. [111] performed a comparative performance assessment of four different small-scale gasifier systems with combined heat and power (CHP) engines operated in South Tyrol (Italy). The investigated technologies were three different downdraft gasifiers for wood chips designed for an electric power output ranging from 45-300 kW and a rising co-current pellet gasifier with a CHP unit providing 180-190 kW electric power output. The pellet gasifier's design is unique in that it has the same zone distribution as a downdraft gasifier, but the biomass input is provided from the bottom and the producer gas exits at the top, while the air is fed in a way that it creates a vortex above the combustion zone similar to a fluidised bed. The reported gas qualities were H_2 at 15-20 vol%, CO at 18-24 vol%, CH_4 at 1-2 vol%, CO_2 at 6-10 vol% and N_2 at 48-52 vol%, with the pellet gasifier delivering the highest hydrogen content and thus the highest heating value.

Marcello et al. [112] present results from a pilot scale steam-oxygen circulating fluidised bed gasification of commercial torrefied wood pellets. The equivalence ratio and the steam to biomass ratio was varied and the gasification temperature was set to about 850 °C. The

gas composition was measured with a gas chromatograph. Depending on the settings and the type of torrefied pellets, the gas quality varied with the approximate values on dry basis being H_2 30-40 vol%, CO 11-15 vol%, CH_4 4-5 vol% and CO_2 40-50 vol%. The water content in the product gas was approximately 37-60 vol%. Higher hydrocarbons in the fuel gas (other than tar) were not measured. Torrefaction showed to improve the gas quality in terms of combustible components and lower total tar content, while also improving the gas yield.

Biagini et al. [113] investigated the gasification of agricultural residues (corn cobs) in a demonstrative plant. The reactor used was of the downdraft type with throat using air as gasification agent and was originally designed to operate with wood chips with a nominal thermal throughput of 350 kW. The product gas composition was measured with a gas chromatograph and a Fourier-transform infrared spectrometer. The reported dry output gas composition (mean values of all tests) was as follows: CO at 22.4-22.6 vol%, H_2 at 15.8-17.3 vol%, CO_2 at 11.3-12.3 vol%, CH_4 at 1.9-2.3 vol%, C_2H_4 at 0.34-0.39 vol% and approximately 0.05 vol% of both C_2H_6 and C_2H_2, with the rest being nitrogen. Water and tar in the produced syngas were not quantified.

Kurkela et al. [114] studied the steam-oxygen gasification of forest residues and bark in a circulating fluidised bed reactor applying hot gas filtration and catalytic reforming of tars. Steam and oxygen were used as the main fluidising agents. The dry gas composition was measured on-line with a gas chromatograph. The combustible constituents (dry basis) were CO 17.3-18.6 vol%, H_2 29.7-31.3 vol%, CH_4 6.6-7.2 vol%, C_2H_2 0-0.01 vol%, C_2H_4 0.9-0.99 vol% and C_2H_6 0.1-0.15 vol%. The diluents were CO_2 33.5-34.6 vol% and N_2 7.6-10.1 vol%. Higher hydrocarbons C3-C5 were below the detection limit of the gas chromatography. The water content in the wet gas ranged from 33.8 to 37.6 vol%. After reforming the H_2 content increased to 34.4-37.4 vol%, with CO 19.3-21.96 vol%, CH_4 1.22-2.67 vol%, C2-C5 not detectable, CO_2 32.5-34.9 vol% and N_2 6.9-10.1 vol% (dry basis all). The water

content after reforming increased to 37.4-42.2 vol%. The total concentration of tar and benzene in the raw gas was 17.5-19.3 g/m³ and could be effectively reduced through catalytic reforming by 98 % and 93 … 97 % respectively. Additional trace gases detected in the product gas after reforming were NH_3, H_2S, COS and HCN.

Dahlquist et al. [115] performed a study comparing the gas quality from the gasification of black liquor and wood pellets using modelling and experimental results from a pilot scale plant. The gasifiers used for black liquor and wood pellets were both of the circulating fluidised bed type and were equipped with a gas cleaning system with bag filters and a scrubber. The syngas composition was measured with a gas chromatograph (wood pellets) and near-infrared spectroscopy (black liquor). The experimental results were used to calibrate a partial least squares model for predicting the gas qualities. Black liquor was found to produce substantially more hydrogen in the syngas, while syngas from wood pellets showed higher contents of CO and CH_4. The simulated gas composition (wet basis) from black liquor for different set points was H_2 8.7 … 13 vol%, CO 1.68 … 2.8 vol%, CH_4 0.96 … 1.33 vol%, CO_2 9.8 … 12 vol%, N_2 37.2 … 46.9 vol% and water 29.4 … 39.9 vol%. H_2S ranged from 0.52 to 0.58 vol%. In the case of the wood pellets the gas composition is reported after condensation to 20 °C, so that part of the water was already removed from the product gas. The respective shares were as follows: H_2 1.9 … 3.4 vol%, CO 8.4 … 16.8 vol%, CH_4 0.9 … 6.6 vol%, CO_2 23.5 … 54 vol%, N_2 30.3 … 49.9 vol% and water 1.3 … 1.5 vol%.

Katsaros et al. [116] studied the low temperature gasification of poultry litter in a lab-scale bubbling fluidised bed reactor at 700 °C and different equivalence ratios using air as gasification agent. The gas composition was measured with an on-line gas-chromatograph. At the lowest equivalence ratio the gas composition was found to be (dry basis): H_2 7.87 vol%, CO 6.37 vol%, CH_4 2.04 vol%, C_2H_4 1 vol%, C_2H_6 0.22 vol%, CO_2 11.47 vol%. The nitrogen and water content in the product gas were not explicitly given by the authors.

With increasing equivalence ratio the yield of H_2 and CO increased up to 9.2 and 7.7 vol% approximately, albeit with an increase in CO_2 to about 14 vol%, while CH_4 decreased slightly down to 1.7 vol% and C_2H_4 remained stable at around 1 vol%. Trace gases were found to be COS, H_2S and higher hydrocarbons C_6H_6 and C_7H_8 all at less than 0.05 vol%.

2.3.4 Pyrolysis gas

Pyrolysis processes can be classified according to the residence time as slow, intermediate, fast and flash pyrolysis [1]. The residence time is in the range of minutes in the case of slow and intermediate pyrolysis, while for fast and flash pyrolysis it is in the range of seconds. Accordingly the required heating rates are highest for flash and fast pyrolysis, which usually requires a finely ground biomass feed [1]. As presented in Table 2-5 the yield of liquid products (pyrolysis oil and pyrolysis water) is highest for flash pyrolysis, followed by fast pyrolysis. The intermediate and slow processes feature lower yields of liquids, but return higher yields of gas and char. Fast pyrolysis is usually targeted at the production of bio-oils (see Bridgewater [117]), therefore less attention is paid to the energetic utilisation of the gas fraction and many authors focus merely on the liquid fraction and do not publish detailed data on the pyrolysis gas composition (e.g., [118–124]). This is different in the case of intermediate pyrolysis, where the gas fraction is an important product of the process.

Table 2-6 shows typical compositions of the gas fraction obtained by fast and intermediate pyrolysis of biomass and organic residues. *Pyroformer* and *Thermo-Catalytic Reforming (TCR)* represent intermediate pyrolysis processes developed at the *European Bioenergy Research Institute* and *Fraunhofer UMSICHT* respectively. TCR is an evolution of the Pyroformer and introduces an additional post-reforming step (see [4] and [125]). In addition to the gas fraction the Pyroformer and TCR processes deliver high quality bio-oils, which can be further upgraded to transportation fuels [126] or directly used in stationary engines [127].

From Table 2-6 it can be seen that in contrast to the typical methane fuels, such as natural gas and anaerobic digester gas (biogas), the methane concentration in the pyrolysis gas is generally below 10 vol%, peaking at about 12 vol% for TCR pyrolysis of wood. The main combustible constituents of pyrolysis gas are carbon monoxide (CO) at up to 50 vol% and hydrogen (H_2). The product gas is typically diluted with inert gases, mainly CO_2. The Pyroformer process delivers very high contents of carbon dioxide (CO_2) up to 70 vol%, which indicates a poor energy content and low reactivity of the gas fraction. By contrast, the TCR process consistently delivers very high hydrogen (H_2) contents of up to 40 vol% and thus presents a considerable progress with regard to the energy content of the gas, while at the same time introducing new challenges for engine operation due to the high reactivity and fast combustion of hydrogen. Neumann et al. [4] showed that the formation of H_2 can be mainly attributed to the post-reforming step and that the H_2-content rises with increasing post-reforming temperature. This is confirmed by the findings of Ahmad et al. [128]. Higher post-reforming temperatures are also beneficial for the gaseous product yield, which peaked at about 44 wt% at 1 023 K post reforming temperature [4].

Table 2-5: Main variants of pyrolysis methods (as presented in [1] adopted from [129])

Pyrolysis process		Slow	Intermediate	Fast	Flash
Temperature (°C)	Range	250 – 750	320 – 500	450 – 1 050	550 – 1 300
	Typical	350 – 400	350 – 450	550 – 750	1 050 – 1 150
Time	Range	min	15 min	0.5 – 10 s	< 1 s
	Typical	2 – 30 min	4 min	0.5 – 5 s	< 1 s
Heating rate (°C/s)		1 – 50	10 – 100	100 – 500	> 1000
Particle size (mm)		5 – 50	5 – 50	< 1.0	< 0.2
Yields on dry basis (wt-%)					
Char	Range	2 – 60	19 – 73	15 – 35	10 – 35
	Typical	25 – 35	30 – 40	20 – 25	10 – 20
Liquid	Range	0 – 60	25 – 60	20 – 75	20 – 65
	Typical	20 – 50	35 – 45	46 – 53	46 – 71
Gas	Range	0 – 60	20 – 40	10 – 25	11 – 28
	Typical	20 – 50	20 – 30	11 – 15	15 – 22

For most of the data presented in Table 2-6 it is not known whether the gas composition is measured on a dry or on a wet basis. However, judging from the measurement devices applied (usually gas-chromatographs, infrared photometers and thermal conductivity detectors which require gas drying before analysis) the values refer to a dry basis. The water content in the product gas is not reported by any of the authors. In practical applications the product gas is probably wet up to the saturation level at the given condensation temperature of the pyrolysis vapours, but this has not yet been investigated in detail.

Some authors report higher hydrocarbons (C_xH_y) in the product gas, which are however not specified. This is particularly problematic since it is the higher hydrocarbons that limit the applicability of a gaseous fuels due to end gas knock limitations [130]. A detailed analysis of C2-C5 hydrocarbons in the product gas is reported by Greenhalf et al. [131] showing considerable levels of ethene, ethane, propene, propane and n-butane, but the experiments were performed in a bench-scale reactor where the pyrolysis gases were heavily diluted with nitrogen, so it is not possible to transfer the results to production-scale applications.

Furthermore, in the majority of the published data a comparatively large fraction of the mixture was not identified. Conti [132] and Neumann [133] argue that judging from the heating value of the product gas, which was measured separately with an on-line gas calorimeter, the non-detectable components are hydrocarbons like ethylene or propane. Ahmad attributes the non-detectable fraction to the formation of alkenes [128], while Meyer [134] closes the balance with nitrogen. The latter seems only reasonable if nitrogen is used for inertisation or as a diluent in the experiments. Consequently, there is still a need to further investigate the product gas quality and composition of intermediate pyrolysis gas with regard to engine applications.

Table 2-6: Pyrolysis gas composition from different feedstocks and processes

Source	Process / feedstock / post reforming temperature [a] / gas yield	Heating value [b]	H_2	CO	CH_4	CO_2	N_2	C_xH_y	Not detected / others
			vol%	vol%	vol%	vol%	vol%	vol%	vol%
Conti [132]	TCR / wood chips / 973 K / 62.7 wt%	-	24.0	22.0	12.0	22.0	-	2.0	18.0
	TCR / digestate / 973 K / 31.7 wt%	-	33.0	16.0	8.0	23.0	-	2.0	18.0
	TCR / sewage sludge / 973 K / 18.5 wt%	-	38.0	12.0	3.0	15.0	-	3.0	29.0
	TCR / paper sludge / 973 K / 19.1 wt%	-	40.0	10.0	1.0	27.0	-	3.0	19.0
Neumann [133]	TCR / digestate / - / 18 wt%	LHV 9.7 MJ/m³	7.0	43.0	6.0	40.0	-	-	4.0
	TCR / digestate / 773K / 20 wt%	LHV 13.1 MJ/m³	21.0	14.0	5.0	40.0	-	-	20.0
	TCR / digestate / 1 023K / 35 wt%	LHV 14.4 MJ/m³	37.0	12.0	3.0	28.0	-	-	20.0
Jäger [135]	TCR / vine shoots / 973 K / 57 wt%	-	36.0	15	10.0	27.0	-	1.5	10.5
	TCR / evergreen oak / 973 K / 58 wt%	-	36.0	16.0	12.0	27.0	-	1.0	8
	TCR / olive tree / 973 K / 60 wt%	-	33.0	16.0	12.0	27.0	-	1.5	10.5
Mahmood [136]	Pyroformer / brewers spent grain / - / 33-34 wt%	1-2 MJ/m³	1.6	19.7	9.4	64.2	4.6	-	O_2 0.45
Ouadi [125]	Pyroformer / de-inking sludge 1 /- / -	HHV 5.5 MJ/m³	0.0	22.7	6.1	71.2	-	-	-
	Pyroformer / de-inking sludge 2 /- / -	HHV 6.2 MJ/m³	1.9	25.5	6.3	66.3	-	-	-
Yang [137]	Pyroformer / wood pellets / - / 17.7 wt%	HHV 7.27 MJ/m³	2.2	34.7	7,2	50.3	5.5	-	-
	Pyroformer / barley straw /- / 20.9 wt%	HHV 6.92 MJ/m³	1.5	21.7	10.5	60.1	4.7	-	O_2 0.42
Louwes [138]	Fast pyrolysis wood & torrefied wood /- / ≈ 30% wt%	HHV 5.0-9.9 MJ/kg	0.6-3.2	42.1-53.5	-	43.3-54.2	-	-	-
Wu [139]	Shenwu rotating bed reactor / rice straw / 973 K [c] / ≈ 30 wt%	HHV 14.5 MJ/m³	37.2	20.2	8.5	19.6	-	5.4	-
	Shenwu rotating bed reactor / maize straw / 973 K [c] / ≈ 30 wt%	HHV 17.1 MJ/m³	45.4	30.1	7.5	10.7	-	6.3	-
	Shenwu rotating bed reactor / wheat straw / 973 K [c] / ≈ 30 wt%	HHV 14.1 MJ/m³	39.9	28.9	5.7	18.0	-	4.5	-

[a] if applicable, [b] as reported, [c] pyrolysis temperature
LHV: lower heating value; HHV: higher heating value

2.3.5 Quality assessment of fuel gases

Most biogenous fuel gases, such as biogas and producer gas, exhibit lower heating values than natural gas, although this might be compensated to some extent by a lower stoichiometric air requirement. While the loss of power production of an engine due to a lower energy content of a fuel is readily understood and can be compensated for, the knock-resistance is the parameter that can limit its usability [96]. Admixtures of higher hydrocarbons are especially challenging in this regard [130], while for hydrogen, pre-ignition and backfire seem to be more critical than classical knock caused by auto-ignition in the end gas [140]. Water vapour might increase the ignition energy demand [67] and also influences the thermodynamic properties of the mixture due to its high heat capacity. Trace gases such as ammonia and hydrogen sulphide should also not be neglected [67], but can be accounted for by gas conditioning and do not critically influence the combustion characteristics.

One of the most widely used measures for the knock resistance of gaseous fuels is the *methane number (MN)* in analogy to the octane number used for liquid fuels. The original methane number was developed by the company AVL in the 1960s based on experimental data from a test engine with variable compression ratio [27, 141]. For the determining the methane number the compression ratio of the engine is continually increased until knock is detected at the *critical compression ratio (CR_c)*. The test is then repeated with variable mixtures of methane and hydrogen keeping the identified critical compression ratio constant and increasing the hydrogen content until knock is detected again. The obtained mixture of methane and hydrogen defines the methane number, with hydrogen being equivalent to MN = 0 and methane to MN = 100. For gases with even higher knock resistance CO_2 is added on top resulting in methane numbers > 100 [27]. The AVL data was first summarised in ternary mixture diagrams, which allowed the graphical/numerical determination of the methane number without the need for engine experiments. Since then it has been transferred into

algorithms for computation, for example, by Andersen [142] and MWM [143]. The methane number calculation according to the MWM method is implemented in a free software tool available from the *European Association of Internal Combustion Engine Manufacturers EU-ROMOT* [144].

The AVL methane number has some shortcomings, especially for syngas with high shares of H_2 and at the same time CO [96] as well as for gases containing higher hydrocarbons with methane numbers less than approximately 50 [130]. Furthermore, it was developed from a specific test engine operating under stoichiometric conditions and it is therefore discussed if the method is suitable for the actual diversity of engine designs and modern machines, that tend to operate under fuel-lean conditions and at higher pressures [145]. Therefore, other proprietary knock indexes have been developed by different engine manufacturers, for example, Cummins Westport [146] and Waukesha, which are however not necessarily compatible with each other [27] and have their own shortcomings.

Van Essen et al. [145, 147] developed a new knock characterisation method for fuel gases based on the auto-ignition delay time in the compressed end gas during the engine cycle which is determined with the help of a two-zone thermodynamic model using detailed chemical kinetics. The model was derived from experimental tests on a 6-cylinder gas engine applying mixtures of CH_4 and Dutch natural gas with H_2, CO and higher hydrocarbons, such as ethane and propane, iso-butane and n-butane. A ranking tool was constructed, in which a mixture of methane and propane showing the same simulated auto-ignition behaviour as the test gas, serves as a benchmark, analogous to the methane/hydrogen mixture applied to the AVL methane number. The obtained result is referred to as *propane knock index (PKI)* and can be calculated using the online calculator available from DNV GL [148]. Compared with

experimental data the model shows excellent experimental power and according to the authors it is superior to the AVL methane number especially with regard to mixtures containing higher hydrocarbons.

A similar approach is followed by Virnich et al. [149] in their prediction model for knocking combustion in natural gas engines using detailed chemical kinetics, although the model is not focused on rating a specific fuel but on predicting safe operating conditions for a particular engine. The model is based on a two-zone approach with an unburned and a burned zone, where flame propagation is simulated with an entrainment model based on the laminar flame speed and on assumptions about the turbulent flow field in the cylinder. The two-zone model is coupled with a reaction kinetics calculation using the Cantera [150] solver with the AramcoMech 1.3 mechanism [59]. Knock is assumed to happen when the temperature in the unburned end-gas suddenly rises above a threshold of 1,300 K due to auto-ignition. The respective cycle is considered as knocking cycle and the crank angle at which auto-ignition is detected is defined as the onset of knock. Once calibrated, the model showed a very good correlation between measured and simulated knock and could be used to predict knock and other operating points. The authors state that in prior investigations the model also provided adequate estimations for a variation of the methane number in the range from 76 to 100.

Saikaly et al. [151, 152] present a preventive knock protection technique based on a two-zone thermodynamic engine model with detailed chemical kinetics (GRI-Mech 3.0 [54]), which is used to calculate a *knock risk estimator*. The knock risk estimator is applied to determine the methane number requirement (MNR) of a particular engine for different operating conditions. By generating an engine map with adequate settings for satisfying the condition MNR < MN, a preventive knock protection technique can be implemented, where the engine adapts itself to the current methane number of the gas supply.

Roy et al. [153] present a novel prediction model for determining the methane number of natural gas with varying composition in real-time. The model is based on multiple and support vector regression and takes easily measurable physical gas properties, such as the thermal conductivity, sound velocity, pressure and temperature as input. Using a support vector regression with a Gaussian kernel, a high accuracy in predicting the methane number was achieved. According to the authors, the model can be successfully implemented and used in a sensor to predict the methane number in a real-world environment, for example in a natural gas engine.

Beshouri et al. [92] present the concept of a virtual air/fuel ratio sensor based on the trapped equivalence ratio for the control of pipeline gas engines operating with varying gas qualities in the United States. In order to assess the effects of the fuel composition on combustion behaviour, the authors studied over 4 000 unique natural gas compositions of varying C1-C5 components, using the open-source chemistry solver Cantera [150] to compute ignition delay and laminar flame speed. Regression models were fitted to the results, showing good prediction accuracy. The laminar flame speed was found to have a rather insensitive response to varying fuel composition, while ignition delay revealed stronger influence by non-methane components. However, the investigation just covers natural gas compositions occurring in gas pipelines with comparatively little admixture of higher hydrocarbons. The authors propose developing a correlation between fuel-species-influenced ignition delay and the corresponding influence on kinetically-driven combustion behaviour to be implemented in the virtual air/fuel ratio sensor.

Schultze et al. [69] experimentally and numerically investigated the utilisation of hydrogen-rich fuel gases in large gas engines. In order to assess the usability of fuel gases in internal combustion engines, they developed a numerical model based on detailed chemical kinetics considering both the laminar flame and ignition delay. They applied the GRI-Mech

3.0 mechanism [54] and their own modification optimised for H_2 and CO-rich fuel gases, using Cantera [150] as solver. The laminar flame speed was calculated using the model of a premixed, one-dimensional, freely propagating flame. For modelling auto-ignition, a piston reactor model was set up, which is analogous to an ideal homogenous charge compression ignition engine. The reactor is referred to as *rapid compression machine (RCM)* model by the authors. From prior investigations they infer that the laminar flame speed is suitable for estimating the required equivalence ratio for engine operation: the equivalence ratio at which the same laminar flame speed as for the reference gas is obtained corresponds to the one required at full engine load. This correlation can be adequately reproduced in the model, but only for gases with a high content of H_2 and CO and only when the optimised reaction mechanism is used. The piston reactor model was found to be suitable for qualitative predictions of knock-resistance, although the trends of the experimental results could not be reproduced in all cases. Still, the authors consider the model to be a better approach than the methane number for gases with high contents of H_2 and at the same time CO.

Hiltner [91] proposes a methodology for combustion system development and simulation of engines operating on gasified biomass fuel based on the laminar flame speed of the fuel. He presents laminar flame speeds for typical gas compositions found in oxygen blown and wet air blown gasifiers obtained from chemical kinetics calculations using the DARS code by CD Adapco. The biomass fuels all showed laminar flame speeds greater than natural gas, which according to Hiltner leads to a higher combustion rate and higher peak cylinder temperatures. This is confirmed by experimental data showing a clear relationship between the laminar flame speed and the early burn duration, albeit with asymptotic limits for very large and very slow flame speeds. The latter is often the case for fuels with high water vapour

content [91]. Hiltner concludes that for a given set of engine hardware the early burn duration, main burn duration and combustion efficiency are all directly related to the laminar flame speed of the fuel as a function of relative air/fuel ratio.

Wise [96] studied the utilisation of producer gas from biomass gasification in high performance natural gas engines both experimentally and numerically, using a Cooperative Fuel Research (CFR) F-2 fuel research engine and applying chemical kinetics simulation with CHEMKIN. Prior experiments with the same engine covering digester gas, landfill gas, natural gas, coal gas and different syngases were carried out by Malenshek [154] and Arunachalam [155]. Wise investigated a total of 35 different blends based on real producer gas compositions encountered in practice, and experimentally determined both the critical compression ratio at the onset of knock and the corresponding methane number of a CH_4/H_2 blend. In some cases the experimental results differ considerably (up to 30 units, average 11.1 units) from the calculated methane numbers according to the AVL method, with the largest overprediction occurring for blends with large CO and H_2 content and very little methane content. With regard to diluents (CO_2 and N_2) no observable trend could be detected regarding the AVL method accuracy compared to the experimental results. According to Wise the methane number correlates with the ignition delay and – judging from the combustion evolution in the research engine – with the laminar flame speed of the fuel gas. The methane number, however, did not correspond with the lower heating value of the fuel, but was determined by the percentage of pro-knock species (CO and H_2) instead, which is more critical than the fuel energy content. In order to predict the methane number numerically, Wise implemented a homogenous charge compression (HCCI) reactor model using the CHEMKIN code with detailed chemical kinetics to model auto-ignition. However, the results were not consistent with the experimental measurements, since the HCCI model does not consider flame propa-

gation as it occurs in real engines. In addition, Wise presented a second approach for prediction of the methane number using an artificial neural network which showed better consistency than the AVL method, but needs improvement with more data sets for training. Nonetheless, Wise concludes that the methane number is a fuel property that could be ascertained solely through knowledge of the constituent make-up of the fuel.

Building upon the methodology developed by Wise, Montoya et al. [156] investigated the methane number and critical compression ratio of twelve blends of biogas with methane, propane and hydrogen. They used the same test engine and CHEMKIN model as Wise, but applied several different reaction mechanisms in order to identify the most suitable for the given fuel blend. The best overall mechanism for the prediction of the critical compression ratio was found to be the USC-II mechanism [55], while for the methane number it was the San Diego mechanism [66]. It was, however, not possible to find an optimal mechanism for all gaseous blends to reproduce both the critical compression ratio and the methane number.

A very different approach is followed by Bates et al., who applied the detonation theory to assess the knock propensity of fuels [71]. The authors determined the ignition delay and excitation times of stoichiometric mixtures of methane/air at different pressures using the Mech_56-54 comprehensive kinetic scheme from NUI Galway [72]. The results confirm the strong resistance to knock of CH_4/air with the mixture only entering the regime of developing detonation when being compressed up to 15 MPa. Additionally, Bates developed reduced kinetic schemes for the calculation of ignition delay and excitation times in order to reduce the computation time. While this proved to produce satisfactory results for the ignition delay time after suitable tuning of the reduced schemes, the excitation times were underpredicted by an order of magnitude.

2.4 Summary

Two major conversion routes, either bio-chemical or thermo-chemical conversion, lead to gaseous biofuels. Depending on which route is chosen, the product will either be a methane-rich gas diluted with carbon dioxide or a *syngas* rich in hydrogen and carbon monoxide, with comparatively less hydrocarbons.

While the combustion of anaerobic digester gas from bio-chemical conversion is similar to natural gas, albeit with lower reactivity due to the dilution and the absence of higher hydrocarbons, syngas features vastly diverging combustion characteristics. Comprehensive data with regard to the combustion characteristics of fuel gases from thermo-chemical conversion with compositions encountered in practice is still lacking. Many authors focus only on single aspects, such as ignition delay or laminar flame speed, often using synthetic laboratory gas mixtures. Combustible mixtures including residual gas and water vapour are also rarely considered. Fuel gases from intermediate pyrolysis have not been comprehensively investigated with regard to their combustion characteristics up to now.

The main parameters for assessing the combustion characteristics are the chemical ignition delay time and the laminar flame speed, both of which are intrinsic properties of a particular combustible mixture and independent of a specific combustion system layout. The experimental determination of these parameters is complex and often not possible for practical gas compositions at operating conditions encountered in modern internal combustion engines. Therefore, simulation techniques based on detailed chemical kinetics are commonly applied. The adiabatic, constant volume reactor and the freely propagating, adiabatic, laminar flame are the two main models used, the former for the calculation of ignition delay, the latter for the determination of laminar flame speed. A variety of detailed chemical reaction

mechanisms and software tools for chemically reacting systems has been developed throughout the years, allowing the implementation of such simulations into engine and fuel development processes.

Methods have been sought for translating the complex phenomena associated with ignition and combustion into a single measure indicating the usability of fuel gases for internal combustion engines. While the methane number is possibly the best known of these rating methods, it suffers from some serious drawbacks particularly with regard to syngas blends that feature high shares of H_2 and at the same time CO. The same applies to fuels which contain higher hydrocarbons. Thus, several more sophisticated methods have been developed to account for the variety of engine designs and fuel options encountered today. A promising alternative is the ξ-ε *diagram* for fuels which is based on the *detonation theory* by Bradley [99] and has recently been extended in its applicability by Bates [71]. The required values for construction of the diagram are the ignition delay time τ_i and the excitation time τ_e, which can both be obtained from chemical reaction kinetic simulations. Thus, the ξ-ε diagram has the potential to be used for a priori characterisation of the auto-ignition propensity of fuels without the need for experimentation.

Chapter 3 Experimental methodology

3.1 Intermediate pyrolysis plant

In order to supplement the data from literature (Table 2-6), pyrolysis gas measurements were performed at an industrial scale TCR® 300 intermediate pyrolysis plant built by Susteen Technologies and operated at the Fraunhofer UMSICHT premises in Sulzbach-Rosenberg, Germany. The pilot plant was designed to process up to 300 kg/h of sewage sludge from municipal waste-water treatment.

Thermo-Catalytic Reforming (TCR®) is an intermediate pyrolysis process developed by Fraunhofer UMSICHT capable of operating on a wide range of residue biomass feedstocks. The TCR reactor is basically a multi-zone auger reactor with different zones through which the feedstock is transported by the screw conveyor while being heated using a specific temperature profile [4]. In the auger reactor, pyrolysis and a first reforming step take place at temperatures of about 623 K to 723 K with residence times from 5 to 10 min [126]. The resulting intermediates are then conveyed into a post-reformer, where the organic fraction is catalytically reformed at a maximum temperature of 1 023 K [126] resulting in an essential upgrade of all phases [4]. The yield of gas increases as the post-reformer temperature rises [133]. Typical product yields of the TCR process when using sewage sludge and digestate as feedstocks are 30 to 50 wt% char, 5 to 10 wt% oil and 30 to 40 wt% gas [4, 132]. The remainder is an aqueous phase of low energetic value [132, 133]. On an energy basis, the oil accounts for 12 to 20 % of the total output, while gas and char both contribute in the range of 30 to 50 %, and about 5 to 10 % are conversion losses [4, 132]. A schematic of the process is presented in Figure 3-1.

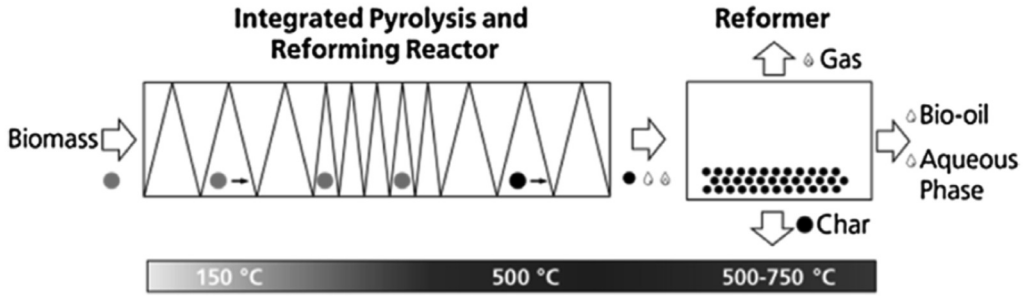

Figure 3-1: Schematic of the TCR process [4]

The TCR® 300 plant at Fraunhofer UMSICHT was equipped with a gas flare for experimental operation. However, in the final design the produced gas is to be used in a co-generation engine for on-site combined heat and power production. Both spark ignition and dual fuel engines are conceivable for this application. In the latter the bio-oil fraction from the TCR process could be used as pilot fuel.

3.2 Measurement of pyrolysis gas composition

The composition of permanent gases from the pyrolysis plant was measured with a mobile micro gas chromatograph (micro GC) of type Agilent 490. The micro GC is equipped with a thermal conductivity detector and four independent columns each designed to separate a different range of gaseous compounds (see Table 3-1). Helium is used as carrier gas except for the hydrogen measurement where argon is required since the thermal conductivities of helium and hydrogen are too similar and detection would not be possible otherwise. The micro GC is enclosed in a protective field case and equipped with an independent carrier gas supply and an electric supply by batteries for on-site measurements (see Figure 3-2).

The maximum sampling pressure is 0.1 MPa and the maximum possible sampling temperature is 383 K. In order to protect the gas chromatograph from particles and moisture a

sampling line with active cooling and washing flasks for retaining the condensable fraction was designed (see Figure 3-2). The samples were taken downstream of the TCR reactor and post reformer in the supply line to the gas flare. At this point the gas quality is expected to be equivalent to what it would be for engine use.

Table 3-1: Column specifications of the Agilent 490 micro GC

Column #	Column type	Carrier gas	Detectable components
1	Molesieve	Argon	Helium, Neon, H_2
2	Molesieve	Helium	O_2, N_2, CH_4, CO
3	PPQ	Helium	CO_2, C_2H_4, C_2H_6, C_3H_8, H_2O
4	Al_2O_3	Helium	iso-C_4H_{10}, n-C_4H_{10}, iso-C_5H_{12}, n-C_5H_{12}, C6+

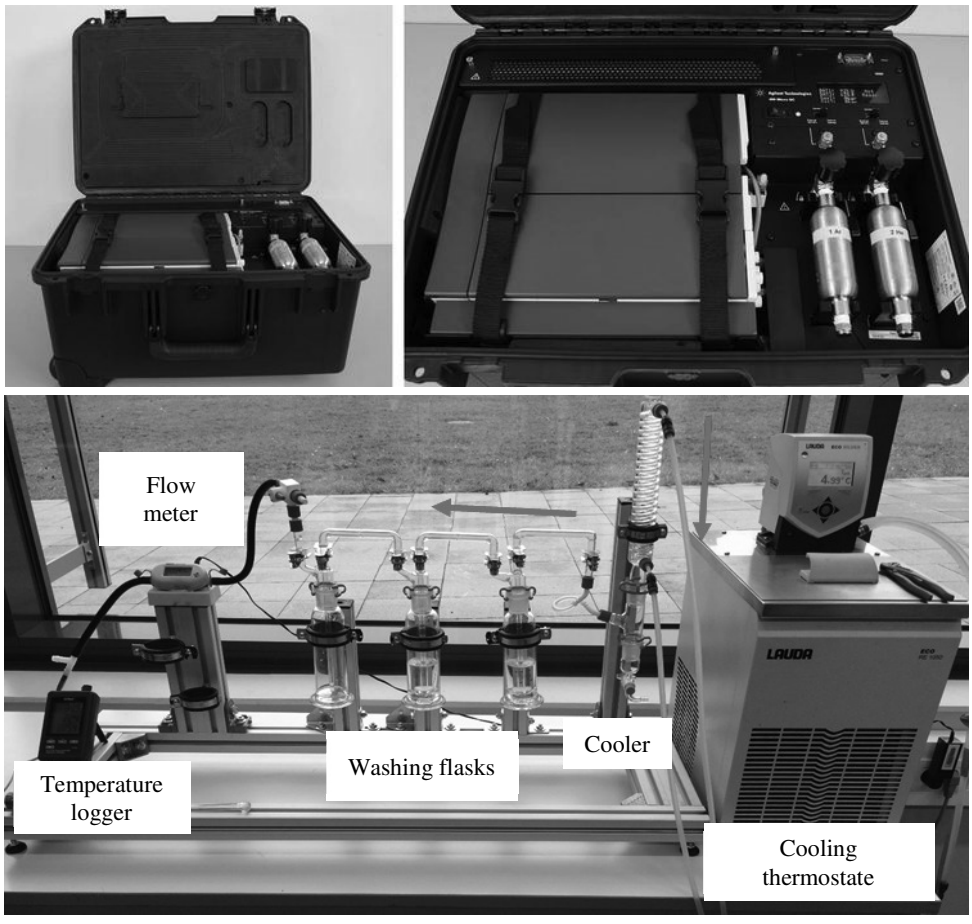

Figure 3-2: Micro GC setup in field case (upper figure) and sampling line with cooler and washing flasks (lower figure); arrows indicate the direction of flow

3.3 Summary

In order to supplement the data from the literature, gas measurements were performed at an industrial scale TCR® 300 intermediate pyrolysis plant built by Susteen Technologies GmbH and operated at the Fraunhofer UMSICHT premises in Sulzbach-Rosenberg, Germany. The plant was designed to process up to 300 kg/h of sewage sludge from municipal waste water treatment. The measurements were taken with a mobile micro gas chromatograph downstream of the pyrolysis reactor and the post reformer in the supply line to the gas flare. The gas quality at this point is expected to be approximately equivalent to what it would be for engine use.

Chapter 4 Modelling methodology

4.1 Overview

In order to assess the combustion characteristics of syngas blends, a modular modelling methodology is applied, consisting of several independent submodels, as displayed in Figure 4-1. The major parameters to be determined are the *laminar flame speed* and the auto-ignition characteristics, more precisely the *chemical ignition delay time* and the *excitation time*. Based on these values, the reactivity and auto-ignition propensity of the respective fuel blend can be assessed.

First, it is necessary to model the *combustion gas*, that is, the chemically reacting mixture of fuel, oxidiser and residual gas. The combustion gas is represented by a mixture of chemical species reacting with each other according to a defined set of one-step chemical reactions. The respective species, reactions and rate constants are provided through a chemical reaction mechanism. Additionally, the thermodynamic properties and the transport properties for the individual species are required.

In real combustion engines, the gas exchange will never be fully complete, and a small amount of burned residual gas from the previous cycle will always remain trapped in the cylinder and add to the total cylinder charge. In addition to this *residual gas fraction*, a certain amount of burned gas may deliberately be recirculated to the intake of the engine. This procedure is known as *exhaust gas recirculation (EGR)*. The composition of the residual gas is determined by a separate *residual gas model*.

Both the combustion gas and the residual gas model are complemented by a *water vapour model* which is used to control the humidity of the mixture.

The chemical ignition delay and the excitation time are determined by simulating the combustion of a homogenous mixture of fuel and oxidiser in a closed batch reactor with

constrained volume and adiabatic walls. This *homogenous constant volume reactor* is the model equivalent of an ideal *rapid compression machine (RCM)* where a homogenous combustible mixture is set to ignition conditions (high temperature and pressure) by a single, fast compression stroke. The ignition delay time and the excitation time can be obtained by evaluating the temporal evolution of the temperature, the pressure or the species concentrations in the reactor.

When it comes to real engine processes, the constant volume reactor model has its limitations since it does not consider the varying pressure and temperature conditions evoked by the constantly changing reactor volume due to the movement of the piston. This applies especially to simulation of knock in the compressed end gas, where auto-ignition depends critically on the temperature and pressure history of the unburned mixture during the combustion cycle [157]. Thus, to approximate the conditions in real engines, a homogenous piston reactor model was designed based on a model presented by Schultze et al. [69]. The reactor is the model equivalent of an ideal *homogenous charge compression ignition engine* (HCCI engine), where fuel and oxidiser are homogenously mixed. The mixture in the cylinder auto-ignites by compression through the piston. In *this study*, the HCCI reactor model is used to determine a *critical compression ratio* CR_c which is defined as the minimum compression ratio required for auto-ignition of the mixture with a given reactor geometry and a given set of initial conditions.

Both the constant volume and the HCCI reactor model are zero-dimensional models. These are sufficient when only the temporal profiles are to be evaluated. However, in case of the laminar flame speed, additional information about the spatial evolution of species and temperature is needed in order to determine the speed at which the reacting gases move through the flow domain (cf. definition of the laminar flame speed in section 2.2.2). For

laminar flames the problem can be reduced to one dimension. In *this study*, the model of a *freely-propagating, adiabatic, premixed flame* is applied to determine the flame speed.

The results of the constant volume reactor simulations – the ignition delay time τ_i and the excitation time τ_e – are used to determine the possible auto-ignition regimes for the respective fuel blend at the given initial conditions by applying the ξ-ε *diagram* for fuels according to the methodology by Bates [74] (cf. section 2.2.3). Additionally, the *Sankaran criterion* (cf. [102]) is applied to further define the auto-ignition regimes in the ξ-ε diagram by evaluating the laminar flame speed from the one-dimensional flame simulation and the chemical ignition delay time τ_i from the constant volume reactor simulation.

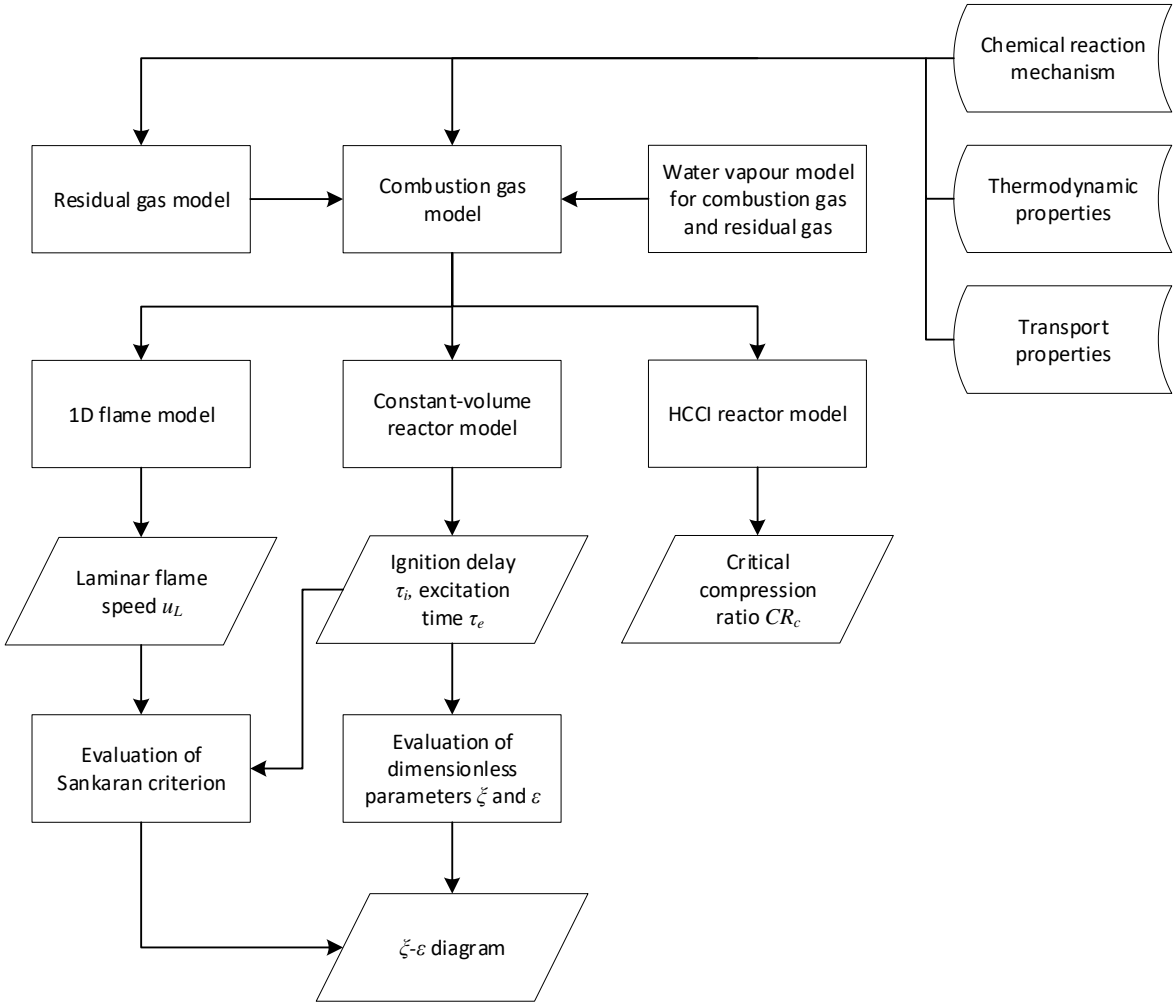

Figure 4-1: Overview of modelling methodology

4.2 Combustion gas

4.2.1 Fluid properties

The principal thermodynamic properties required in the combustion gas model are [150]:

a) The molar heat capacity $C_p^o\ (T)$ at constant pressure for a range of temperatures at the reference pressure P_0.

b) The molar enthalpy $H(T_0, P_0)$ at the reference pressure and temperature P_0, T_0.

c) The absolute molar entropy $S(T_0, P_0)$ at (T_0, P_0).

These properties can be computed for each of the species in the combustion gas by using the *NASA polynomial parameterization*, which is available as an older 7-coefficient polynomial [158] and a newer 9-coefficient polynomial [43]. It should be noted, however, that the two versions are not compatible [150].

With the 7-coefficient polynomial the thermodynamic properties in standard state for each species j can be computed as:

$$\frac{C_{pj}^o(T)}{R} = a_0 + a_1T + a_2T^2 + a_3T^3 + a_4T^4 \tag{4-1}$$

$$\frac{H_j^o(T)}{RT} = a_0 + \frac{a_1}{2}T + \frac{a_2}{3}T^2 + \frac{a_3}{4}T^3 + \frac{a_4}{5}T^4 + \frac{a_5}{T} \tag{4-2}$$

$$\frac{S_j^o(T)}{R} = a_0 lnT + a_1T + \frac{a_2}{2}T^2 + \frac{a_3}{3}T^3 + \frac{a_4}{4}T^4 + a_6 \tag{4-3}$$

where T is the temperature, R is the universal gas constant and a_0 to a_6 are the tabulated coefficients of the polynomial [150]. From the values obtained by Equation (4-1) to (4-3) other thermodynamic properties such as the heat capacity at constant volume C_{vj}^o, the internal energy U_j^o and the standard state Gibbs free energy G_j^o can be easily computed [159]:

$$C_{vj}^o = C_{pj}^o - R \tag{4-4}$$

$$U_j^o = H_j^o - RT \tag{4-5}$$

$$G_j^o = H_j^o - TS_j^o \tag{4-6}$$

The 7-coefficient polynomials are valid for a temperature range from 200 to 6 000 K with two different parameter sets for the intervals from 200 to 1 000 K and 1 000 to 6 000 K. The standard state for gases is ideal gas at a pressure of 10^5 Pa and the standard state for condensed species is the crystalline or liquid substance at the same pressure [158]. The reference state is the thermodynamically stable state at 298.15 K [158].

In case of an ideal gas, the standard state specific heats, enthalpies, and internal energies are also the actual values and the superscript o on those quantities can be dropped [159]. If the properties are needed in mass units rather than in molar units, they can be converted by introducing the molecular weight W_j of the species [159], for example:

$$c_{pj} = \frac{C_{pj}}{W_j} \tag{4-7}$$

where c_{vj} and C_{vj} are the mass-based and molar heat capacities at constant volume respectively. Likewise the other properties can be obtained in mass units.

In combustion systems usually mixtures of gases are dealt with, and it is often convenient to use mole fractions X_j to specify the composition of the mixture. Mole fractions are obtained by dividing the number of moles of the single species n_j by the total number of moles n of all constituents in the mixture:

$$X_j = n_j / \sum_j n_j = \frac{n_j}{n} \tag{4-8}$$

In the case of an ideal gas, the mole fraction is related to the partial pressure p_j of species j in the mixture and the individual partial pressures sum up to the total pressure P according to Dalton's law:

$$\frac{p_j}{P} = \frac{n_j}{n} = X_j \tag{4-9}$$

$$P = \sum_{j=1}^{n} p_j \tag{4-10}$$

The same applies to the volumetric fraction, so that for ideal gases the volumetric fraction, mole fraction or partial pressure can be used in an equivalent way to specify the composition of a mixture:

$$\frac{V_j}{V} = \frac{n_j}{n} = \frac{p_j}{P} = X_j \tag{4-11}$$

The mole fraction can also be easily related to the mass fraction Y_j by considering the molecular weight W_j of the individual species and the total molecular weight W of the mixture:

$$Y_j = \frac{m_j}{m} \tag{4-12}$$

$$Y_j = \frac{X_j W_j}{W} \tag{4-13}$$

$$W = \sum_{j=1}^{n} X_j W_j = \frac{1}{\sum_{j=1}^{n} (Y_j / W_j)} \tag{4-14}$$

The mixture-averaged properties in molar and mass units can be obtained considering the mole fraction X_j respectively the mass fraction Y_j of the individual species [159], as shown for the heat capacity at constant pressure and applicable likewise to the heat capacity at constant volume, the enthalpy and the internal energy:

$$C_p = \sum_{j=1}^{n} C_{pj} X_j \tag{4-15}$$

$$c_p = \sum_{j=1}^{n} c_{pj} Y_j = C_p / W \tag{4-16}$$

In the case of the entropy, the Gibbs free energy and the Helmholtz free energy the actual values of the mixture are different from the standard state values and pressure and entropy-of-mixing terms must be considered for computing the mixture-averaged values [159]:

$$S = \sum_{j=1}^{n} \left(S_j^0 - R\ln X_j - R\ln(P/P_0) \right) X_j \tag{4-17}$$

$$s = S/W \tag{4-18}$$

$$G = \sum_{j=1}^{n} \left[H_j - T_j \left(S_j^0 - R\ln X_j - R\ln(P/P_0) \right) \right] X_j \tag{4-19}$$

$$g = G/W \tag{4-20}$$

The pressure P_0 is the standard state pressure of 10^5 Pa.

Another important property of the combustion gas is the acoustic velocity a which will determine the speed at which a pressure wave travels through the mixture. For an ideal gas the acoustic velocity depends only on the temperature and can be calculated as follows:

$$a = \sqrt{\frac{c_p}{c_v}\frac{P}{\rho}} = \sqrt{\frac{c_p}{c_v}\frac{RT}{W}} \tag{4-21}$$

In addition to the thermodynamic properties, the transport properties, namely the dynamic viscosity μ, the thermal conductivity λ, the thermal diffusivity α and the mass diffusivity D are required for solving problems involving chemically reacting flow, such as modelling of laminar flames. Multicomponent transport phenomena in fluids are highly complex and require to consider the interactions between the molecules in the mixture. Different mixture-averaged and multicomponent transport models have been developed for this purpose. For a comprehensive introduction to molecular transport one can refer to Kee et al. [160].

In this work the Cantera software package [150] was used for evaluating the thermodynamic and the transport properties, applying the methodology originally developed by Kee et al. for the CHEMKIN computer code [159, 161, 162]. The required species-specific gas-phase transport parameters are the geometry of the molecule (monatomic, linear or non-linear), the Lennard-Jones collision diameter and potential well-depth, the dipole moment, the polarizability and the rotational relaxation collision number [162].

4.2.2 Modelling of chemical reacting systems

According to Glassmann et al. [68] the stoichiometric relation describing a one-step chemical reaction for a system of *m* reactions can be represented by Equation (4-22), where ν'_{ji} are the stoichiometric coefficients of the reactants and ν''_{ji} the stoichiometric coefficients of the products, M_j is an arbitrary chemical species and *n* the total number of species involved. The index *j* represents the species, the index *i* refers to the reactions 1 through m of the mechanism.

$$\sum_{j=1}^{n} \nu'_{ji} M_j \rightleftarrows \sum_{j=1}^{n} \nu''_{ji} M_j \quad i = 1, \dots, m \tag{4-22}$$

The reaction rate for the *i*th reaction is given by Equation (4-23), with $k_{f,i}$ and $k_{b,i}$ being the reaction rate constants for the forward and backward reaction respectively and the square brackets around the species symbol $[M_j]$ signifying the molar or mass concentration of this species [68].

$$q_i = k_{f,i} \prod_{j=1}^{n} [M_j]^{\nu'_{ji}} - k_{b,i} \prod_{j=1}^{n} [M_j]^{\nu''_{ji}} \tag{4-23}$$

The change of concentration of a species *j* from the forward and backward reactions of the *i*th reaction is expressed by [68]:

$$\dot{\omega}_j = [\nu''_{ji} - \nu'_{ji}] q_i = \nu_{ji} q_i \tag{4-24}$$

The overall rate of change of concentration of species *j* resulting from all *m* reactions is [68]:

$$\dot{\omega}_j = \sum_{i=1}^{m} \nu_{ji} q_i \tag{4-25}$$

For a temporally reacting system at constant temperature the evolution of the *n* species can be described by [68]:

$$\frac{d[M_j]}{dt} = \dot{\omega}_j \quad j = 1, \dots, n \tag{4-26}$$

The molar concentration $[M_j]$ of species is related to the mole fraction X_j by the ideal gas equation, where R is the universal gas constant, P is the pressure and T is the temperature [68]:

$$X_j P = [M_j] RT \tag{4-27}$$

The reaction rate constant k is usually expressed in the *modified Arrhenius* form, Equation (4-28), where A is the kinetic pre-exponential factor taking into account collision rates and steric probabilities for the collision of molecules leading to a reaction. The exponential term exp*(-E/RT)* is the *Boltzmann factor,* which refers to the required activation energy *E,* the universal gas constant R and the temperature T. The term T^n is introduced in the modified form of the Arrhenius equation to account for the temperature dependency of the pre-exponential term [68]:

$$k = AT^n \exp\left(-\frac{E}{RT}\right) \tag{4-28}$$

The reaction rate constant k in the Arrhenius expression is pressure-independent [68], which implies that the reaction rate depends only on temperature. However there are certain classes of reactions that are also pressure-sensitive, essentially *three-body reactions* (e.g., radical recombination) which involve a third body that absorbs excess energy and stabilises the recombined molecule that otherwise would decompose into the original radicals again [68]. Another important exception are *pseudo-first-order reactions* that can change their order as the pressure changes, as was first addressed by Lindemann [68]. These reactions feature an upper limit rate constant and first order kinetics at high pressures and second order kinetics and a low limit rate constant at lower pressures. The region between the high and low pressure limits is called the *fall-off range* and is important for many combustion systems [68]. Different *fall-off functions* have been developed to account for this behaviour, for example, by Gilbert ([163] in [150]) and Kee [159].

The equations describing the chemical reaction system are a set of nonlinear first-order ordinary differential equations. Since the rate of reactions can be vastly different, the time-scales at which the species concentrations change can vary significantly resulting in stiff ordinary differential equations that require specialised numerical integration routines [68].

4.2.3 Combustion products and chemical equilibrium

The global combustion chemical reaction of a generic fuel containing carbon, hydrogen, nitrogen and oxygen reacting with air consisting of 21 vol-% oxygen and 79 vol-% nitrogen can be written as

$$C_aH_bO_cN_d + \frac{n_{O_2}}{\phi}(O_2 + 3.762N_2) \rightarrow aCO_2 + \frac{b}{2}H_2O + \left(\frac{1}{\phi} - 1\right)O_2 + \left(\frac{n_{O_2}}{\phi}3.762 + \frac{d}{2}\right)N_2 \quad (4\text{-}29)$$

with n_{O_2} being the number of O_2 molecules required for complete combustion [17]

$$n_{O_2} = a + \frac{b}{4} - \frac{c}{2} \quad (4\text{-}30)$$

and ϕ defined as the *fuel/air equivalence ratio* with m_{fuel} being the mass of fuel and m_{air} the mass of air and the subscripts *act* and *stoic* representing the actual and stoichiometric mixtures [26]:

$$\phi = \frac{\left(m_{fuel}/m_{air}\right)_{act}}{\left(m_{fuel}/m_{air}\right)_{stoic}} \quad (4\text{-}31)$$

The composition of the products given by Equation (4-29) may not occur in practice, since at normal combustion temperatures a significant dissociation of CO_2 and H_2O will happen [17] and even at moderate temperatures at least 1 % dissociation takes place [68]. In the case of fuel-rich combustion, that is, with less than the stoichiometric air requirement there is insufficient oxygen to fully oxidise the fuel, and the product composition cannot be determined from an element balance alone so that additional assumptions about the chemical

composition of the product species are required [17]. It has to be noted that in chemical equilibrium, the products formed in combustion are determined by the atomic ratios and the specific atoms that are introduced rather than by the specific reactants [68]. Thus, the equilibrium composition will be the same for any C-H-O-N system and will only be determined by temperature, pressure and the C/H/O/N ratio of the mixture [68].

The equilibrium reaction among arbitrary products can be written as (cf. [17]):

$$\nu_a M_a + \nu_b M_b \ + \cdots \rightleftarrows \ \nu_r M_r + \nu_s M_s + \cdots \tag{4-32}$$

where

$$\sum \nu_j M_j = 0 \tag{4-33}$$

The change in number of moles dn_j of species j is proportional to the total change in moles dn [17]:

$$dn_j = \nu_j dn \tag{4-34}$$

From the first and second law of thermodynamics it follows that in chemical equilibrium at constant temperature and pressure the change of the Gibbs free energy of reaction (4-32) must be zero [17, 68]:

$$(\Delta G)_{T,P} = 0 \tag{4-35}$$

By introducing the *chemical potential* or *partial molar free energy* μ_j

$$\mu_j = \left(\frac{\partial G}{\partial n_j}\right)_{T,P,n_{i(i\neq j)}} \tag{4-36}$$

this condition can be expressed as follows, where dn_j is the change in moles of species j [17]:

$$(\Delta G)_{T,P} = \sum_j \mu_j \, dn_j \tag{4-37}$$

Assuming an ideal gas, which is a valid approximation at the high temperatures occurring in combustion [68], it follows that:

$$\mu_j = \mu_j^o(T) + RT \ln\left(\frac{p_j}{p_0}\right) \tag{4-38}$$

Where μ_j^o is the *standard chemical potential* of species j [17]. Substitution in Equation (4-37) gives, at chemical equilibrium [17]:

$$\sum_j \left(\mu_j^o + RT \ln\left(\frac{p_j}{p_0}\right)\right) dn_j = 0 \tag{4-39}$$

and:

$$\sum_j \left(\mu_j^o + RT \ln\left(\frac{p_j}{p_0}\right)\right) \nu_j dn = 0 \tag{4-40}$$

where p_0 is the standard state pressure. This can be rearranged to:

$$\sum \ln\left(\frac{p_j}{p_0}\right)^{\nu_j} = -\frac{\sum \mu_j^o \nu_j}{RT} = -\frac{\Delta G^o}{RT} = \ln K_p \tag{4-41}$$

$$K_p \equiv \prod_j \left(\frac{p_j}{p_0}\right)^{\nu_j} \tag{4-42}$$

where K_p is the equilibrium constant at constant pressure [17].

Different methods have been developed for computing chemical equilibrium. One approach is to use the equilibrium constants K_p, which are tabulated in thermochemical databases like the NIST-JANAF tables [164] or in the database developed by Burcat et al. [165]. Due to computational considerations, this approach is mainly applied for reduced sets of chemical reactions (cf. [68, 166]). The second approach is based on the minimisation of free energy, that is, either the Gibbs or the Helmholtz free energy, or the maximisation of entropy [68]. These methods can be stoichiometric or non-stoichiometric. While the former method is based on the Gibbs free energy the latter corresponds to the chemical potentials of each species [167].

In Figure 4-2 the chemical equilibrium composition for the stoichiometric combustion of methane at a pressure of 0.1 MPa and temperatures between 300 K and 2 500 K is displayed. Dissociation and radical formation can be observed to start at about 1 600 K leading

to the appearance of radicals as dissociated species, such as H, N, O and OH. Since the processes in combustion engines are fast, chemical equilibrium will usually only be reached during short periods of the working cycle when the temperatures are high. Thus, a common approach for modelling the burned gas in combustion engines is to assume chemical equilibrium above 1 600 … 1 700 K and a *frozen* composition below 1 600 … 1 700 K [17] [166].

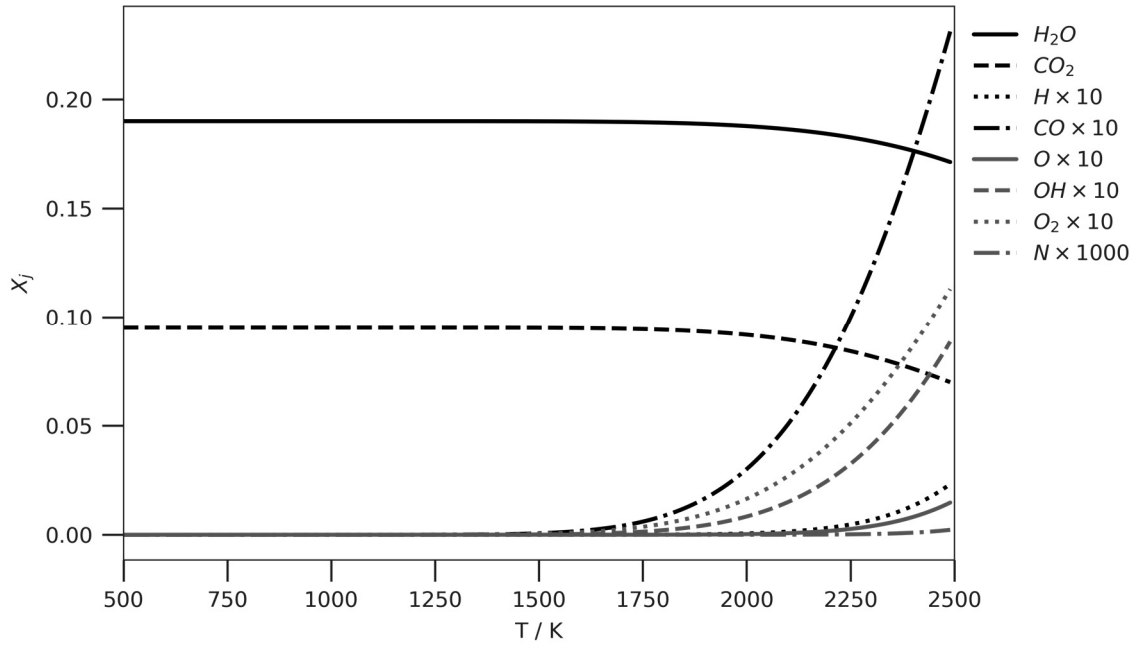

Figure 4-2: Equilibrium composition for combustion of methane at ϕ = 1 and P = 0.1 MPa

4.2.4 Residual gas fraction and exhaust gas recirculation

The *residual gas mass fraction* Y_r which remains trapped in the cylinder from the previous cycle is defined as [17]:

$$Y_r = \frac{m_{residual}}{m_{charge}} \tag{4-43}$$

Additionally, in modern spark ignition and diesel engines a fraction of the engine exhaust gases is deliberately recirculated to the intake of the engine to dilute the fresh mixture, primarily for the control of NO_x emissions. According to [17] the *exhaust gas recirculation*

(EGR) ratio can be defined as the percentage of the total intake mixture m_{intake} which is recirculated exhaust m_{EGR}:

$$EGR(\%) = \frac{m_{EGR}}{m_{intake}} \cdot 100 \tag{4-44}$$

In an alternative definition, EGR is related to the fresh mixture of fuel m_{fuel} and air m_{air}:

$$EGR(\%) = \frac{m_{EGR}}{m_{air} + m_{fuel}} \cdot 100 \tag{4-45}$$

The total *burned gas fraction* in the cylinder charge is the sum of the recirculated exhaust gas and the residual gas masses divided by the cylinder charge [17]:

$$Y_B = \frac{m_{EGR} + m_{residual}}{m_{charge}} \tag{4-46}$$

The burned gas will consist mainly of CO_2, H_2O and N_2. These species dilute the cylinder charge and thus reduce the combustion temperatures. Moreover, they change the thermodynamic properties of the cylinder charge thus affecting the temperature and pressure during compression. They also participate in the chemical reactions to some extent. Additionally, products from incomplete combustion may be present in the burned gas together with dissociated molecules and radicals, forming a pool of reactive species participating in the autoignition and combustion reactions. For chemical kinetics calculations it is thus necessary to model the composition of the burned gas fraction in detail considering also the dissociated species and radicals. The following assumptions are made:

a) No distinction is made between the residual gas fraction and the exhaust gas recirculation; instead, a burned gas fraction is defined, which is the sum of the residual gas fraction and the EGR fraction (cf. Equation (4-46)).

b) The fresh mixture of fuel and oxidiser and the burned gas are treated as two independent fractions with different compositions which do not interact prior to the start of the simulation; once the simulation starts they are instantly and perfectly mixed to form a homogenous chemically reacting gas (zero-dimensional model).

c) The burned gas composition is the result of the combustion of the specified fuel and oxidiser mixture at the given fuel/air equivalence ratio; it can be specified to be either in chemical equilibrium at the ambient conditions of the cylinder charge or to be frozen at an arbitrary temperature.

d) The burned gas composition can be specified as either "wet" or "dry"; if dry conditions are assumed, the species H_2O is eliminated from the burned gas (see also next section).

4.2.5 Water vapour fraction

The fact that the oxidiser, the fuel and the residual gas fraction may contain a certain amount of water vapour has to be taken into account when dealing with real combustion systems. In the case of the oxidiser, this amount of vapour is usually be determined by the humidity of the air at the respective intake ambient conditions, unless water is deliberately added. In fuels water is not a desirable constituent due to the corrosion of materials and possible deterioration of the fuel, so that both fuel gases and liquid fuels are usually kept technically dry. However, when dealing with anaerobic fermentation or thermo-chemical conversion, the fuel gas might contain water vapour up to a relative humidity of 100 %, if not specially dried. Additionally, the residual gas trapped in the cylinder and the recirculated exhaust gas also contains water vapour which in this case is a product of the combustion; see also Equation (4-29). Water may influence the combustion process in two ways: due to its high heat capacity it cools the combustion system; in addition it participates as species in the chemical reacting system. Thus, the amount of water vapour in the mixture has to be considered in the combustion gas model.

Since fuel, oxidiser and residual gases are treated as homogenous mixtures of ideal gases and phase changes are not considered, the mole fraction of water vapour can be determined from its partial pressure p_{H_2O} and the total pressure P:

$$X_{H_2O} = \frac{n_{H_2O}}{n} = \frac{p_{H_2O}}{P} \tag{4-47}$$

The maximum possible content of water is determined by its pure phase saturation vapour pressure $p_{H_2O,sat}$ at the given temperature:

$$X_{H_2O,max} = \frac{p_{H_2O,sat}}{P} \tag{4-48}$$

The saturation vapour pressure is determined according to the IAPWS industrial formulation for the thermodynamic properties of water and steam, which is valid along the entire vapour-liquid saturation line from the triple point temperature to the critical temperature (273.15 K to 647.096 K and 611.213 Pa to 22.064 MPa) [168].

The relative humidity is obtained by dividing the partial pressure by the saturation vapour pressure:

$$\varphi = \frac{p_{H_2O}}{p_{H_2O,sat}} \tag{4-49}$$

In the combustion gas model water will be automatically removed from the mixture if the partial pressure of the water vapour fraction exceeds the saturation pressure at the given conditions. The water vapour content will then be set to the maximum possible amount (100 % relative humidity) and the mixture composition will be corrected to equal one again. This ensures that no unrealistically high concentrations of gaseous water occur in the mixture. This is mostly relevant for the initial mixture before combustion and for exhaust gas recirculation, since during combustion the temperature will be high enough to allow for arbitrary contents of water vapour.

In practice humid gases will not behave exactly as an ideal gases and the actual quantity of saturated water vapour in the mixture may differ from that obtained by using the pure phase approximation. Enhancement factors have been developed to account for this effect, such as those by Greenspan [169] for moist air and recently by Sairanen and Heinonen [170]

for humid methane gas. However, since no consistent methodology exists so far for calculating these enhancement factors for arbitrary gases and because the real gas effects are not very large at normal engine intake conditions, they are not considered in the combustion gas model.

4.3 Reactor models

4.3.1 Constant volume and constant pressure reactor model

The constant volume reactor is assumed to be filled with an initial homogenous mixture of fuel species and oxidiser at a given equivalence ratio, temperature and pressure (cf. Figure 4-3). Additionally, a fraction of already burned gas consisting of residual gas trapped in the cylinder and recirculated exhaust gas may be considered. The mixture is assumed to be compressed instantaneously to the initial pressure and temperature at time zero (cf. [71]) so that the initial temperature and pressure of the constant volume reactor correspond to the conditions in the RCM at the end of the compression stroke. Whether auto-ignition happens within the simulation time period depends on the reactivity of the mixture and the initial conditions.

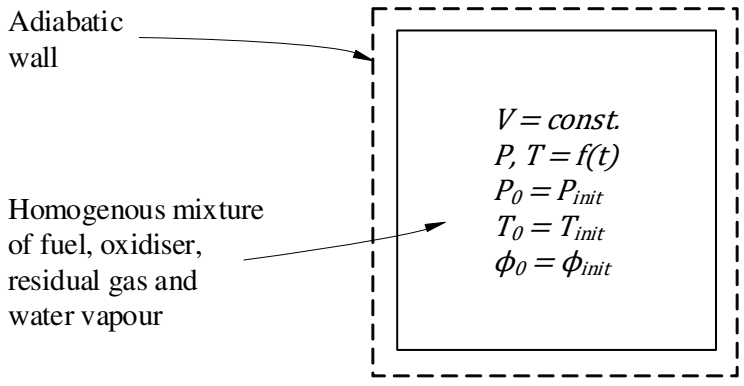

Figure 4-3: Adiabatic constant-volume reactor

The chemical reacting system in the constant-volume reactor is modelled according to section 4.2.2; additionally, the governing equations for a closed reactor with fixed mass have to be considered. As presented by Glassmann [68] these are species conservation and energy conservation. Since the overall mass conservation for a closed reactor with fixed mass yields $dm/dt = 0$, the mass change of the individual species can be described as

$$\frac{dm_j}{dt} = V\dot{\omega}_j W_j \tag{4-50}$$

with $\dot{\omega}_j$ being the rate of change of concentration of species V the volume of the system and W_j the molecular weight of species j [68]. Wall effects are not considered.

By introducing the mass fraction Y_j and the density $\rho = m/V$, Equation (4-50) can be rewritten as [68]:

$$\frac{dY_j}{dt} = \frac{\dot{\omega}_j W_j}{\rho} \quad j = 1, \dots, n \tag{4-51}$$

When working with gaseous fuels it can be more convenient to use mole fractions rather than mass fractions. The conversion between the two units is performed with Equation (4-13).

In the case of an adiabatic *constant-pressure reactor* the first law of thermodynamics reduces to [68]:

$$dh = 0 \tag{4-52}$$

The total enthalpy for a mixture is given by

$$h = \sum_{j=1}^{n} Y_j h_j \tag{4-53}$$

and the derivative is

$$\frac{dh}{dt} = \sum_{j=1}^{n} Y_j \frac{dh_j}{dt} + \sum_{j=1}^{n} h_j \frac{dY_j}{dt} \tag{4-54}$$

For an ideal gas mixture, the enthalpy can be related to the temperature by the specific heat capacity at constant pressure [68]:

$$dh_j = c_{p,j} dT \tag{4-55}$$

Substituting this term into Equation (4-54) yields [68]:

$$\frac{dh}{dt} = \sum_{j=1}^{n} Y_j c_{p,j} \frac{dT}{dt} + \sum_{j=1}^{n} h_j \frac{dY_j}{dt} = 0 \tag{4-56}$$

By introducing the mass-weighted specific heat

$$\sum_{j=1}^{n} Y_j c_{p,j} = c_p \tag{4-57}$$

and substituting Equation (4-51) into Equation (4-56) the system energy equation can be written in terms of temperature [68]:

$$\frac{dT}{dt} = \frac{-\sum_{j=1}^{n} h_j \dot{\omega}_j W_j}{\rho c_p} \tag{4-58}$$

For the closed *constant-volume reactor* the internal energy *u* becomes zero

$$du = 0 \tag{4-59}$$

and Equation (4-58) can be rewritten accordingly by replacing the enthalpy by the internal energy *u* and the specific heat at constant pressure by its equivalent c_v at constant volume [68]:

$$\frac{dT}{dt} = \frac{-\sum_{j=1}^{n} u_j \dot{\omega}_j W_j}{\rho c_v} \tag{4-60}$$

4.3.2 HCCI reactor model

The constant volume reactor and its experimental equivalent, the rapid compression machine, are appropriate tools for general studies of auto-ignition and chemical ignition delay. However, when it comes to real engine processes, the model has its limitations since it does not consider the varying pressure and temperature conditions evoked by the constantly

changing reactor volume due to the movement of the piston. This applies especially to simulation of knock in the compressed end gas, where auto-ignition depends critically on the temperature and pressure history of the unburned mixture during the combustion cycle [157]. Thus, to approximate the conditions in real engines, a homogenous piston reactor model was designed based on a model presented by Schultze et al. [69]. The reactor is the model equivalent of an ideal *homogenous charge compression ignition engine* (HCCI engine), where fuel and oxidiser are homogenously premixed outside the cylinder and auto-ignite by compression through the piston. In *this study* the HCCI reactor model is used to determine a *critical compression ratio* CR_c which is defined as the minimum compression ratio required for auto-ignition of the mixture with a given reactor geometry and a given set of initial conditions.

The HCCI reactor is modelled as a closed cylinder with fixed walls representing the cylinder head and cylinder liner and one moving wall representing the piston. There is no gas exchange neither through valves nor due to leakages. Again, wall surface effects are neglected, but as opposed to the batch reactor, which is always assumed to be adiabatic within the scope of this thesis, the HCCI reactor model allows for heat transfer through the walls. For this, a heat transfer model according to Woschni was implemented, as documented, for example, in [17, 34]. Simulations are possible both in adiabatic mode or with heat transfer enabled.

As in the case of the constant-volume reactor, the governing equations for the HCCI reactor are mass, species and energy conservation, and Equations (4-50) and (4-51) apply likewise. Since neither pressure nor volume are constant in the piston reactor, energy conservation has to be considered in a more general form, but still without inbound and outbound fluxes, since the reactor is closed:

$$\frac{du}{dt} = -p\frac{dV}{dt} - \frac{dQ}{dt} \tag{4-61}$$

The moving wall of the HCCI reactor follows the kinematics of a piston in a reciprocating engine (see Figure 4-4). The volume V of the reactor can thus be described as a function of the *crank angle* θ

$$V(\theta) = V_c + \frac{\pi B^2}{4}\, s(\theta) \tag{4-62}$$

where V_c is the *clearance volume* (minimum reactor volume), B is the *bore* and s is the piston displacement as a function of the crank angle θ.

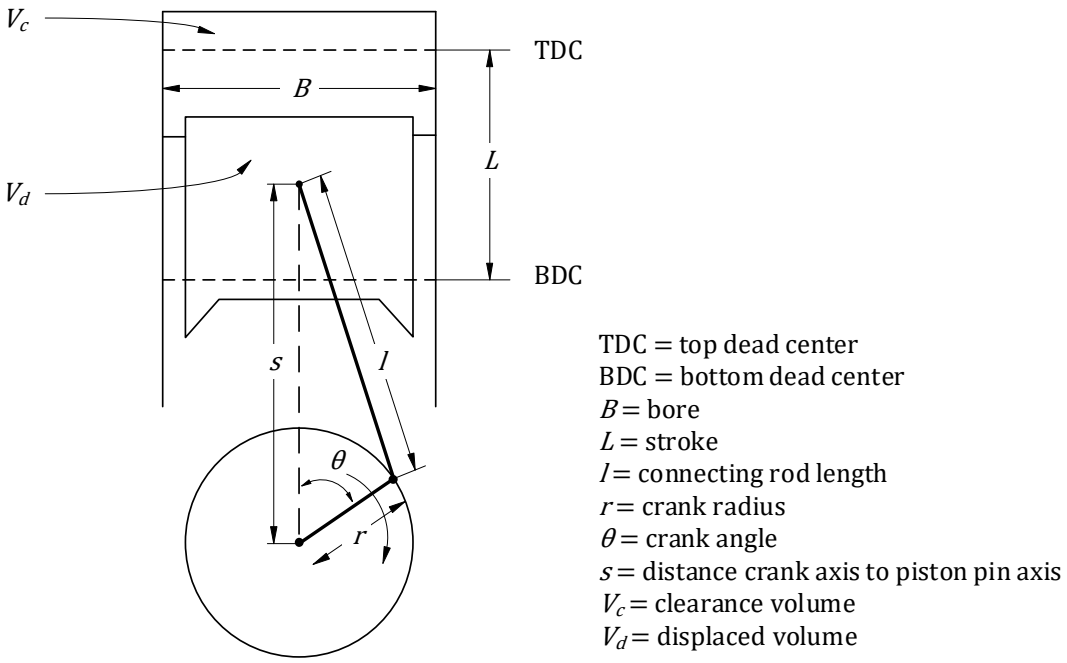

Figure 4-4: Geometry of the HCCI reactor (adapted from [17])

The maximum reactor volume is related to the clearance volume through the *compression ratio* CR, where V_d is the *displaced volume*:

$$CR = \frac{V_d + V_c}{V_c} \tag{4-63}$$

By inserting the compression ratio in Equation (4-62) one obtains:

$$V(\theta) = \frac{V_d}{CR - 1} + \frac{\pi B^2}{4}\, s(\theta) \tag{4-64}$$

The reactor volume changes as a function of crank angle according to:

$$\frac{dV}{d\theta} = \frac{\pi B^2}{4}\frac{ds}{d\theta} \tag{4-65}$$

By introducing the *angular velocity* ω

$$\frac{d\theta}{dt} = \omega \tag{4-66}$$

the piston velocity can be written as

$$\frac{ds}{dt} = \frac{ds}{d\theta}\frac{d\theta}{dt} = \omega\frac{ds}{d\theta} \tag{4-67}$$

and the change of reactor volume can be related to time:

$$\frac{dV}{dt} = \frac{\pi B^2}{4}\frac{ds}{dt} \tag{4-68}$$

For the HCCI reactor model the following approximation of the piston velocity is used. More details on crank drive kinematics can be found in [34] and [17]:

$$\frac{ds}{dt} = r\omega\left(\sin(\omega t) + \frac{1}{2R}\sin(2\omega t)\right) \tag{4-69}$$

Where a is the crank radius and R the ratio of the connecting rod length l to the crank radius r and accordingly to the *stroke L*:

$$L = 2r \tag{4-70}$$

$$R = \frac{l}{r} = \frac{2l}{L} \tag{4-71}$$

The angular velocity ω can be calculated from the *rotational frequency* f in 1/s, and hence from the *rotational speed* n in 1/min:

$$\omega = 2\pi f = 2\pi\frac{n}{60} \tag{4-72}$$

The influencing factors on the auto-ignition in the HCCI reactor are the available time and the temperature/pressure profile. The former is determined by the piston speed and hence

the rotational speed, and the latter is determined by the initial conditions and the geometry of the reactor. The HCCI model reactor thus allows the numerical study of auto-ignition in fuel/oxidiser mixtures based purely on the time, pressure and temperature available for the chemical reactions, while using a setting close to a real combustion engine.

An example for the results of a HCCI simulation is presented in Figure 4-5. The geometry of a CFR F-2 engine according to Wise [96] was used for the calculation with a compression ratio of CR = 21 and Woschni heat transfer enabled. On the left the pressure profile in the reactor is displayed showing a sharp peak slightly after top dead centre caused by auto-ignition of the mixture. Additionally, the pressure profile which would result from the compression and expansion of a chemically inert mixture with the same thermodynamic properties is shown as baseline (see also concept of baseline reactors in the next section). On the right the heat release rate and the molar concentration profiles of formaldehyde C_2HO and hydroxyl radicals (OH) are displayed, showing the formation of CH_2O prior to ignition and its fast consumption during combustion accompanied by the formation of OH radicals.

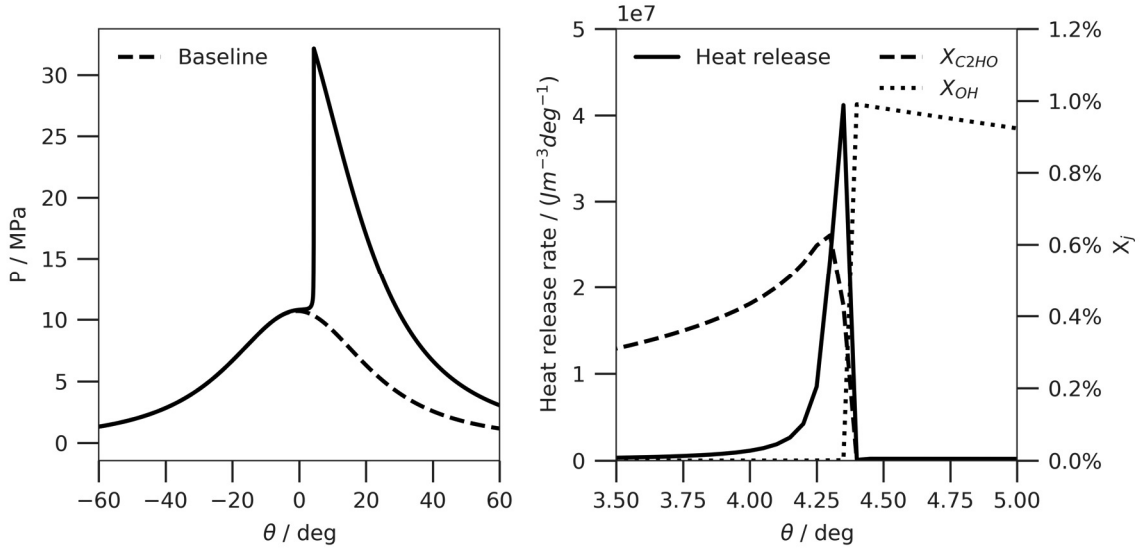

Figure 4-5: HCCI pressure, heat release and species profiles for combustion of CH_4/air in a CFR F-2 engine at ϕ = 1.0, P_{init} = 0.2 MPa and T_{init} = 400 K

4.3.3 Concept of baseline reactors

For all reactor simulations a *baseline reactor* is simulated parallel to the actual reactor. The baseline reactor contains the same initial combustible mixture and is set to the same initial conditions as the actual reactor, but is assumed to be chemically inert. In both reactors the thermodynamic properties of the mixture (see also section 4.2.1) are fully considered for every simulation time step, but the chemically reacting system is only evaluated in reactor 1, while in reactor 2 the reaction rate constants are set to zero. Thus, the baseline reactor reproduces how an inert mixture with the same initial thermodynamic properties as the reacting mixture would behave under the same conditions. This is necessary especially for the HCCI reactor model, where a compression/expansion baseline history of temperature and pressure is required as datum for the detection of ignition. An example for the pressure profiles of the baseline and actual reactor is presented in Figure 4-5.

4.3.4 Detection of auto-ignition

For both the constant-volume and the HCCI reactor model, a method for detecting the moment t_i at which ignition takes places and for calculating the ignition delay τ_i is required. Since the simulation starts with a perfectly homogenous gaseous mixture of fuel, oxidizer and residual gas and no physical processes such as mixing and evaporation are considered, the chemical ignition delay is equivalent to the period from the start of the simulation at t_0 until ignition:

$$\tau_i = t_i - t_0 \tag{4-73}$$

Different criteria are conceivable for determining t_i, following two basic approaches:

a) A change of the chemical composition in the reactor indicating the beginning of combustion, such as a rise of the concentration of OH radicals.

b) A change of the physical state in the reactor, such as temperature and pressure or internal energy and enthalpy.

Regardless of which approach is followed, different algorithms can be applied for determining t_i based on the reactor history for an arbitrary variable, for example, the temperature, the pressure or the heat release in the reactor:

a) The time at which the function y reaches a user-defined threshold with regard to the initial state (threshold criterion).

b) The time at which the first derivative of the variable or the variable itself reaches its maximum (maximum criterion).

c) The intersection of the extrapolated value of the variable at t_0 with the extrapolated tangent at the point of inflexion (extrapolation criterion).

The different methods are exemplarily displayed in Figure 4-6 for the temperature profile in a constant-volume reactor. As can be seen from the figure the different methods may deliver different results for t_i.

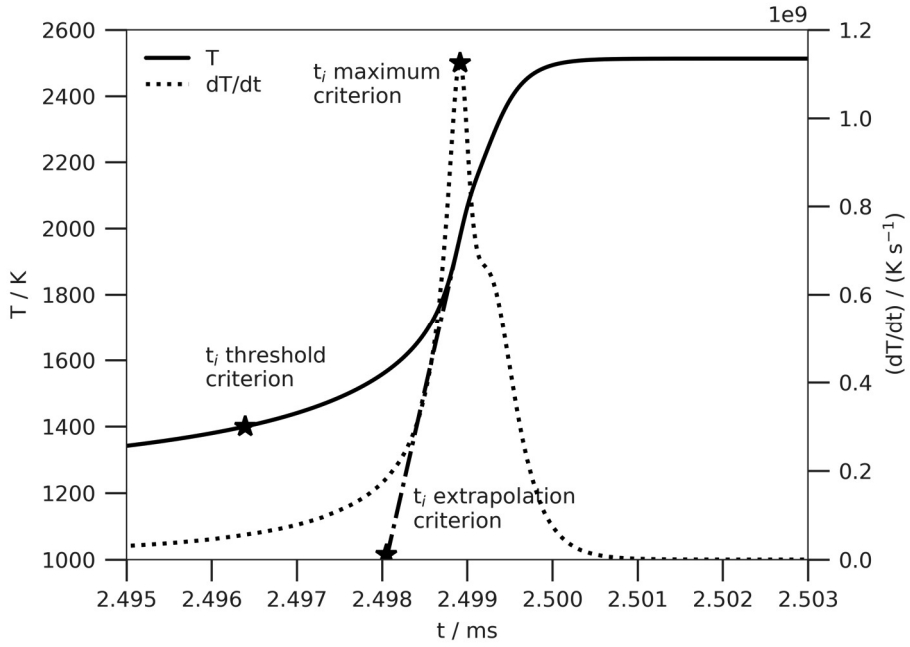

Figure 4-6: Ignition detection according to different methods

Special care has to be taken when dealing with fuels that feature a two-step ignition profile due to cool-flame reactions, such as n-heptane. In this case the actual ignition is assumed to happen in the second step when the main reaction starts, such as displayed in Figure 4-7 for a stoichiometric mixture of n-heptane and air at 1.0 MPa and different initial temperatures. From Figure 4-7 the effect of a *negative temperature coefficient* can also be observed: despite the earlier onset of pre-ignition reactions in the cool-flame zone the actual ignition delay time increases with increasing temperature. This behaviour normalises at higher initial temperatures when leaving the cool-flame regime.

In the case of the HCCI reactor a simple threshold criterion is not applicable, since the temperature and pressure vary as a function of the reactor geometry, even when no ignition occurs. Thus, the threshold always has to be related to an appropriate baseline, which in the case of the HCCI reactor is the compression/expansion of a chemically inert mixture with the same thermodynamic properties as the reacting mixture (see also [69]). This is accomplished by evaluating the history of the baseline reactor.

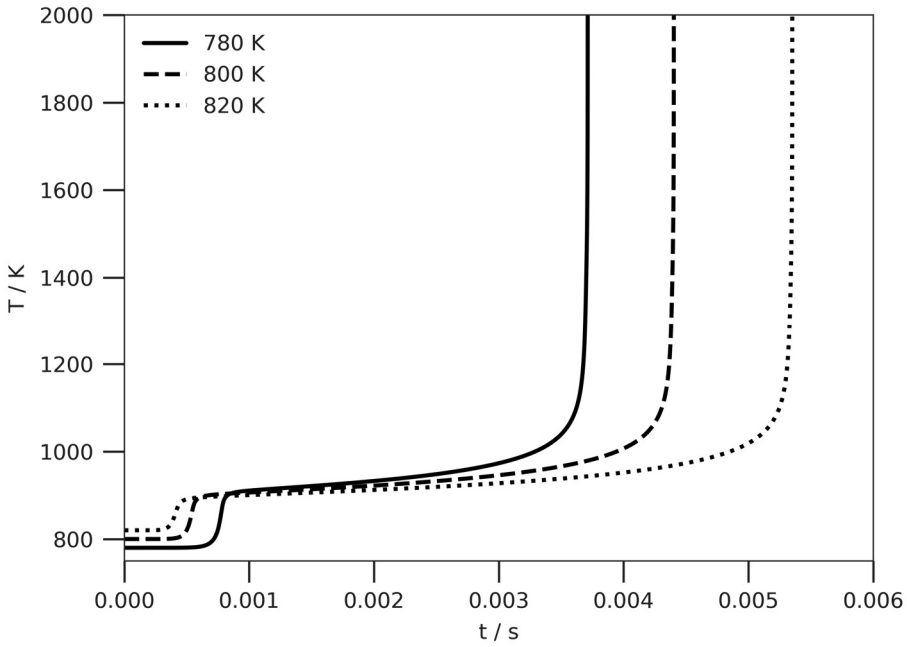

Figure 4-7: Two step ignition of n-heptane/air at ϕ = 1.0 and P = 1.0 MPa

4.3.5 Reactor root finding

In order to characterise the reactivity of fuel/oxidiser mixtures it may be necessary to determine the threshold of a specific target variable at which ignition happens in the model reactors. This can be, for example, the initial temperature required for ignition in the constant-volume reactor or the minimum compression ratio needed for ignition in the HCCI reactor. This task is accomplished by a scalar root finding routine, in which the target variable is automatically modified until a zero crossing of a defined search function is detected. The search function uses the threshold criterion for detection of ignition, where the evaluated variable should preferably be a straightforward indicator for ignition, for example, the temperature profile in the reactor. Brent's method is used for root finding (cf. [171]).

4.4 Laminar flame speed model

4.4.1 Laminar flame structure

According to the thermal theory a laminar flame front of thickness δ_L can be thought of consisting of a preheat zone with thickness δ_{PH} and a reaction zone with thickness δ_R, which are separated at the point where the next layer ignites, defined by an ignition temperature T_i [68], as illustrated in Figure 4-8. T is the temperature and z the flame coordinate, with T_U being the temperature of the unburned mixture and T_B the temperature of the burned mixture which is equivalent to the flame temperature. Heat diffuses from the reaction zone to the preheat zone and the reactants diffuse, in opposite direction, from the preheat zone into the reaction zone [172]. Both mechanisms are related by the *Lewis number* Le, with α denoting the thermal diffusivity and D the mass diffusivity [172]:

$$Le = \frac{\alpha}{D} \tag{4-74}$$

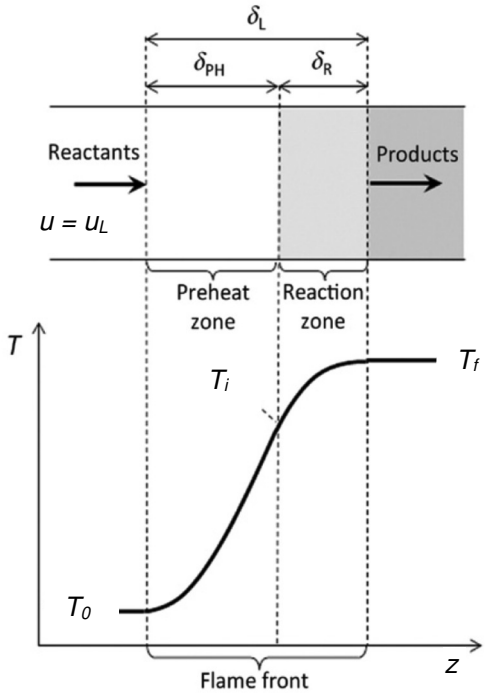

Figure 4-8: Schematic of a one-dimensional planar and unstretched flame front (adapted from [172])

The flame thickness is proportional to the ratio of the thermal diffusivity α and the flame speed and can thus be correlated to the mass flow $\dot{m}''$ per unit area of the unburned gases by using the definition of α as the thermal conductivity λ divided by the density ρ and the specific heat capacity c_p [68]:

$$\dot{m}'' \equiv \rho u_L \sim P^{n/2} \tag{4-75}$$

$$\alpha = \frac{\lambda}{c_p \rho} \tag{4-76}$$

$$\delta_L \sim \frac{\alpha}{u_L} \sim \frac{\lambda}{c_p \rho u_L} \sim \frac{\lambda}{c_p \dot{m}_U} \tag{4-77}$$

While u_L may decrease with decreasing pressure in hydrocarbon combustion systems, the mass burning rate increases proportional to $P^{n/2}$ with n being the overall order of the reaction [68]. Because λ/c_p does not vary with pressure, the flame thickness decreases as the pressure rises [68].

The thermal theory is a simplification of the actual laminar flame structure and modern computational methods as presented in the next section consider the steady-state mass, species, and energy conservation equations with complete reaction mechanisms for the fuel-oxidiser systems which specifies the heat release [68].

Under engine operating conditions the laminar flame speed should be understood as a characteristic scale rather than a measurable property of a flame [173]. Moreover, in real engine processes the flame regime will be mostly turbulent and laminar flames are not likely to appear in practice. Still, the laminar flame speed is an important parameter for assessing the reactivity of mixtures of fuel, oxidiser and residual gas, since it is purely dependent on the physico-chemical properties of the mixture and not on engine specific design parameters. Thus, the laminar flame speed can be used to assess the chemical time scale at which combustion proceeds for different mixtures of fuel, oxidiser and residual gas, without having to make additional assumptions concerning the flow-field and turbulence level, which would only be valid for a particular engine design.

4.4.2 Freely propagating premixed laminar flame

The model of a *freely-propagating, one-dimensional, adiabatic, premixed flame* is applied for calculating the laminar flame speed. According to Kee et al. [160] the set of conservation equations for a one-dimensional premixed laminar flame evolving in direction of coordinate z is as follows:

State conservation:

$$\rho = \frac{PW}{RT} \tag{4-78}$$

Overall mass continuity:

$$\frac{\partial \rho}{\partial t} + \frac{\partial (\rho u)}{\partial z} = 0 \tag{4-79}$$

Axial momentum:

$$\rho \frac{\partial u}{\partial t} + \rho u \frac{\partial u}{\partial z} = -\frac{\partial p}{\partial z} + \frac{\partial}{\partial z}\left(\mu \frac{\partial u}{\partial z}\right) \tag{4-80}$$

Species continuity:

$$\rho \frac{\partial Y_j}{\partial t} + \rho u \frac{\partial Y_j}{\partial z} = -\frac{\partial j_{j,z}}{\partial z} + \dot{\omega}_j W_j \tag{4-81}$$

Thermal energy:

$$\rho c_p \frac{\partial T}{\partial t} + \rho u c_p \frac{\partial T}{\partial z} = \frac{\partial}{\partial z}\left(\lambda \frac{\partial T}{\partial z}\right) - \sum_{j=1}^{n} c_{pj} j_{j,z} \frac{\partial T}{\partial z} - \sum_{j=1}^{n} h_j \dot{\omega}_j W_j \tag{4-82}$$

Where ρ is the density, p the pressure, R the universal gas constant, T the temperature, W the molecular weight, u the axial velocity, μ the dynamic viscosity, Y the mass fraction, j the diffusive mass flux, $\dot{\omega}$ the molar production rate, c_p the specific heat capacity at constant pressure, λ the thermal conductivity and h the enthalpy. The index j refers to the individual species in the mixture and n to the total number of species.

These equations can be further reduced in the case of a strictly one-dimensional flat flame at steady flow conditions by assuming a constant net mass flux $\dot{m}''$ and by dropping the axial momentum equation (4-80), which is possible in this case since the pressure gradients associated with flow are negligibly small compared to the magnitude of the pressure itself [160]:

$$\dot{m}'' = \rho u \tag{4-83}$$

$$\rho \frac{\partial Y_j}{\partial t} + \dot{m}'' \frac{\partial Y_j}{\partial z} = -\frac{\partial j_{j,z}}{\partial z} + \dot{\omega}_j W_j \tag{4-84}$$

$$\rho c_p \frac{\partial T}{\partial t} + \dot{m}'' c_p \frac{\partial T}{\partial z} = \frac{\partial}{\partial z}\left(\lambda \frac{\partial T}{\partial z}\right) - \sum_{j=1}^{n} c_{pj} j_{j,z} \frac{\partial T}{\partial z} - \sum_{j=1}^{n} h_j \dot{\omega}_j W_j \tag{4-85}$$

The diffusive mass flow j_j of the individual species in the mixture can be computed either with a mixture-averaged or a multicomponent formulation. The latter one is more accurate and has the advantage that total mass conservation is preserved when solving the species-continuity equations, but it causes higher computational expenses, especially when

many species are involved [160]. The mixture-average diffusive mass flux is an approximation rather than being accurate and requires a correction procedure to ensure that the sum of the mass fluxes is zero [160]. It can be calculated as follows, where D_{jm} is the mixture-averaged diffusion coefficient of species j and Equation (4-87) accounts for the mass flux correction [150]:

$$j_j^* = \rho \frac{W_j}{W} D_{jm} \frac{\partial X_j}{\partial z} \tag{4-86}$$

$$j_j = j_j^* - Y_j \sum_i j_i^* \tag{4-87}$$

The multicomponent formulation is based on the multicomponent diffusion coefficient $D_{j,i}$ for species j in direction i and can be written as [150]:

$$j_j = \frac{\rho W_j}{W^2} \sum_i W_i D_{j,i} \frac{\partial X_i}{\partial z} \tag{4-88}$$

For a rigorous theory of transport properties including the equations for the computation of multicomponent diffusion coefficients one can refer to [160].

The problem of the laminar flame is solved in the reference frame of the flame by imposing a fixed coordinate system, where the boundary condition is that all gradients, both at the cold and hot boundary, must vanish [160]. For practical computation the size of the domain has to be adjusted such that the cold boundary gradients nearly vanish and at the same time the mass flux fractions equal the mass fractions of the unburned mixture [160]. The laminar flame speed is then found by evaluating the velocity at the cold boundary z_0 once the net mass flux $\dot{m}''$ is determined [160]:

$$u_L = \frac{\dot{m}''}{\rho} \tag{4-89}$$

4.5 Auto-ignitive regimes and detonation theory

4.5.1 Ignition delay and excitation time

The chemical auto-ignition delay time τ_i of a given fuel at a specific pressure and equivalence ratio is strongly dependent on the respective temperature T and can be expressed in an equation of the Arrhenius form

$$\tau_i = Ce^{\frac{E}{RT}}, \tag{4-90}$$

where C is a fuel-dependent constant, E is an apparent activation energy for the fuel auto-ignition process and R is the universal gas constant [17, 23].

The gradient of the auto-ignition delay time with temperature is an important parameter for assessing the reactivity of fuels and is often denominated the *thermal sensitivity*:

$$\frac{\partial \tau_i}{\partial T} = -\tau_i \frac{E}{RT^2} \tag{4-91}$$

The fraction E/R is the localised auto-ignitive activation temperature [23] characteristic for a specific fuel. The ratio E/R can conveniently be determined as the gradient from the associated differences in delay times between different temperatures at constant pressure in plots of $\ln \tau_i$ versus $1/T$ (cf. also Figure 4-9) [97]:

$$\frac{\partial \ln \tau_i}{\partial \left(\frac{1}{T}\right)} = \frac{E}{R} \tag{4-92}$$

The release of energy during an auto-ignition is not instantaneous but takes place over a finite amount of time determined by the heat release rate [74]. The time span in which the majority of heat is released is denominated the *excitation time* and is usually defined as the time span between the point where 5 % of the maximum heat release rate is reached and the point where the maximum is attained (see also Figure 4-9) [71, 98]:

$$\tau_e = t\left(\frac{dQ}{dt}\right)_{max} - t\left(\frac{dQ}{dt}\right)_{5\%} \tag{4-93}$$

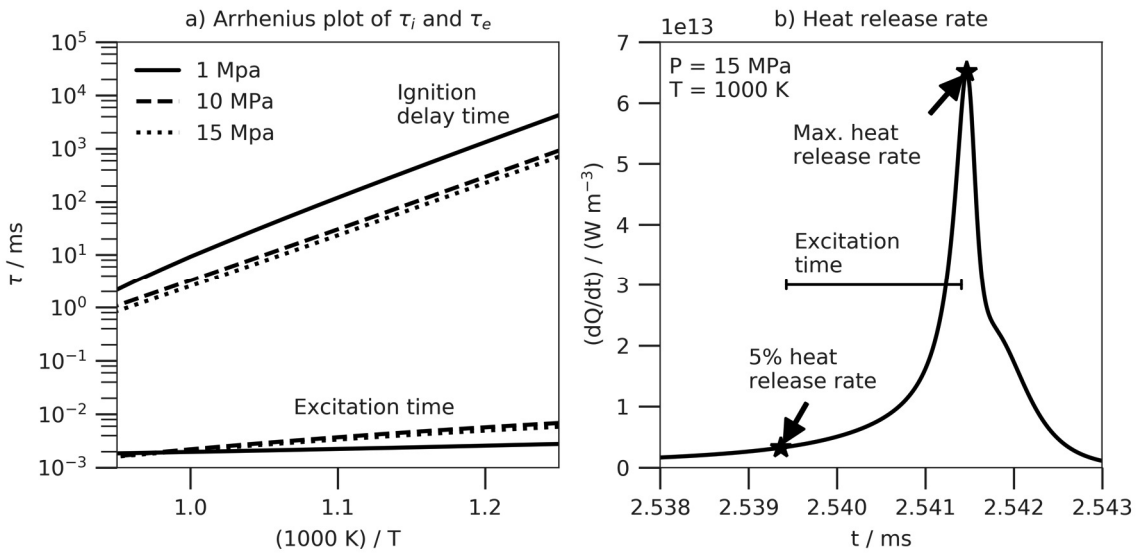

Figure 4-9: a) Arrhenius plot and b) heat release for combustion of H_2/CO/N_2 = 40/20/40 vol%, ϕ = 0.5

It should be noted that the excitation time cannot be measured with current experimental methods and therefore can only be ascertained through numerical simulations [71]. Thus, it is important to accurately reproduce the heat release profiles by adequately detailed chemical kinetics and sufficiently small simulation time steps which increases the computational costs. Moreover, different definitions of the excitation time are conceivable and the interpretation according to Equation (4-93) and Figure 4-9 b) is a convention rather than being based on physical evidence. In the strict sense it would only be applicable for auto-ignition events with equally shaped heat release profiles where the majority of energy is released during the excitation time and only to a lesser extent after the point of maximum heat release. It is important to be aware of these drawbacks when using the excitation time for subsequent analyses such as for the construction of the ξ-ε diagram presented in section 4.5.3. Nevertheless, the excitation time is still an appropriate metric for the reactivity of combustible mixtures and plays an important role for classifying the possible auto-ignition regimes evolving from ignition hot spots in internal combustion engines (cf. [23]).

4.5.2 Auto-ignition propagation from secondary hot spots

The reaction zone evolving from an ignition *hot spot* can have different speeds ranging from the premixed laminar flame speed to infinity [26, 98]. Assuming that the temperature gradient is the only non-uniformity in an otherwise homogenous mixture, successive points along the gradient will have different ignition delay times, leading to the propagation of an *auto-ignition wave* travelling at the *auto-ignition propagation speed* u_p relative to the unburned gas, which is equal to the inverse gradient of the auto-ignition delay time [98]:

$$u_p = \left(\frac{\partial \tau_i}{\partial r}\right)^{-1} \tag{4-94}$$

Decomposing the gradient of the auto-ignition delay time τ_i into a product of the thermal gradient $\partial T/\partial r$ and the thermal sensitivity $\partial \tau_i/\partial T$ yields [98]:

$$u_p = \left(\frac{\partial T}{\partial r}\frac{\partial \tau_i}{\partial T}\right)^{-1} \tag{4-95}$$

If the temperature gradient attains a critical value $(\partial T/\partial r)_c$ inducing an auto-ignition velocity in the range of the acoustic velocity a, the auto-ignition wave can couple with the pressure wave, such that both mutually reinforce each other, leading to a developing detonation [26, 98]:

$$u_p = \left(\frac{\partial \tau_i}{\partial T}\right)^{-1}\left[\left(\frac{\partial T}{\partial r}\right)_c\right]^{-1} = a \tag{4-96}$$

The critical temperature gradient in a hot spot at which this resonance occurs can be determined from [98]:

$$\left(\frac{\partial T}{\partial r}\right)_c = a^{-1}\left(\frac{\partial \tau_i}{\partial T}\right)^{-1} \tag{4-97}$$

By normalising the actual initial temperature gradient in the hot spot with the critical gradient the dimensionless parameter ξ is obtained, which can be regarded as an approximate indicator for a developing detonation in the region of chemical resonance which occurs at $\xi = 1$ [23, 98]:

$$\xi = \left(\frac{\partial T}{\partial r}\right)\left(\frac{\partial T}{\partial r}\right)_c^{-1} \tag{4-98}$$

In real systems the conditions for a developing detonation will occur in a range marked by the upper and lower values ξ_l and ξ_u rather than at a sharp threshold [98]. An example for a developing detonation regime with $\xi = 3$ from the DNS simulations by Gu et al. [98] is displayed in Figure 4-10.

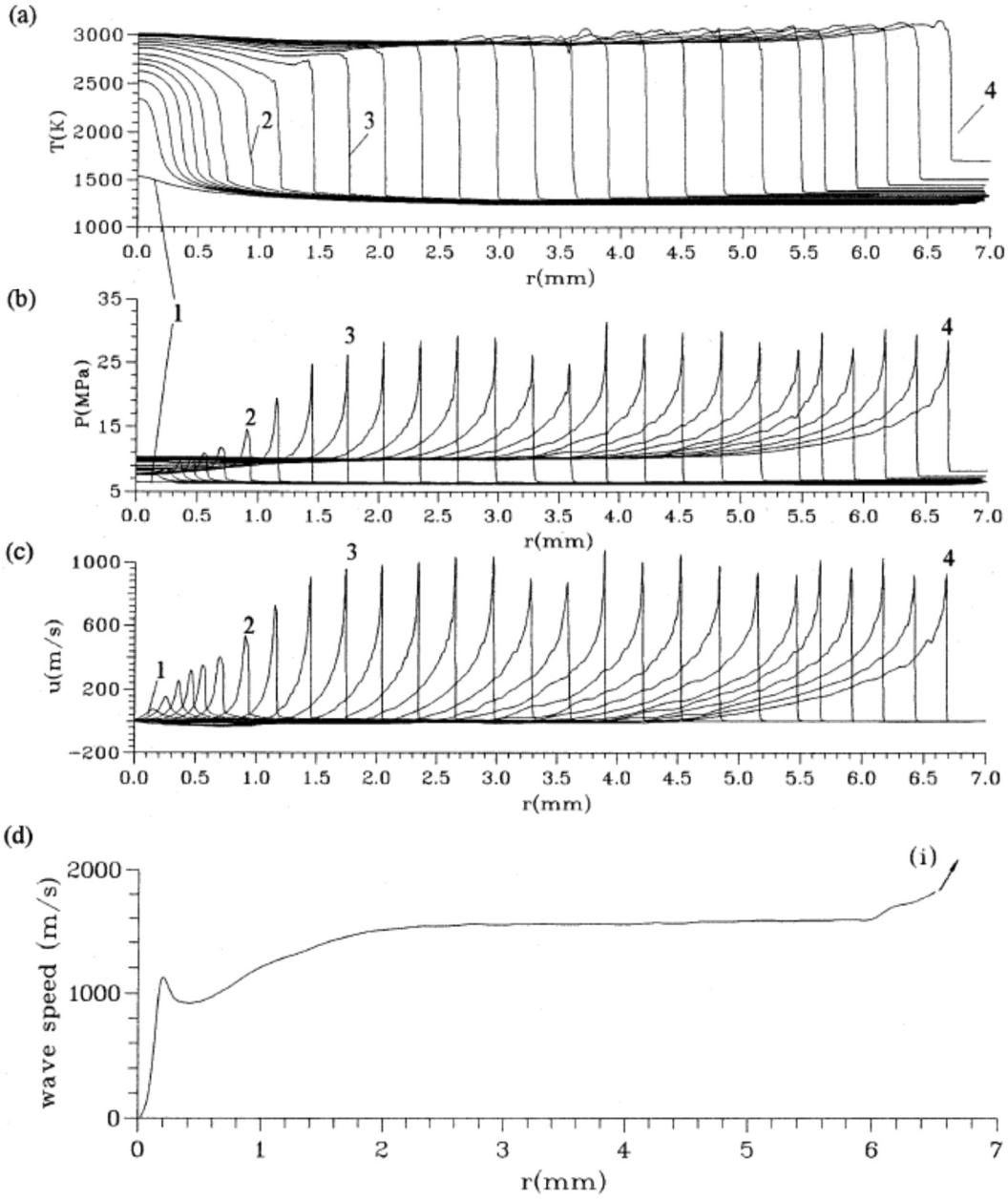

Figure 4-10: Developing detonation and thermal explosion for a hot spot of radius 3 mm for stoichiometric H_2/CO = 50/50 vol% in air, P = 5.066 MPa, ΔT = 0.5067 K, τ_i = 1.4225 ms [98]

By combining Equations (4-96) and (4-98) the parameter ξ can be related to the auto-ignition propagation speed [98]:

$$u_p = \left(\frac{\partial \tau_i}{\partial T}\right)^{-1} \left[\left(\frac{\partial T}{\partial r}\right)_c\right]^{-1} \xi^{-1} = a\xi^{-1} \tag{4-99}$$

According to Gu [98] the following five regimes of auto-ignition propagation can be distinguished based on the condition defined in Equation (4-99):

a) $\xi = 0$: no temperature gradient, homogenous thermal explosion after τ_i

b) $0 < \xi < \xi_l$: supersonic rapid auto-ignitive deflagration

c) $\xi_l \leq \xi < \xi_u$: developing and developed detonation (see also Figure 4-10)

d) $\xi_u \leq \xi < au_L^{-1}$: subsonic auto-ignitive deflagration

e) $\xi \geq au_L^{-1}$: laminar burning deflagration at the laminar flame speed S_L

The modes b) to e) will probably be terminated by a thermal explosion [98].

4.5.3 ξ-ε diagram

The methodology developed by Bates et al. [23, 25, 71, 74], cf. section 2.2.3, is used to construct a ξ-ε diagram for fuels based on the concept of auto-ignition propagation from secondary hot spots. The secondary hot spot is idealised as a sphere with radius r_0 and a temperature gradient $\partial T/\partial r$ along the radius, with T_0 being the temperature at the centre and T the temperature of the surrounding mixture (cf. Figure 4-11). Assuming an otherwise homogenous mixture this temperature gradient is the sole driver for the reactivity gradient in the hot spot, and the auto-ignition propagation velocity u_p can be obtained from Equation (4-95).

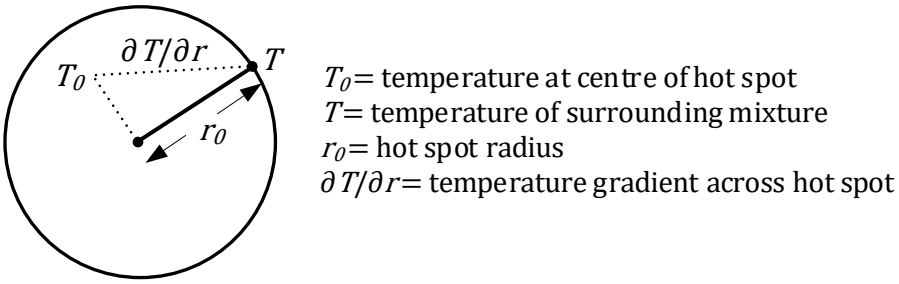

Figure 4-11: Idealised spherical hot spot with linear temperature gradient

By rearranging Equation (4-99), Bates defines the dimensionless parameter ξ, relating the auto-ignition propagation velocity to the acoustic velocity a [23]:

$$\xi = \frac{a}{u_p} = \frac{\partial T}{\partial r}\frac{\partial \tau_i}{\partial T}a \tag{4-100}$$

Based on the general expression for the auto-ignition delay time for a given fuel at a specific pressure and equivalence ratio – see also Equations (4-90) and (4-91) – the expression for ξ can be rewritten as

$$\xi = -\tau_i \frac{E}{RT^2}\frac{\partial T}{\partial r}a \tag{4-101}$$

A second dimensionless parameter ε is defined as the time the acoustic wave with the velocity a moves through the hot spot of radius r_0 divided by the excitation time τ_e [23]:

$$\varepsilon = \frac{r_0}{a\tau_e} \tag{4-102}$$

The parameter ε relates the acoustic wave transit time r_0/a through the hot spot to the time τ_e during which the majority of heat is released and is thus a measure for the energy transferred into the acoustic front [23].

Reorganising Equation (4-101)

$$\xi = -\left(\frac{\tau_i E}{RT}\right)\left(\frac{\partial T}{T}\frac{r_0}{\partial r}\right)\left(\frac{a}{r_0}\right) \tag{4-103}$$

and introducing the excitation time τ_e yields

$$\xi\varepsilon = -\bar{E}\left(\frac{\partial lnT}{\partial \bar{r}}\right) \tag{4-104}$$

with

$$\bar{E} = \frac{\tau_i}{\tau_e}\frac{E}{RT} \tag{4-105}$$

and $\bar{r}$ being the dimensionless hot spot radius [23]:

$$\bar{r} = \frac{r}{r_0} \tag{4-106}$$

The term $\partial lnT/\partial \bar{r}$ can be approximated by $\ln(T/T_0)$ with little error[2] if the temperature gradient $\partial T/\partial r$ across the hot spot is assumed to be linear, with T_0 being the temperature at the centre of the hot spot [23]. The actual structure of hot spots in combustion devices may be very complex, as DNS studies show, and the assumption of spherical hot spots is a significant simplification [23]. According to Bates, the radius r_0 should thus be essentially regarded as a length over which the temperature gradient is almost constant [23].

Both dimensionless values, ξ and ε, can be easily determined if τ_i and τ_e are known, for example, from constant-volume reactor simulations. The hot spot radius and the thermal gradient along the hot spot are often assumed to be $r_0 = 5$ mm and $\partial T/\partial r = -2$ K/mm for engine operating conditions [23, 71].

Based on plots of ξ versus ε, the different auto-ignition regimes can be characterised as shown in Figure 4-12 compiled by Bates [74]. The detonation peninsula is marked by the upper and lower boundaries of ξ_u and ξ_l which separate the region of dominating deflagration from strong thermal explosions with the transition regime of developing detonations in between. In the region above the upper limit ξ_l of the detonation peninsula, Bates introduces

[2] The resulting error ranges from 0.05 % for temperature gradients of -1 K/mm to 4.7 % for -100 K/mm [23] and is thus negligible for typical engine operating conditions, where the temperature gradients are in the range of -2 K/mm [71]

an additional criterion for the onset of deflagration by applying the parameter $-\bar{E}(\partial lnT/\partial \bar{r})$ [23].

By evaluating the Sankaran criterion using data presented by Mansfield [102] for syngas-air mixtures ($n_{H_2}/n_{CO} = 0.7$, $\phi = 0.5$) with a temperature gradient of -5 K/mm, a hot spot radius of 3 mm and $\bar{E} = 110 \times 10^3$ at 1 100 K, Bates found a value of $-\bar{E}(\partial lnT/\partial \bar{r})$ =1 490 ≈ 1 500 which was defined as tentative threshold for the onset of deflagration above the upper limit of the peninsula [23]. The actual threshold is probably a range of $-\bar{E}(\partial lnT/\partial \bar{r}) \approx 900 \ldots 6000$ rather than a fixed value as the evaluation of experimental and computational data indicates [71]. According to Bates the curves of constant $-\bar{E}(\partial lnT/\partial \bar{r})$ are indicators for the intensity of ignition, and $\bar{E}$ can be regarded as a parameter for detonation stability encapsulating the properties of the fuel [74]. Small values of $\bar{E}$ lead to stable detonations and when combined with small temperature gradients $\partial lnT/\partial \bar{r}$ detonation and super knock are likely to occur [74].

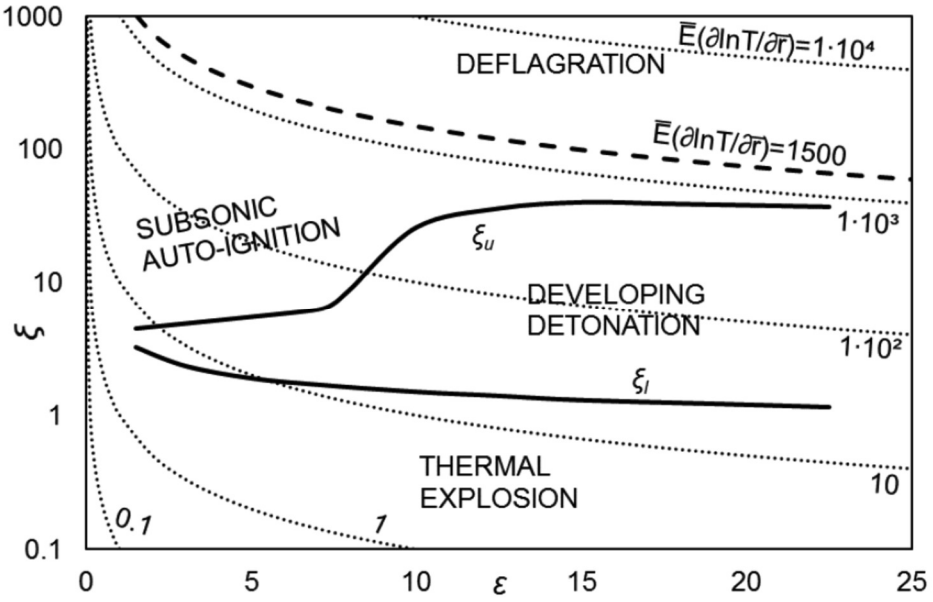

Figure 4-12: ξ-ε diagram by Bates with addition of curves of constant $\bar{E}(\partial lnT/\partial \bar{r})$ [74]

4.5.4 Sankaran criterion

Based on the results of a high fidelity DNS of the auto-ignition of hydrogen-air mixtures, Sankaran [101] distinguishes two prominent ignition regimes emanating from thermal hot spots: a wide-range spontaneous explosion and a narrow flame-like deflagration. To describe the transition between the two regimes Sankaran introduces a dimensionless parameter $\beta = C_\beta \, u_d / u_p$ by relating the deflagrative wave speed u_d to the auto-ignitive propagation speed u_p [101]. Building upon the work of Sankaran, Mansfield et al. [102, 174] propose a definition of β which sets the deflagrative reaction front speed equal to the laminar flame speed u_L and relates it to the speed u_p of the spontaneous propagation reaction front which is equal to the inverse of the gradient of the auto-ignition delay time $(\partial \tau_i / \partial r)^{-1}$:

$$\beta = \frac{u_L}{u_p} = \frac{u_L}{\left(\frac{\partial \tau_i}{\partial r}\right)^{-1}} \tag{4-107}$$

Values of $\beta < 1$ correspond to a dominance of strong ignition (homogenous explosion) and values of $\beta > 1$ to a dominance of mixed or weak ignition (inhomogenous deflagration front) [102].

Based on the definition of the auto-ignition propagation speed in Equation (4-95), Mansfield defines the *Sankaran criterion* as

$$\frac{\partial \tau_i}{\partial T} < \left(\frac{\partial T}{\partial r} u_L\right)^{-1} \tag{4-108}$$

where strong ignition will occur if the inequality is true and mixed or weak ignition will occur if the inequality is false [102]. Equation (4-108) highlights the importance of thermal sensitivity of the ignition delay time with regard to auto-ignition [102].

Typical thermal gradients $\partial T / \partial r$ occurring in experimental devices are in the range of -5 to -10 K/mm [102, 174], while in internal combustion engines about -2 K/mm are most probable [71]. By applying these gradients the evaluation of Equation (4-108) requires solely

knowledge of the laminar flame speed and the ignition delay time or its thermal sensitivity. Both values can be calculated using the methodology presented later in sections 4.3 and 4.4. The Sankaran criterion is thus a tool that can be used for the a priori prediction of the strong ignition limit for different fuels and initial conditions, with no experimentation necessary for its application [102, 174].

4.6 Summary

In order to simulate the auto-ignition and laminar flame speed of combustible mixtures it is first necessary to model the *combustion gas*, that is, the chemically reacting mixture of fuel, oxidiser and residual gas. The complex chemical processes taking place in the combustion gas are split into a system of one-step chemical reactions, in which the reaction rate constant of the single reaction can be expressed in an *Arrhenius* form and the whole system is described by a *chemical reaction mechanism*. The combustion gas is assumed to be a mixture of ideal gases. The required fluid properties (thermodynamic and transport data) are obtained from databases, for example, in *NASA polynomial parameterization* for thermodynamic data.

For modelling the influence of the *residual gas fraction* and the *exhaust gas recirculation* it is necessary to consider the composition of the burned gas. Since combustion in real systems is never perfect and products other than carbon dioxide and water will appear, the burned gas is modelled as an ideal gas mixture in *chemical equilibrium*. Alternatively, a *frozen* composition can be assumed in order to better reproduce typical engine exhaust gas, in which chemical equilibrium is usually not reached. Additionally, the mixture has to be controlled for water vapour which can only be present up to the saturation pressure. When assuming ideal gas behaviour the volume fraction of water vapour is equivalent to its partial

pressure and the maximum possible amount can be calculated from the saturation pressure of the pure substance according to the IAPWS formulation.

The chemical ignition delay and excitation time of fuel mixtures are studied in constant-volume reactor simulations which are the numerical equivalent to an ideal *rapid compression machine (RCM)*. Alternatively, a piston reactor model emulating an ideal *homogenous charge compression ignition (HCCI)* reactor can be used to simulate auto-ignition under conditions closer to the compression process in a real combustion engine. The *laminar flame speed* is obtained from the simulation of a *freely-propagating, one-dimensional, adiabatic, premixed flame.*

The ignition delay time and the laminar flame speed are important characteristic parameters of combustible mixtures. However, without further characterisation only limited information with regard to the suitability for engine operation can be derived from these parameters. Therefore, additional assessment criteria are necessary. One possible measure is the Sankaran criterion [101] as defined by Mansfield et al. [102, 174] which relates the thermal sensitivity of the ignition delay time to the laminar flame speed and allows the a priori determination of strong ignition limits based solely on simulations without the need for experimentation. A second methodology is presented by Bates et al. [23, 25, 71, 74] based on the ξ-ε diagram applying two dimensionless parameters representing the auto-ignition propagation velocity normalised by the acoustic velocity (ξ) and the energy transferred into the acoustic wave front moving through a hot spot (ε). The respective values of ε and ξ define the regimes of subsonic auto-ignition, deflagration, detonation and thermal explosion. By assuming a constant hot spot radius $r_0 = 5$ mm and a thermal gradient $\partial T/\partial r = -2$ K/mm through the hot spot, the ξ-ε diagram can be constructed solely with the simulated ignition delay and excitation times τ_i and τ_e and thus enables fuel characterisation based only on reaction kinetic calculations without the need for experimentation.

Chapter 5 Implementation of the models – CoPa toolbox

5.1 CoPa simulation toolbox

Based on the methodology presented in Chapter 4, a modular, object-oriented simulation toolbox – the *Combustion Parameters toolbox (CoPa)* – was developed. The toolbox was implemented in *Python* (64-bit version 3.7.3, https://www.python.org/) and built upon the *Cantera* software package [150]. Cantera was chosen as chemical kinetics solver since it is widely used at research institutions and companies for solving problems related to combustion [175] and features a well-documented, powerful interface to Python and Matlab, which facilitates its integration into user-specific applications. Cantera is one of the few comprehensive chemical reaction kinetics codes that can be expected to remain open source and available for all to use [176]. The CoPa toolbox essentially provides a high-level interface to Cantera for computing characteristic combustion parameters of combustible mixtures in an automatized workflow. Since *CoPa* is intended for automatising Cantera calculations, it can also be conveniently used to compute tabulated chemistry data.

In Figure 5-1 a schematic overview of the simulation workflow is displayed. The CoPa toolbox consists of several individual *modules* grouped into a *package* and is supplemented by predefined processing scripts that can be used to generate the simulation input files and process the simulations (see Table 5-2). The main features of the individual modules and processing scripts are presented in detail in Appendix B.

The first step of the workflow is to generate a simulation input file in which the relevant data for the respective simulation runs are defined. The data are arranged in a spreadsheet style using a *Pandas DataFrame* [177], where each row represents a single simulation run and the columns contain the required input data for each simulation, such as the mixture definition or the reactor geometry.

The simulation input file is then processed using the *copa_processor.py* script, which performs the pre-processing, main processing and post-processing by calling the respective modules. The pre-processing routine involves loading the simulation input file and preparing the data for the subsequent steps. Again, a Pandas DataFrame is used to store the data during processing. After pre-processing, the main routine takes over and calls *sim_module.py*, which interacts with the Cantera software package to perform the actual simulations. The simulation module first calls *gas_module.py*, which initialises a mixture of fuel, oxidiser and residual gas and performs additional tasks, such as controlling the water vapour content or freezing the equilibrium composition. The gas module interacts with Cantera to define a *Cantera solution object*, which is then handled back to the simulation module. According to the selected simulation mode, the simulation module initialises either a *Cantera reactor network* or a *Cantera flame object* with the Cantera solution object obtained from the gas module and calls the respective Cantera solver. The simulation results for each time step (or grid point for flames) are aggregated by the simulation module and handled back to the simulation processor script.

Since each setup in the input file is considered separately, a single call of the simulation module is necessary for each simulation run. Thus, in a normal Python implementation, the simulations would be processed serially, one after another, using just one process at a time. In order to speed up calculations on machines with multiple cores, the *pathos framework* [178, 179] is used to add multiprocessing capabilities, so that various simulations can be computed in parallel, limited only by the number of available cores.

The simulation results received from the multiprocessing pool are stored in a Pandas DataFrame and handled over to the post-processing step which calls the respective functions from *postproc_module.py*. The post-processing results are added to the results DataFrame and finally stored in an output file, which then can be used for further processing or plotting.

The figures presented in this thesis were created with *Matplotlib* [180] (version 3.0.3 https://matplotlib.org/).

The CoPa toolbox consistently uses SI units according to Table 5-1. If other units should be used, conversion factors have to be applied in the simulation generation and/or post-processing. Since the CoPa toolbox is designed in a modular, object-oriented approach, it is easy to include new features by adding functions or classes in the respective modules while retaining the general processing framework.

Table 5-1: Base units used in the CoPa simulation toolbox

Parameter	Unit
Angular dimensions	radians
Amount of substance	mol
Energy	J
Linear dimensions	m
Mass	kg
Rotational speed / frequency	1/s
Time	s
Velocity	m/s
Volume	m^3

Table 5-2: Modules of the CoPa simulation toolbox

Name	Description
copa	Simulation package containing the individual modules of the simulation toolbox. Can be imported into Python scripts or interactive environments and makes the functions and classes of the modules available in the namespace.
__init__.py	Initialisation file for the copa package.
gas_module.py	Module for initialising mixtures of fuel, oxidiser and residual gas. High-level interface to Cantera for defining combustible mixtures occurring in internal combustion engines. Contains all classes and functions required for setting the gas mixture and state, and interacts with Cantera to create a Cantera Solution object according to the mixture specification.
helpers.py	Helper functions, e.g., for rounding or data type conversion
postproc_module.py	Post-processing module. Contains all functions required for post-processing of the reactor and flame simulation results, e.g., for calculating ignition delay and excitation times.
sim_module.py	Simulation module. High-level interface to Cantera for determining characteristic combustion parameters of combustible mixtures based on auto-ignition in reactors and flame speeds. Contains all functions for defining and solving chemically reacting systems based on the Cantera reactor and flame models.
copa_generator.py	Script for defining simulations and generating simulation input files.
copa_processor.py	Script for processing simulations including multiprocessing capabilities. Performs pre-processing, main processing and post-processing steps and calls the relevant functions from the copa package.

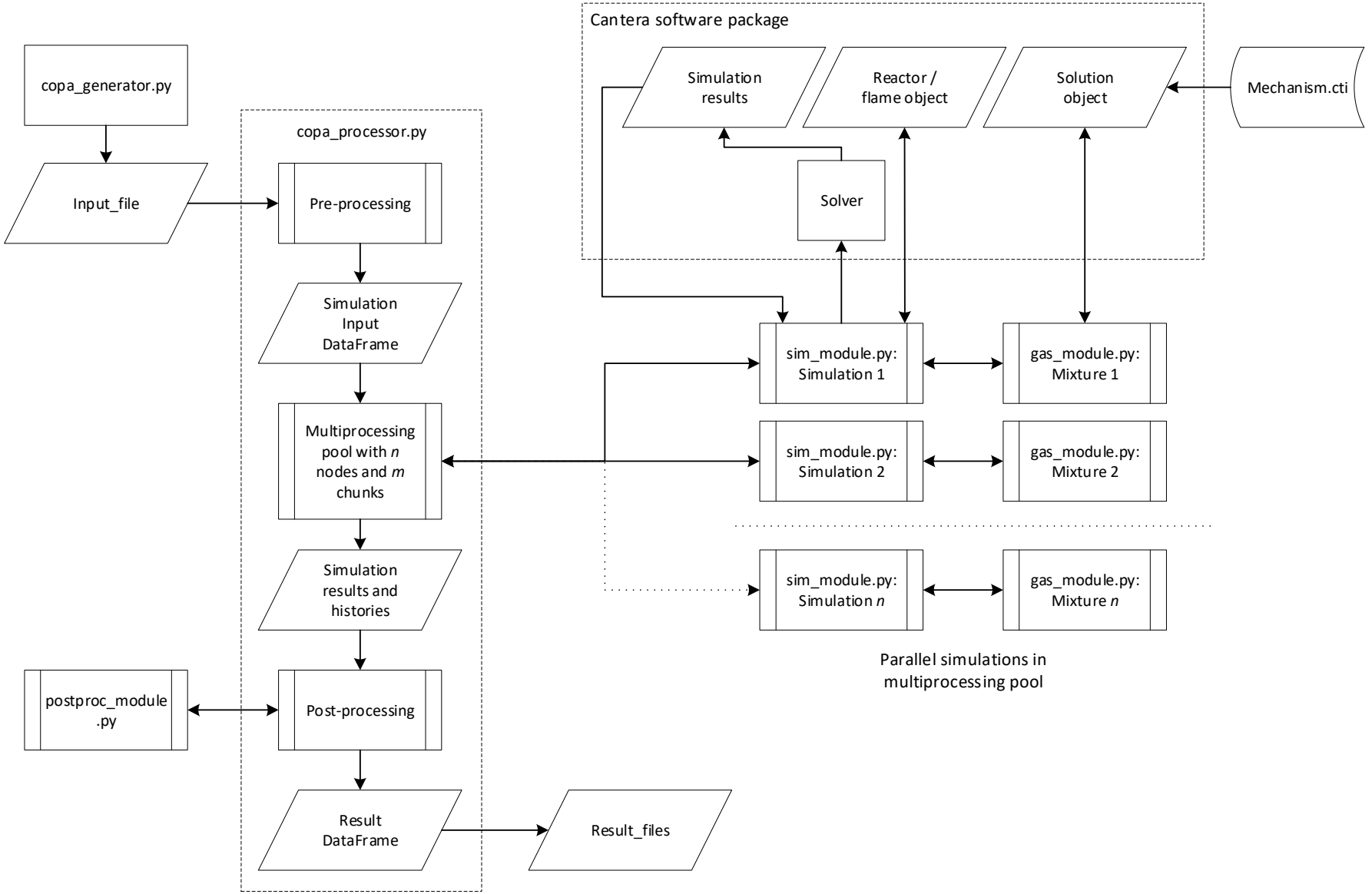

Figure 5-1: Schematic diagram showing the workflow of the CoPa simulation toolbox

5.2 Verification of the models

The fundamentals for modelling chemically reacting systems in ideal reactors and laminar flames as presented in Chapter 4 are state-of-the-art knowledge published in several textbooks [68, 160, 181, 182] and can thus be considered to be a validated methodology. The same applies to the Cantera software package which has been used by many researchers to prepare data which has been published on conferences and in scholarly journals (see [21, 71, 90, 92, 149, 183–186]). Nevertheless, it is necessary to verify that the implementation of the Cantera models in the CoPa toolbox is correct[3]. Data from literature was used for this purpose and the *coefficient of determination* r^2 was calculated to assess the goodness of fit.

5.2.1 Constant-volume reactor

Data published by Bates et al. [71] was used for the verification of the constant-volume reactor model. Bates presents ignition delay and excitation times for CH_4/air obtained from Cantera constant-volume reactor simulations with two different reaction mechanisms at different pressures and temperatures. The ignition delay was defined as the time from zero to the onset of the maximum heat release rate, and the excitation time was evaluated as the time span between 5 % of the maximum heat release rate and its maximum value [71].

The verification results for ignition delay and excitation time are displayed in Figure 5-2 and Figure 5-3. The according coefficients r^2 are given in Table 5-3. The values obtained with the CoPa toolbox are in very good agreement with the data published by Bates. This confirms that both the constant-volume reactor model and the post-processing routines for detection of ignition and calculation of the excitation time perform as intended. This was to be expected, since both simulations are based on the same Cantera reactor model an apply

[3] The verification of the Cantera constant-volume reactor and laminar flame model was to some extent subject of a master's thesis supervised as part of this PhD project, cf. Goßner, T.: Design and validation of open source based program codes for simulation of combustion kinetics parameters. Master's thesis, Ostbayerische Technische Hochschule Amberg-Weiden (2018)

the same reaction mechanism. Ideally, r^2 should be ≈ 1.0 in all cases. However, since the reference data was digitised from plots, minor deviations are possible. Additionally, the simulation settings (time step, error tolerances) might differ, leading to slightly deviant results.

Figure 5-2 additionally includes experimental data from several sources as compiled by Bates [71]. While the experimental values show good agreement with the simulated curves at low pressure (Figure 5-2 a) there is generally much more scatter at higher pressure (Figure 5-2 b). At higher pressure the Mech 56.54 mechanism [72] captures the general trend better than the GRI-Mech 3.0 [54] which has been optimised only up to 1.01 MPa [71]. The evaluation of reaction mechanisms was, however, not subject of the present study and the experimental data is presented for information only at this point.

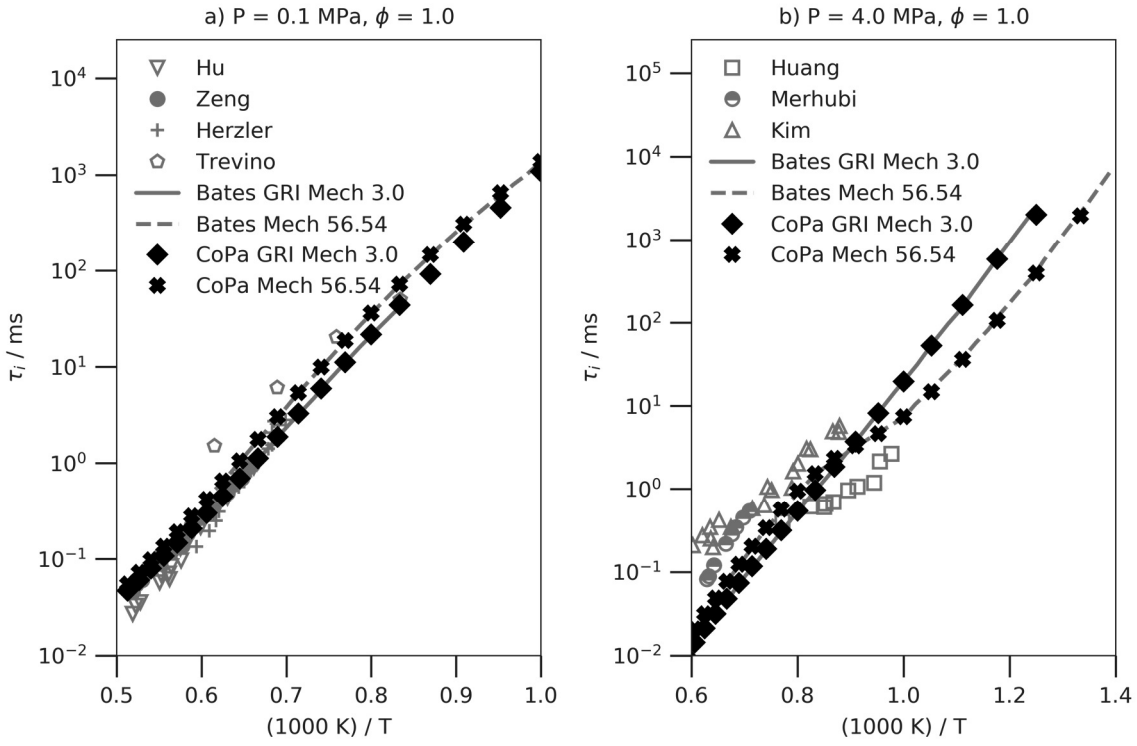

Figure 5-2: Verification of ignition delay simulation for CH_4/air combustion; reference data from [71]

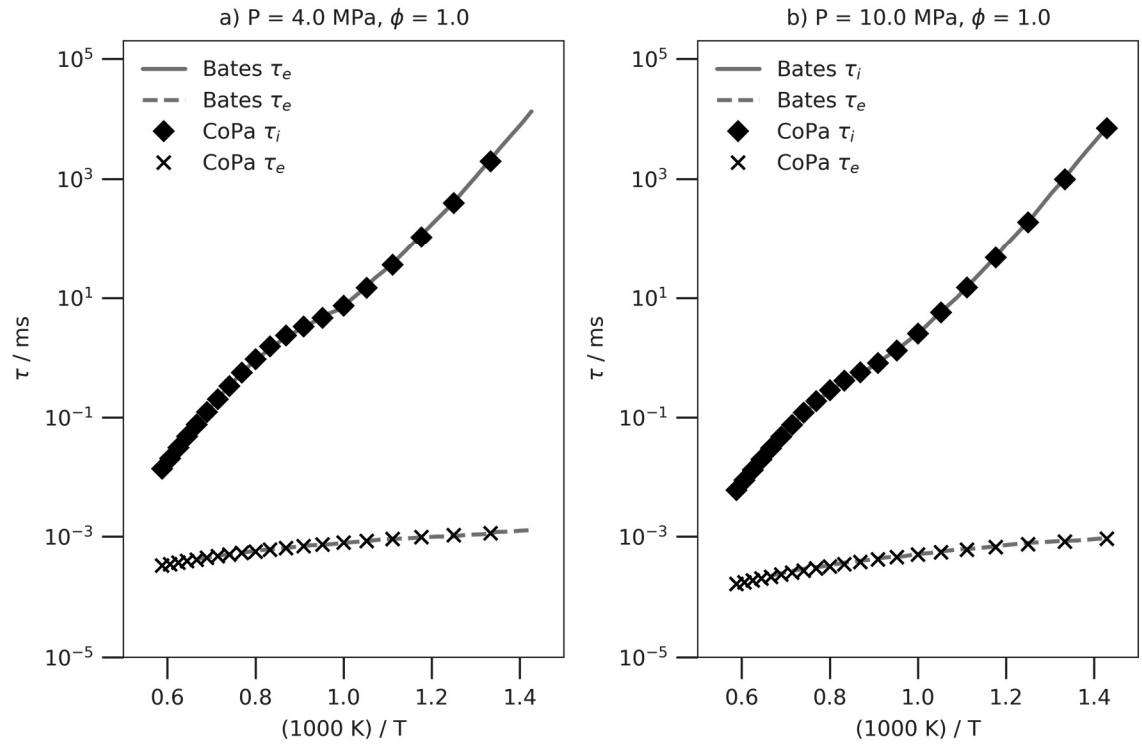

Figure 5-3: Verification of ignition delay and excitation time simulation for CH_4/air combustion; reference data from [71]

Table 5-3: Coefficients of determination r^2 for verification of the constant-volume reactor model[4]

Pressure	Mechanism	r^2 Ignition delay	r^2 Excitation time
0.1 MPa	GRI Mech 3.0	0.9741	-
	Mech 56.54	0.9909	-
4.0 MPa	GRI Mech 3.0	0.9779	-
	Mech 56.54	0.9632	0.9718
10.0 MPa	Mech 56.54	0.9650	0.9628

5.2.2 HCCI reactor

Due to the lack of well documented published reference data, the HCCI reactor model could not be directly verified with experimental or computed data. The model was therefore verified on a qualitative basis only, using data from Wise [96] obtained with the CHEMKIN

[4] The goodness of fit was evaluated in the temperature range of 750 K to 1 400 K

HCCI model. Wise applied the geometry of a CFR F-2 engine operating at 940 1/min with a variable compression ratio (CR) from 10:1 to 13:1. The fuel was a stoichiometric blend of H_2 40 vol%, CO 24 vol%, CH_4 10 vol%, CO_2 23 vol%, and N_2 3 vol% in air. The chemical mechanism applied in *this study* was Mech 56.54 from NUI Galway [72], whereas Wise used an older version of the NUI Galway natural gas mechanism.

The results are displayed in Figure 5-4. Since information about the exact initial conditions (pressure, temperature, settings for heat transfer model) was lacking and a different version of the chemical mechanism was used, the data of Wise could not be reproduced exactly. Thus, the values of r^2 were not evaluated in this case. Nevertheless the qualitative accordance is good and the relevant features of auto-ignition (timing, peak pressure), as well as the trends with increasing compression ratio are reproduced accurately, as can be seen from Figure 5-4.

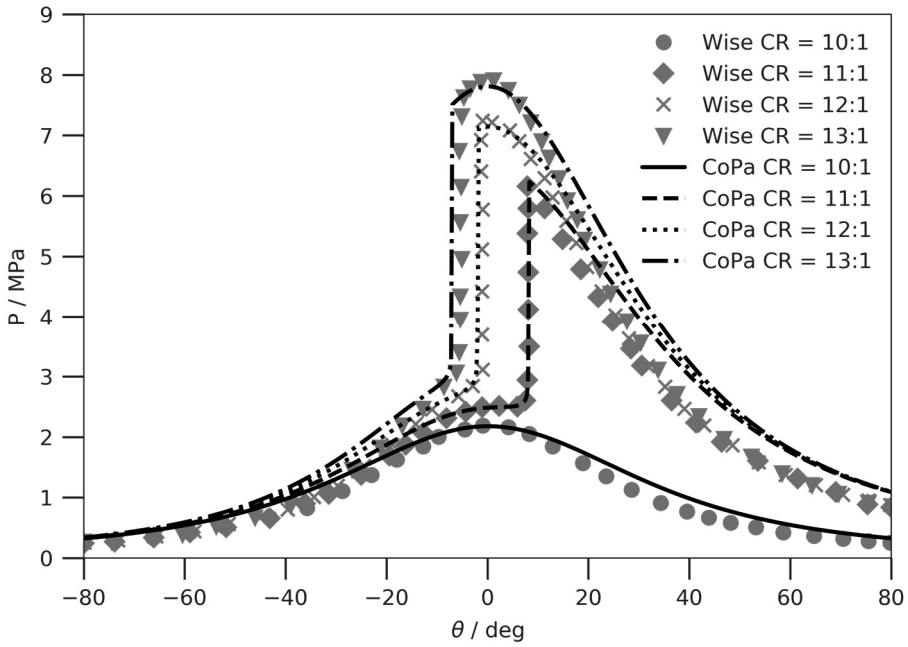

Figure 5-4: Verification of HCCI reactor model; reference data from [96]

5.2.3 Laminar flame speed

For verification of the laminar flame speed model, data from Hu et al. [70] was used. The authors present experimental data for methane/air combustion at elevated temperatures and pressures obtained from constant-volume-bomb measurements. In addition, they performed laminar flame speed simulations using the Premix code [187] with three different reaction mechanisms (GRI Mech 3.0 [54], USC Mech II [55] and AramcoMech 1.3 [59]). Hu et al. used mixture-averaged transport properties for computation.

The results of the verification are presented in Figure 5-5 for the GRI Mech 3.0 and the USC Mech II mechanisms. The experimental data provided by Hu and the simulation results obtained with the AramcoMech 1.3 mechanism were omitted here in favour of readability. The Cantera model implemented in the CoPa toolbox performs well against the Premix code applied by Hu. A slight over-prediction of laminar flame speed can be observed for low pressures and for higher temperatures. However, the deviations are generally less than 2 cm/s which is the in range considered accurate enough by Hu [70] and the general trends with regard to temperature, pressure and equivalence ratio are reproduced very well. This is also confirmed by the r^2-values (cf. Table 5-4). Again, minor deviations can be attributed to some extent to the quality of the reference data which was extracted from plots.

Table 5-4: Coefficients of determination r^2 for verification of the laminar flame model

Pressure	Temperature	r^2 GRI Mech 3.0	r^2 USC Mech II
	300 K	0.9960	0.9959
0.1 MPa	373 K	0.9977	0.9817
	443 K	0.9975	0.9947
0.2 MPa	300 K	0.9930	0.9983
0.5 MPa	300 K	0.9959	0.9990
1.0 MPa	300 K	0.9980	0.9991
2.0 MPa	300 K	0.9979	0.9985

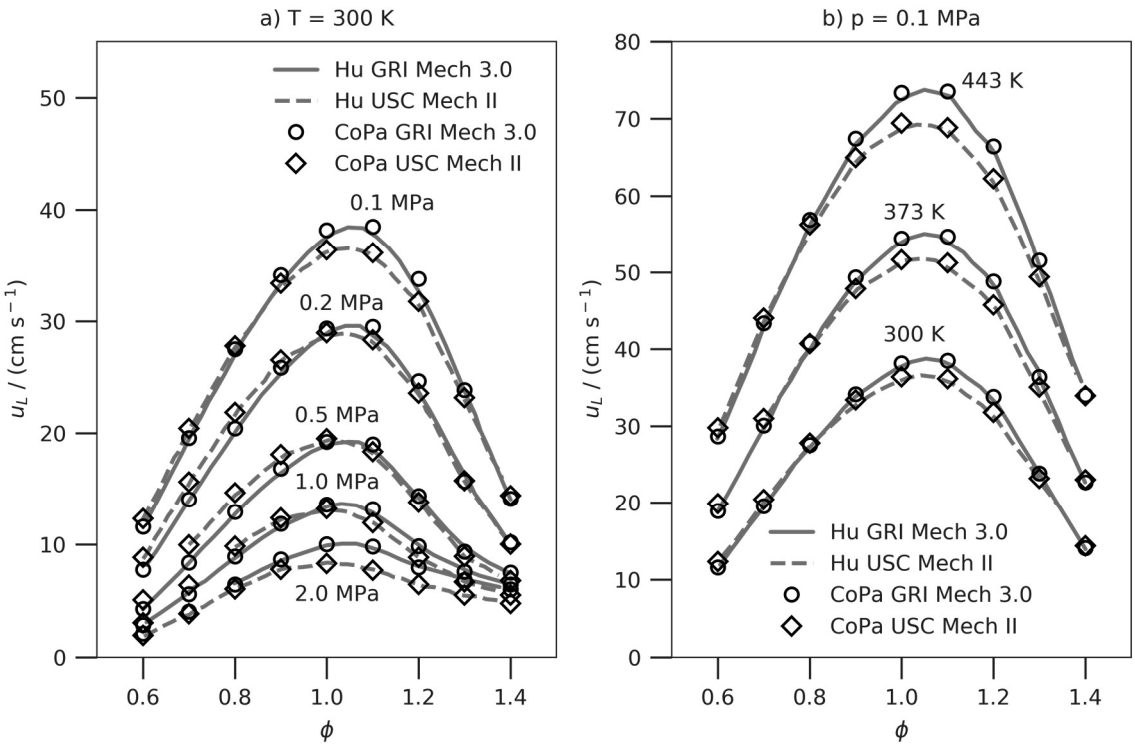

Figure 5-5: Verification of the laminar flame speed model; reference data from [70]

5.2.4 Exhaust gas recirculation

Only little reference data is available with regard to the influence of residual gas and exhaust recirculation on the characteristic combustion parameters. Hann et al. [21] published simulation data comparing the influence of residual gas and equivalence ratio on the laminar flame speed for methane/air combustion. The Cantera flame model with the GRI Mech 3.0 mechanism [54] was used for the calculations. Different temperatures from 300 to 1 000 K were considered with EGR ratios ranging from 0 to 40 wt% and stoichiometric to lean air/fuel equivalence ratios λ = 1.0…1.7 (inverse of fuel/air equivalence ratio $\lambda = 1/\phi$). The pressure was held constant at 0.1 MPa.

Comparative simulations with the CoPa toolbox EGR model show very good agreement with Hann's results for both the equivalence ratio and the EGR sweep[5] (see Figure 5-6 and values of r^2 in Table 5-5). Minor deviations can again be attributed to the reference data being digitised from plots.

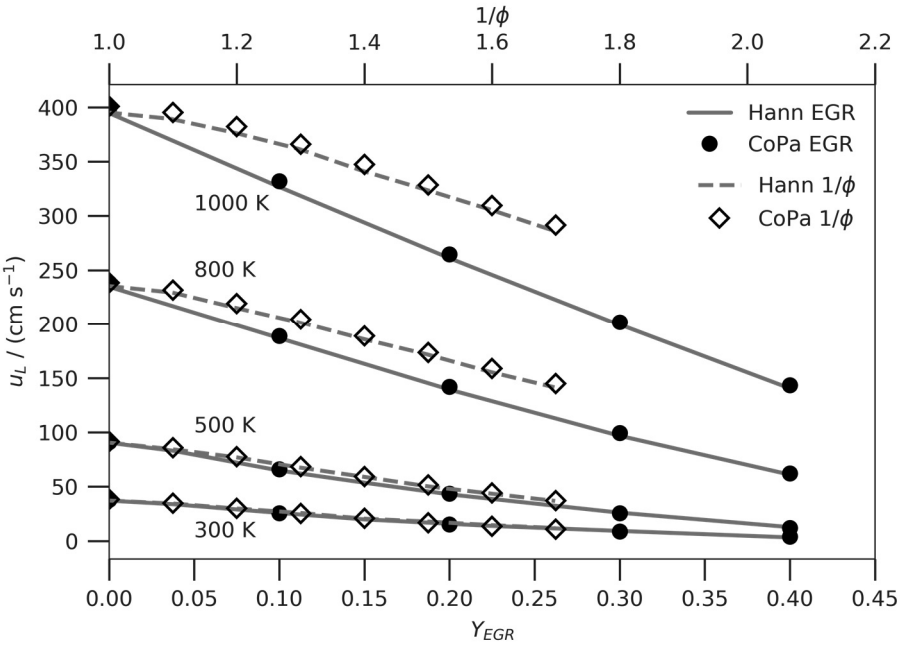

Figure 5-6: Verification of the EGR model; reference data from [21]

Table 5-5: Coefficients of determination r^2 for verification of the EGR model

Temperature	r^2 EGR	r^2 Equivalence ratio
300 K	0.9382	0.9983
500 K	0.9749	0.9996
800 K	0.9999	0.9996
1 000 K	1.0000	0.9997

[5] Hann does not explicitly state if EGR was considered on a dry or wet basis. However, the EGR results of Hann could not be reproduced exactly when assuming dry EGR, while the results with regard to the equivalence ratio were still in very good agreement. This implies that the laminar flame speed model itself performed correctly and the deviations were to be sought in the EGR definition. When assuming wet EGR the results match.

5.3 Computational settings

In order to achieve accurate and reproducible simulation results, it is necessary to determine the computational settings which deliver grid independent results. In the case of reactor simulations, this applies to the required time steps to resolve the time domain with sufficient accuracy to capture the relevant transients in temperature, pressure and species evolution. In the case of one-dimensional flame simulations, the grid resolves a space domain normal to the flame front which must be large enough to ensure that the gradients at the boundaries vanish (cf. section 4.4.2) and at the same time are sufficiently fine to resolve transients of the temperature and the species concentration in the flame front. Adaptive meshes were used both for the reactor and the flame simulations. Theses meshes are comparatively coarse in the beginning and are automatically refined by the solver in regions with high transients according to the defined tolerance levels. By this means, unnecessarily high resolutions in regions with steady-state conditions are avoided and the computation time is reduced.

According to Bates et al. [74] time meshes with steps of 1.0×10^{-7} to 1.0×10^{-10} seconds are required to ensure grid independent solutions for the ignition delay time in constant-volume reactor simulations and 1.0×10^{-12} to 1.0×10^{-14} seconds are needed to achieve grid independency for the excitation times. Since adaptive meshes are used, the time resolution is controlled by the absolute and relative error tolerance while integrating the reactor equations. Error tolerances of 1.0×10^{-9} (relative) and 1.0×10^{-15} (absolute) proved to be sufficient to ensure grid independent results while keeping the computation times at acceptable levels.

The heat release rate from the constant-volume reactor simulations was interpolated using cubic splines at the lower bound (5 % of the maximum heat release rate) in order to determine the excitation times τ_e (cf. [74]). The activation temperatures E/R according to Equation (4-92) were approximated by a least squares linear fit of the logarithmic ignition delay times $\ln \tau_i$ versus $1/T$ in the investigated temperature range.

For the HCCI reactor a fixed simulation step of 0.05 crank-angle degree was used, as proposed by Schultze et al. [69]. This leads to varying time steps according to the rotational speed (e.g., 8.33×10^{-6} s at 1 000 1/min and 2.78×10^{-6} s at 3 000 1/min).

For the laminar flame speed calculations mixture-averaged transport options were used due to computational costs. The associated loss of absolute accuracy is acceptable for the intended purpose of rating fuels qualitatively. In order to determine the necessary grid points in the one-dimensional mesh, a parametric study of grid refinement criteria was performed. The Cantera solver uses basically the same grid refinement approach as implemented in the CHEMKIN code, adding mesh points in regions where the solution has high gradient and curvature (see also [160, 187]). Thus, the number of grid points is controlled by setting the refinement criteria for the maximum difference in slope and curvature for adjacent grid points. Convergence of the flame speed within less than 0.5 % was achieved with about 400 to 500 grid points in most cases. This is accordance with the findings of Kéromnès et al. [58] who investigated syngas mixtures and reported a minimum of about 400 grid points necessary for convergence of laminar flame speed calculations.

A crucial task in kinetic modelling is the selection of suitable reaction mechanisms. Considering the composition of gases from thermo-chemical conversion (both gasification and pyrolysis) the reaction mechanism should include H_2, CH_4 and CO chemistry as well as higher hydrocarbons. Based on these criteria the comprehensive kinetic scheme developed at the Politecnico di Milano was chosen (cf. [65]). The mechanism is hierarchically organised and self-consistent submechanisms are available. In the majority of cases a reduced version of the POLIMI mechanism covering hydrocarbons up to C3 was applied. If hydrocarbons C4+ were present in the fuel an extended version covering primary reference fuels and real fuels was applied. For pure hydrogen the H_2/CO sub-scheme was used.

5.4 Summary

In order to compute the characteristic combustion parameters of combustible mixtures a modular, object-oriented software toolbox – the *Combustion Parameters toolbox (CoPa)* – was developed. The toolbox was implemented in *Python* language and builds upon the open source software package *Cantera*. The CoPa package offers a high-level interface to Cantera for performing automatised calculations with gas phase combustible mixtures of arbitrary fuels, oxidisers and residual gas. The implemented models were verified against literature data showing very good agreement.

Adaptive meshes were used both for the zero-dimensional reactor and the one-dimensional flame simulations in order to ensure accurate results while at the same time limiting computational cost. The computational settings were adjusted to deliver grid independent results. For the zero-dimensional reactor models relative and absolute error tolerances were set at 1.0×10^{-9} and 1.0×10^{-15}, respectively. The HCCI reactor simulations were carried out with a crank angle resolution of 0.05 degree. In the case of the one-dimensional flame, 400 to 500 grid points proved to be sufficient to achieve results with deviations of less than 0.5 % of the final value in most cases.

A hierarchical comprehensive kinetic scheme developed at the Politecnico di Milano was used for the simulations. Depending on the fuel constituents, either a hydrogen submechanism covering only H_2 and CO, or a hydrocarbon submechanism covering fuels up to C3, or an extended version covering also primary reference fuels and real fuels were applied.

Chapter 6 Analysis of fuel gas mixtures

6.1 Results of pyrolysis gas measurement

The results of the pyrolysis gas measurement performed at the TCR® 300 pilot plant are presented in Table 6-1. A total of six samples were taken during stationary operation of the plant. Since the measurements were performed on-site during an experimental campaign, they were subject to some restrictions arising from the test conditions and the limited time available for adapting the GC measurement method. Nevertheless the results prove to be valuable as they provide a first assessment of practical gas compositions from intermediate pyrolysis at industrial-scale production.

Compared to the published results obtained with laboratory scale TCR reactors (cf. Table 2-6) the H_2 content of the produced gas was lower, while the content of CH_4 and CO was considerably higher. This is due to the post-reformer operating at comparatively low temperatures at the investigated operating point. It should be noted that the CO content was determined from the balance of the mixture rather than from direct measurement due to the limited scan time available for the gas chromatography. However, the associated error is estimated to be small, since all other major components including N_2 were detected reliably.

The fraction of higher hydrocarbons consists mainly of C_2H_4 and C_2H_6 with C3 to C5 hydrocarbons all well below 1 vol%. A comparatively high fraction of C6+ was detected which could not be resolved in more detail with the applied measurement method. It cannot be precluded that the high absolute value of the C6+ peak is due to inaccuracies of the measurement. However, the fact that a C6+ signal found indicates that indeed higher hydrocarbons are present as vapour in the gas.

Table 6-1: Measured pyrolysis gas composition

Constituent	Sample					
	1	2	3	4	5	6
H_2	17.174	16.622	16.639	16.649	16.683	16.76
CO	21.68	18.339	18.36	21.1135	21.314	18.268
CH_4	13.235	14.437	14.425	13.133	13.193	14.464
CO_2	16.022	15.768	15.566	15.475	15.464	15.654
C_2H_4	1.739	1.605	1.773	1.779	1.780	1.726
C_2H_6	1.165	1.115	1.167	1.168	1.172	1.151
C_3H_8	0.354	0.346	0.356	0.352	0.354	0.348
iso-butane	0.084	0.081	0.080	0.101	0.083	0.079
iso-pentane	0.030	0.030	0.029	0.029	0.029	0.029
C6+	2.593	2.688	2.344	1.638	2.147	2.548
N_2	25.791	28.473	28.752	28.151	27.584	28.469
O_2	0.078	0.450	0.449	0.255	0.124	0.447
Helium	0.055	0.046	0.060	0.084	0.073	0.057

The measured N_2 content was comparatively high because the plant was inertised with nitrogen for the experiments. In long-term operation the nitrogen content in the gas is expected to be considerably lower and determined mainly by the nitrogen content of the feedstock. For *this study* the nitrogen fraction in the gas was, however, taken as measured. Oxygen and helium (carrier gas for the GC) were detected in trace concentrations. For the subsequent analyses, the average of the six samples was taken and a number of simplifications were made:

a) O_2 and He were neglected and the mixture was filled to 100 vol% with N_2

b) Iso-pentane was assigned to the C6+ fraction, forming a C5+ fraction

c) The primary reference fuels n-heptane and iso-octane were used as representatives of the C5+ fraction including iso-pentane, since the exact composition is not known

d) Three scenarios were considered for the C5+ fraction: 1) a knock-prone C5+ fraction represented by n-heptane; 2) a knock-resistant C5+ fraction represented by iso-octane; 3) the C5+ fraction set to zero and replaced by N_2

6.2 Fuel matrix and investigated conditions

The composition of biogenous fuel gases from thermo-chemical conversion can vary considerably according to the process settings and feedstocks (see section 2.3). A thorough assessment of the combustion characteristics must therefore cover a wide range of fuel compositions. Still there is a risk that some relevant effects and interactions will not be captured adequately with classical experimental methods (i.e., varying one parameter at a time).

Thus, a statistical *design of experiments (DoE)* approach was used to design a fuel matrix covering the relevant range of fuel compositions. The commercial software tool Cornerstone by camLine[6] was used for this purpose. Based on the published fuel data presented in section 2.3, a mixture plan was developed using a D-optimal experimental design with the constraints given in Table 6-2. The gas mixtures were assumed to consist of H_2, CO, CH_4, CO_2, and higher hydrocarbons up to C3. N_2 was used as filler to complete the mixture. C_2H_4, C_2H_6 and C_3H_8 were selected as representatives of higher hydrocarbons. A total of 31 gas mixtures was defined in the DoE plan. Additionally, pure methane, pure propane, pure hydrogen and a biogas mixture consisting of 60 vol% CH_4 and 40 vol% CO_2 were examined as reference fuels. The measured pyrolysis gas composition from the TCR process was considered in three scenarios as introduced in section 6.1.

The investigated fuel matrix is presented inTable 6-4. In order to simplify the nomenclature, the gas compositions #1 to #31 will henceforth be identified as *syngas* mixtures. The measured pyrolysis gas composition from the TCR® 300 pilot plant will be denominated *TCR gas* for differentiation. *Biogas* will be referred to with its full name and *hydrogen, methane* and *propane* with their full names or their chemical symbol for better readability in graphs.

[6] Version 7.1 http://www.camline.com/

For every fuel mixture a range of initial conditions was investigated, covering pressures and temperatures relevant to engine auto-ignition and knock (see Table 6-3). The equivalence ratios range from stoichiometric to ultra-lean with special consideration of the typical lean-operation window of gas engines $\phi = 0.55 \ldots 0.65$. The range of investigated conditions was narrowed for the flame speed calculations due to computational costs. The effects of exhaust gas recirculation and water vapour were examined separately for selected fuels within the range given in Table 6-3.

Table 6-2: Constraints for the DoE mixture plan

Component	Range / vol%
H_2	$0 \leq X_{H2} \leq 40$
CO	$0 \leq X_{CO} \leq 50$
CH_4	$0 \leq X_{CH4} \leq 15$
CO_2	$0 \leq X_{CO2} \leq 50$
C_2H_4	$0 \leq X_{C2H4} \leq 5$
C_2H_6	$0 \leq X_{C2H6} \leq 5$
C_3H_8	$0 \leq X_{C3H8} \leq 5$
N_2	Filler
$H_2 + CO$	$15 \leq X \leq 70$
$CO + CO_2$	$30 \leq X \leq 95$
$H_2 + CO + CH_4$	$30 \leq X \leq 80$
$C_2H_4 + C_2H_6 + C_3H_8$	$0 \leq X \leq 10$
$H_2 + CO + CH_4 + C_xH_y$	$40 \leq X \leq 100$
$H_2 + CO + CH_4 + CO_2 + C_xH_y + N_2$	$80 \leq X \leq 100$

Table 6-3: Investigated range of initial conditions

Parameter	Isochoric reactor	Laminar flame
Temperature	800, 850, 900, …, 1 400 K	800, 850, 900, …, 1 000 K
Pressure	1, 2, 4, 6, 8, 15 MPa	1, 2, 4, 8 MPa
Fuel/air equivalence ratio	1.0, 0.65, 0.5, 0.25	1.0, 0.5
Exhaust gas recirculation	0, 20, 40 vol%	–
Water vapour content	0, 20, 40 vol%	–

Table 6-4: Investigated fuel gas blends

Blend #	H_2 vol%	CO vol%	CH_4 vol%	CO_2 vol%	C_2H_4 vol%	C_2H_6 vol%	C_3H_8 vol%	C_xH_y vol%	N_2 vol%
1	15	50	15	10		5	5		
2	40	30	7.5	10		3.75	2.5		6.25
3		50		45	5				
4		32.5	7.5	50	2.5	2.5	5		
5	40	25	15	10	5		5		
6	10	10	15	40	2.5	2.5			20
7	20	10	15	50	2.5		2.5		
8	20	50		10		1.25			18.75
9	15	50	15	10	5				5
10	15.74	29.26	15	10	2.5	5	2.5		20
11		50		40		5	5		
12	40	10		20		5	5		20
13	40	30		20	5	5			
14	20	10		50	5	2.5	2.5		10
15	15	50		10	5		5		15
16	25	10		50		5			10
17		20	15	50	5	5			5
18	20	50	5	22.5			2.5		
19	5	10	15	40	5		5		20
20	40	10	15	20	5	5			5
21	40	25	15	20					
22	40	10		25	5				20
23	35	10		50			5		
24	5	10	15	50		5	5		10
25		50	5	15	5	5			20
26		30	11.25	50					8.75
27		50	15	25	5	2.5	2.5		
28		50	15	10			5		20
29	20	20	15	30		2.5	5		7.5
30		50	15	30		5			
31		35		40			5		20
32			100						
33			60	40					
34							100		
35	100								
36	16.75	19.85	13.81	15.67	1.73	1.16	0.35	2.45[a]	28.23
37	16.75	19.85	13.81	15.67	1.73	1.16	0.35	2.45[b]	28.23
38	16.75	19.85	13.81	15.67	1.73	1.16	0.35	0.09[c]	30.59

a) iso-C_4H_{10} 0.09 vol%, n-C_7H_{16} 2.36 vol%
b) iso-C_4H_{10} 0.09 vol%, iso-C_8H_{18} 2.36 vol%
c) iso-C_4H_{10} 0.09 vol%

6.3 Energy content and stoichiometric air requirement

The limiting parameter for the power output of a given engine design with a specific fuel is the amount of energy that can be theoretically released from the combustible mixture captured in the cylinder. This value is determined by a) the heating value of the fuel and b) the stoichiometric air requirement, that is, the amount of air per unit of fuel that is minimally required to oxidise the fuel mixture completely consuming all the oxygen available. The key parameter for gas engines in this regard is the volumetric heating value of the combustible mixture at a specific equivalence ratio, since this will dictate how much energy can be trapped in a cylinder of a given volume.

In Figure 6-1 the lower heating values (LHV) of the investigated fuels are plotted against the LHV of the resulting combustible mixtures for stoichiometric and lean fuel/air equivalence ratios. The values are given on mass basis (left) and on volume basis (right) for standard conditions of 273 K and 0.1 MPa. The size of the markers indicates the stoichiometric air/fuel-requirement on mass (left) and mole basis (right). It is apparent that despite the comparatively wide spread of the fuel heating values, the LHV of the resulting fuel-air-mixtures is in a narrow range, especially for lean equivalence ratios, where the dilution with excess air is the determining factor. This observation can be attributed to the fact that the high-calorific fuels also require a comparatively high amount of air for combustion which can be most prominently observed for hydrogen (on mass basis) and propane (on volume basis).

The volumetric heating value of the fuel-air-mixture of the TCR gas blends #36 and #37 is at least on a par with biogas from anaerobic digestion at stoichiometric conditions and even slightly better than pure methane for lean mixtures[7]. This implies that engines operated with TCR gas will essentially be able to deliver the same power output as conventional biogas or natural gas engines, if not limited by other constraints, such as engine knock.

[7] TCR fuel blend #38 was omitted for better readability

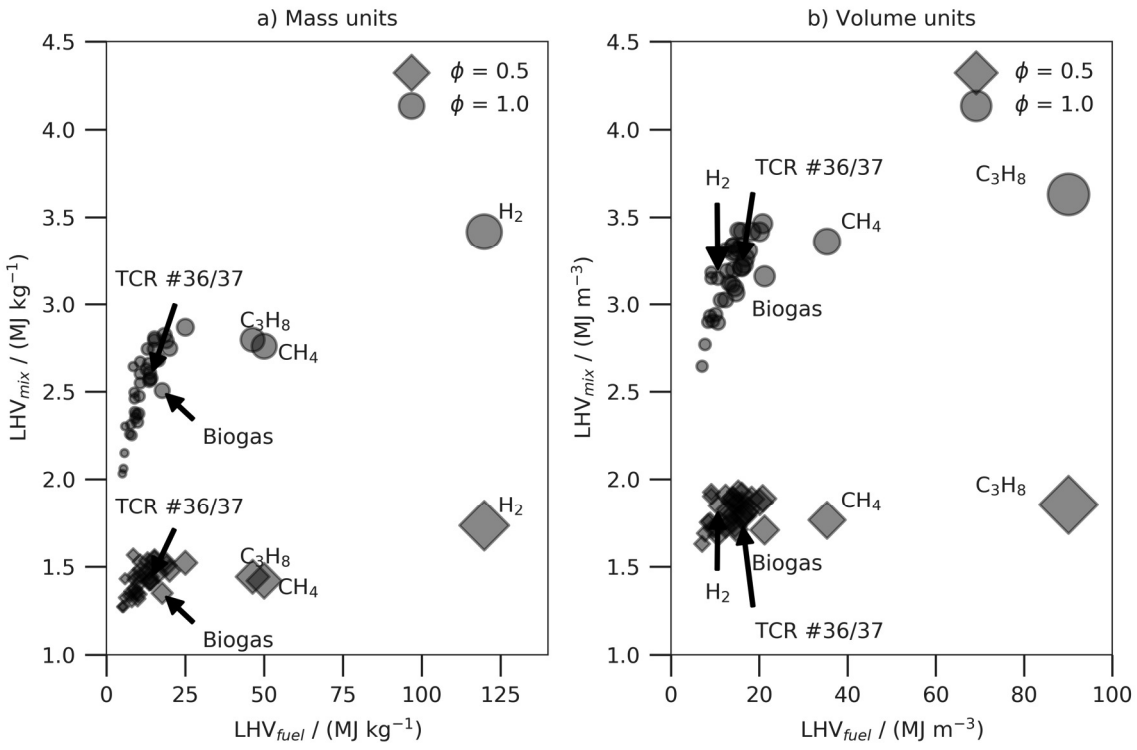

Figure 6-1: Heating value of mixture versus heating value of fuel in a) mass units, b) volume units; size of markers indicates stoichiometric air requirement

6.4 Methane number

The methane numbers of the investigated fuel blends according to Table 6-4 were determined with three different methods using calculator tools available from MWM, Cummins Westport and DNV. The results are displayed in Table 6-5.

First, the MWM method with the computer program provided by EUROMOT [143] was applied. The calculator was in principle able to handle the provided fuel gas compositions in all cases but one, where the calculation failed (fuel blend #25). However, the calculator issued a warning concerning the confidence of the result in half of the cases (cf. Table 6-5) which limits the practical applicability of the method for syngas blends.

The Cummins Westport Fuel Quality Calculator [146] and the DNV Propane Knock Index calculator tool [148] were not able to handle the provided gas compositions in most of the cases, since C_2H_4 is not supported as constituent and either H_2, CO, CH_4 or CO_2 were outside the range of validity. In the case of the DNV Propane Knock Index, the calculation succeeded for pure methane only. Thus, both tools can be considered as not appropriate for the given syngas compositions.

These findings confirm that the existing methods for rating fuel gases based on the methane number or knock index are severely limited with regard to their applicability for syngas blends and need to be supplemented by additional, more advanced methods based on the actual reaction kinetics of the fuel.

Table 6-5: Methane number of the investigated fuel gas blends

Blend	MWM		Cummins		DNV	
#	MN	Comment	MN	Comment	PKI	Comment
1	65	MN not confident	51	Failed H_2 > 0.03 %	-	CO outside range of validity
2	49		30	Failed H_2 > 0.03 %	-	CH_4, CO, H_2 outside range of validity
3	114	MN not confident	-	C_2H_4 not supported	-	C_2H_4 not supported
4	116	MN not confident	-	C_2H_4 not supported	-	C_2H_4 not supported
5	44		-	C_2H_4 not supported	-	C_2H_4 not supported
6	101		-	C_2H_4 not supported	-	C_2H_4 not supported
7	91		-	C_2H_4 not supported	-	C_2H_4 not supported
8	66	MN not confident	57	Failed H_2 > 0.03 %	-	CO, CH_4 outside range of validity
9	66	MN not confident	-	C_2H_4 not supported	-	C_2H_4 not supported
10	64	MN not confident	-	C_2H_4 not supported	-	C_2H_4 not supported
11	109	MN not confident	200		-	CO_2, CO, CH_4 outside range of validity
12	52		49	Failed H_2 > 0.03 %	-	CH_4, H_2 outside range of validity
13	52		-	C_2H_4 not supported	-	C_2H_4 not supported
14	83		-	C_2H_4 not supported	-	C_2H_4 not supported
15	65	MN not confident	-	C_2H_4 not supported	-	C_2H_4 not supported
16	86		197	Failed H_2 > 0.03 %	-	CH_4, CO_2, H_2 outside range of validity
17	113	MN not confident		C_2H_4 not supported	-	C_2H_4 not supported

Table 6-5 (continued)

Blend	MWM methane number		Cummins methane number		DNV propane knock index	
#	MN	Comment	MN	Comment	PKI	Comment
18	75	MN not confident	74	Failed H_2 > 0.03 %	-	CO_2, CO, CH_4 outside range of validity
19	96	MN not confident	-	C_2H_4 not supported	-	C_2H_4 not supported
20	54		-	C_2H_4 not supported	-	C_2H_4 not supported
21	62		53	Failed H_2 > 0.03 %	-	CO, CH_4, H_2 outside range of validity
22	46			C_2H_4 not supported	-	C_2H_4 not supported
23	74		143	Failed H_2 > 0.03 %	-	CO_2, H_2, CH_4 outside range of validity
24	105		186	Failed H_2 > 0.03 %	-	CO_2, CH_4 outside range of validity
25	-	MN invalid	-	C_2H_4 not supported	-	C_2H_4 not supported
26	137	MN not confident	215		-	CO, CO_2, CH_4 outside range of validity
27	91	MN not confident	-	C_2H_4 not supported	-	C_2H_4 not supported
28	80	MN not confident	89		-	CH_4, CO outside range of validity
29	79		100	Failed H_2 > 0.03 %	-	CO, CO_2, CH_4 outside range of validity
30	102	MN not confident	131		-	CO, CO_2, CH_4 outside range of validity
31	120	MN not confident	263		-	CO, CO_2, CH_4 outside range of validity
32 (Methane)	99		100		100	
33 (Biogas)	139		141		-	CH_4, CO_2 outside range of validity
34 (Propane)	34		32		-	CH_4, C_3H_8 outside range of validity
35 (Hydrogen)	1		-	Failed H_2 > 0.03 %	-	H_2 outside range of validity
36 (TCR)	49	MN not confident due to high content of C > C4	-	C_2H_4 not supported	-	C_2H_4 not supported
37 (TCR)	49	MN not confident due to high content of C > C4	-	C_2H_4 not supported	-	C_2H_4 not supported
38 (TCR)	73		-	C_2H_4 not supported	-	C_2H_4 not supported

6.5 Critical compression ratio

Following Wise [96] and Montoya [156] the geometry of a CFR F-2 fuel research engine was used for the determination of the critical compression ratio applying the HCCI reactor model. The initial conditions were set to those of the MON test (cf. Heywood [17] and Wang [77]). The evaluated crank angle range was 360° with a resolution of 0.05° and the compression ratio was automatically varied until auto-ignition at the top dead centre (180° crank angle) occurred. The respective compression ratio was taken as the critical compression ratio CR_c. Heat transfer was not considered (adiabatic reactor). The POLIMI hierarchical kinetic mechanism was used. A summary of the simulation settings is given in Table 6-6.

Table 6-6: HCCI reactor simulation settings for determining CR_c

Parameter	Value
Bore	8.255 cm
Stroke	11.43 cm
Displacement	611.7 cm³
Ratio connecting rod length to crank radius	4.44
Rotational speed	900 1/min
Initial pressure	0.1 MPa
Initial mixture temperature	422 K
Fuel/air equivalence ratio	1.0, 0.5
Evaluated crank angle range / resolution	360° / 0.05°
Auto-ignition crank angle	180° (top dead centre)
Heat transfer	adiabatic
Mechanism	POLIMI[8]

[8] POLIMI C1-C3 high and low temperature mechanism for fuel blends #1 to #34, H_2/CO mechanism for blend #35 (hydrogen) and Primary Reference Fuels (PRF) + PAH + Real Fuels mechanism for the TCR gas blends #36 to #38, all version 1412, December 2014

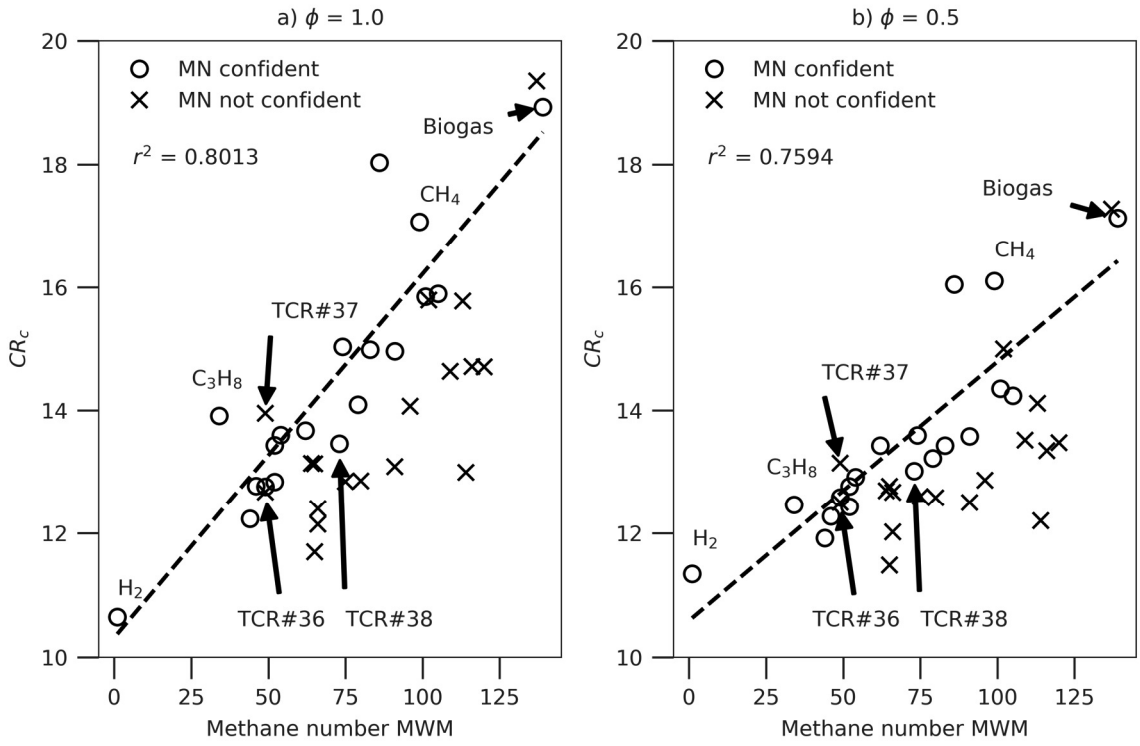

Figure 6-2: Critical compression ratio versus methane number at a) ϕ = 1.0 and b) ϕ = 0.5

The results of the simulation are presented in Figure 6-2 for a) stoichiometric and b) lean mixtures. When sorting out the non-confident MN values (cf. section 6.4), a strong linear correlation between the MWM methane number and the critical compression ratio can be observed for both equivalence ratios. Although the r^2-values are high (r ≈ 0.76…0.80), there is still considerable scatter in the data which does not allow for an unambiguous assignment of the calculated CR_c to a specific value of MN.

The TCR gas blends generally exhibit lower values of CR_c than the average of the investigated fuels, which indicates that they are more prone to auto-ignition and probably knock. As expected, the "knock-resistant" blend #37, which contains iso-octane as representative of higher hydrocarbons, features a higher critical compression ratio than blend #36, to which n-heptane was added. It is interesting that blend #38, in which the C5+ hydrocarbons were replaced by nitrogen and which should be the most knock-resistant of the TCR blends, has

in fact a considerably higher methane number than blend #37, as expected, but shows a slightly lower critical compression ratio. A possible reason for this contradictory behaviour is that the resulting fuel-air-mixture for blend #38 has a higher heat capacity ratio (isentropic expansion coefficient) than that for blend #37, which implies that the temperature and pressure conditions required for auto-ignition are already attained at a lower compression ratio[9]. This might provoke the misconception that blend #38 is more reactive than blend #37, although in fact the lower CR_c is due to thermodynamic effects rather than reaction kinetics.

The same applies to the critical compression ratios obtained for the lean mixtures which are generally lower for most fuels with the exception of hydrogen, compare Figure 6-2 a) versus Figure 6-2 b). Again, these findings can be attributed rather to the heat capacity ratio, which is higher in case of the lean mixtures, than to chemical kinetics. The opposite is true for hydrogen, which explains why in this case CR_c increases when the mixture is leaned.

Because of the overlying thermodynamic effects and other uncertainties, it is not possible to establish a clear link between the critical compression ratio obtained from the HCCI reactor simulation and the calculated methane number for the investigated syngas blends. In fact, fuels with almost identical methane number can exhibit very different values of CR_c, as can be seen from Figure 6-2. However, it should be considered that the methane number itself might not be an accurate measure for the knock propensity of syngas fuels, even if the values are marked as confident in Figure 6-2, since the method was developed primarily for natural gas blends and is not well defined for blends with high shares of hydrogen and carbon monoxide (cf. [69, 96]).

It should also be noted that in the present case, a lower critical compression ratio does not necessarily imply a higher tendency to knock in real engine operation since the HCCI reactor simulation essentially reproduces a homogenous, strong auto-ignition. By contrast,

[9] A higher heat capacity ratio c_p/c_v causes a larger rise of pressure and temperature during compression.

according to the detonation theory knock in the unburned end gas is associated primarily with the auto-ignition propagation from secondary hot spots (cf. [23, 24]) and not with the homogenous auto-ignition of the mixture. Considering its several shortcomings it can be concluded that the critical compression ratio obtained from ideal HCCI reactor simulations is only partially suitable as parameter for assessing the reactivity and knock propensity of syngas blends and must be complemented by additional experimental or numerical methods in order to yield robust results.

6.6 Auto-ignition parameters and laminar flame speeds

6.6.1 Ignition delay and excitation times

The calculated ignition delay times τ_i for the investigated fuels are displayed in the Arrhenius plots – Figure 6-3 to Figure 6-6 – for stoichiometric and lean equivalence ratios ϕ = 1.0 to ϕ = 0.25 at pressures from 1.0 MPa to 15.0 MPa. All values were obtained from constant-volume reactor simulations applying the methodology introduced in section 4.3 and the computational settings presented in section 5.3 with the POLIMI C1-C3 mechanism[10]. The range of ignition delay times covered by the syngas blends #1 to #31 is marked as shaded area in the figures, and the respective blends that confine this area are given in the legend. The reference fuels #32 to #35 (methane, biogas, propane, hydrogen) and the TCR gas blends #36 to #38 are represented by individual lines.

At stoichiometric conditions, the upper boundary of the shaded area (long ignition delay) is determined at all investigated pressures by fuel blend #26 which consists of 30 vol%, 11.25 vol% CH_4, 50 vol% CO_2 and 8.74 vol% N_2. The lower bound (short ignition delay) is determined by fuel blend #3 (CO 50 vol%, CO_2 45 vol%, C_2H_4 5 vol%) with the exception

[10] POLIMI C1-C3 high and low temperature mechanism version 1412, December 2014

of P = 15 MPa, where fuel blend #15 marks the lower limit (H_2 15 vol%, CO 50 vol%, CO_2 10 vol%, C_2H_4 5 vol%, C_3H_8 5 vol%, N_2 15 vol%).

The fuels which contain CH_4 but no higher hydrocarbons (e.g., pure methane, biogas or fuel blend #26) generally feature the longest ignition delay times. A deviation from the straight line Arrhenius behaviour can be observed for these fuels at high temperatures and low pressures, indicated by a curvature in the ignition delay plot. With rising pressure, the ignition delay times reduce and approximately follow a linear Arrhenius behaviour.

Another group of fuels is formed by the blends containing higher hydrocarbons, such as pure propane, syngas blends #3 and #15 and the TCR blends #36 and #37. These fuels generally feature much lower ignition delay times than the methane group fuels. The ignition delay times further reduce with rising pressure and generally follow a linear Arrhenius behaviour at high temperatures. An exception is found for TCR blend #36 which contains n-heptane as representative of higher hydrocarbons. Here, a strong deviation from the straight line Arrhenius behaviour can be found at low temperatures which persists over the whole pressure range and does not normalise at higher pressures. By contrast, TCR blend #38 – which features exactly the same composition as blend #36 except for the higher hydrocarbons – shows an almost perfectly linear Arrhenius behaviour. Thus, the deviation from the straight line Arrhenius behaviour can be attributed to the fraction of n-heptane in the fuel. These findings suggest that TCR blend #36 features a negative temperature coefficient as is known for pure n-heptane (cf. [31]), which, however, could not be captured entirely in the present simulations due to the limited temperature range. A similar behaviour is observed for pure propane at high pressures, albeit less pronounced.

Pure hydrogen takes a special position between the two groups of fuels described above. The ignition delay times follow approximately a linear Arrhenius behaviour, although with a steeper slope than compared to the other fuels, resulting in ignition delay times which are

amongst the shortest at high temperatures, but close to those of the methane group fuels at low temperatures. As opposed to the other fuels the ignition delay times do not necessarily decrease with increasing pressure, but might increase instead, especially in the high temperature range. This can probably be attributed to a chain terminating reaction which moderates the explosion condition at high pressures [68].

The general trends described above persist for lean equivalence ratios down to $\phi = 0.25$ (cf. Figure 6-4 to Figure 6-6). With rising levels of dilution a global increase of ignition delay times for all fuels can be observed, accompanied by a reduced spread between the shortest and longest ignition delay times. The syngas blend #26 marks the upper limit of the shaded area in all cases and either blend #3 or blend #15 confine its lower boundary. In one case (P = 8.0 MPa at $\phi = 0.25$) blend #14 marks the lower limit instead of blend #15, but this should not be over-interpreted, since both fuels are similar in terms of ignition delay. The ignition delay curves increasingly approach a straight line Arrhenius behaviour with rising level of dilution. Still, pure propane and TCR blend #36 present an exception in this regard, but less pronounced than at stoichiometric conditions.

The second important auto-ignition parameter to be analysed is the excitation time τ_e. The calculated excitation times for the investigated fuel blends are exemplified in Figure 6-7 and Figure 6-8 for stoichiometric ($\phi = 1.00$) and very lean conditions ($\phi = 0.25$). Generally, the dependency of the excitation times on temperature and pressure is much less pronounced than it is for the ignition delay times. However, the excitation times are much more influenced by the level of dilution with excess air. From $\phi = 1.00$ to $\phi = 0.25$ the values of τ_e increase by about two orders of magnitude in the low temperature range and by about one order of magnitude in the high temperature range. With rising level of dilution the temperature dependency of the excitation times increases (cf. Figure 6-8). Still, the gradients $\Delta ln\tau_e/\Delta T$ are by two orders of magnitude less than the gradients $\Delta ln\tau_i/\Delta T$.

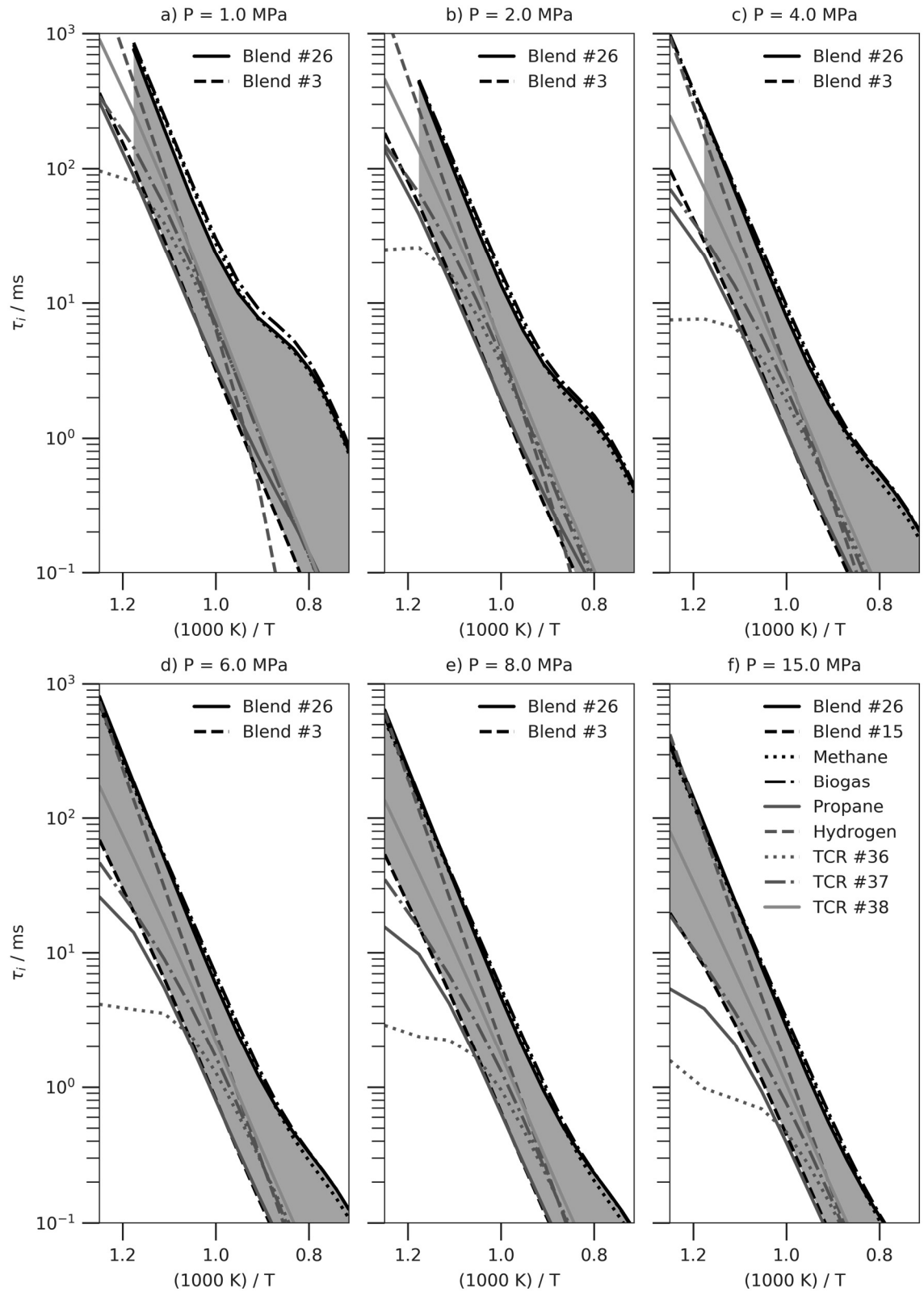

Figure 6-3: Ignition delay times at ϕ = 1.00

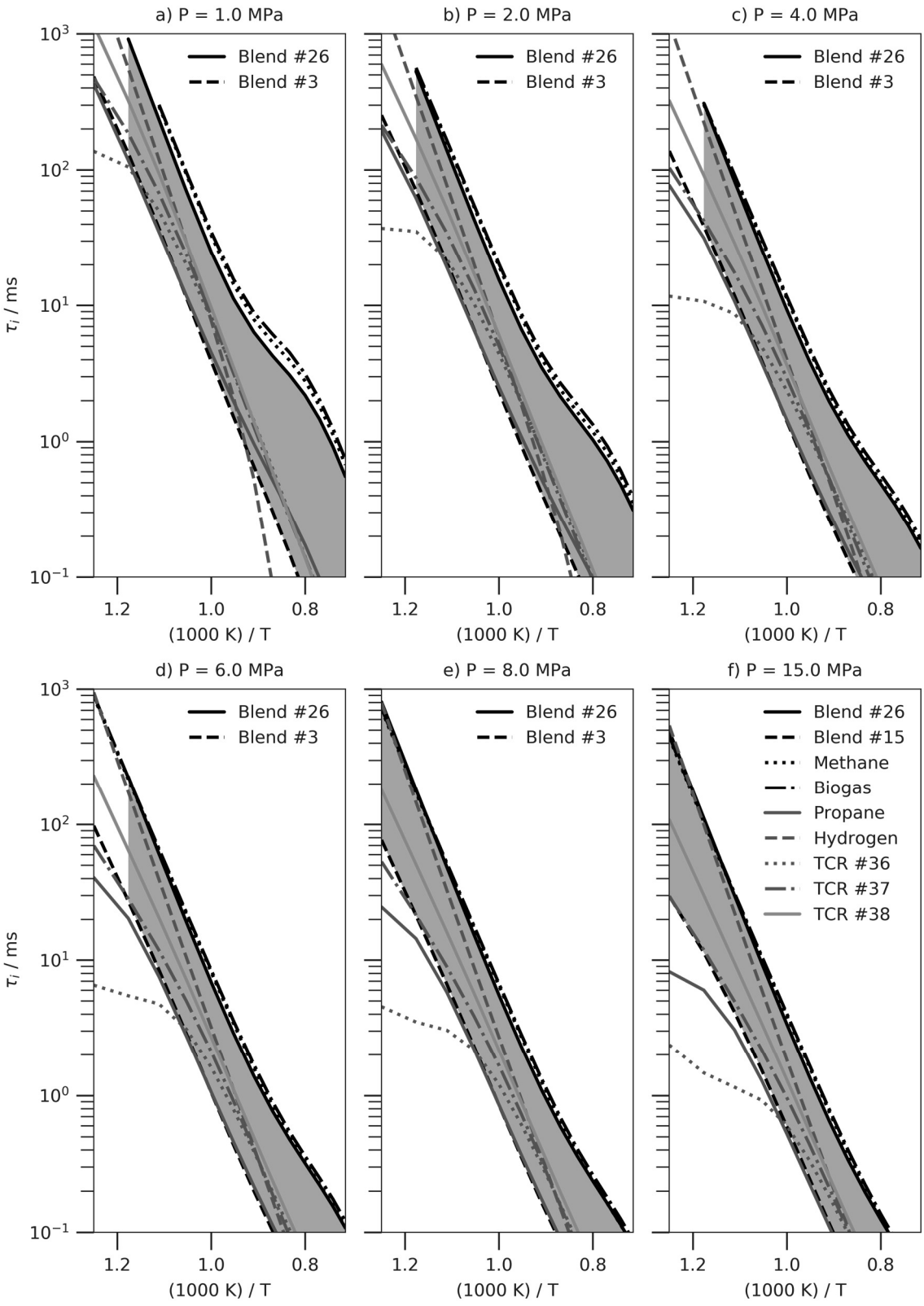

Figure 6-4: Ignition delay times at ϕ = 0.65

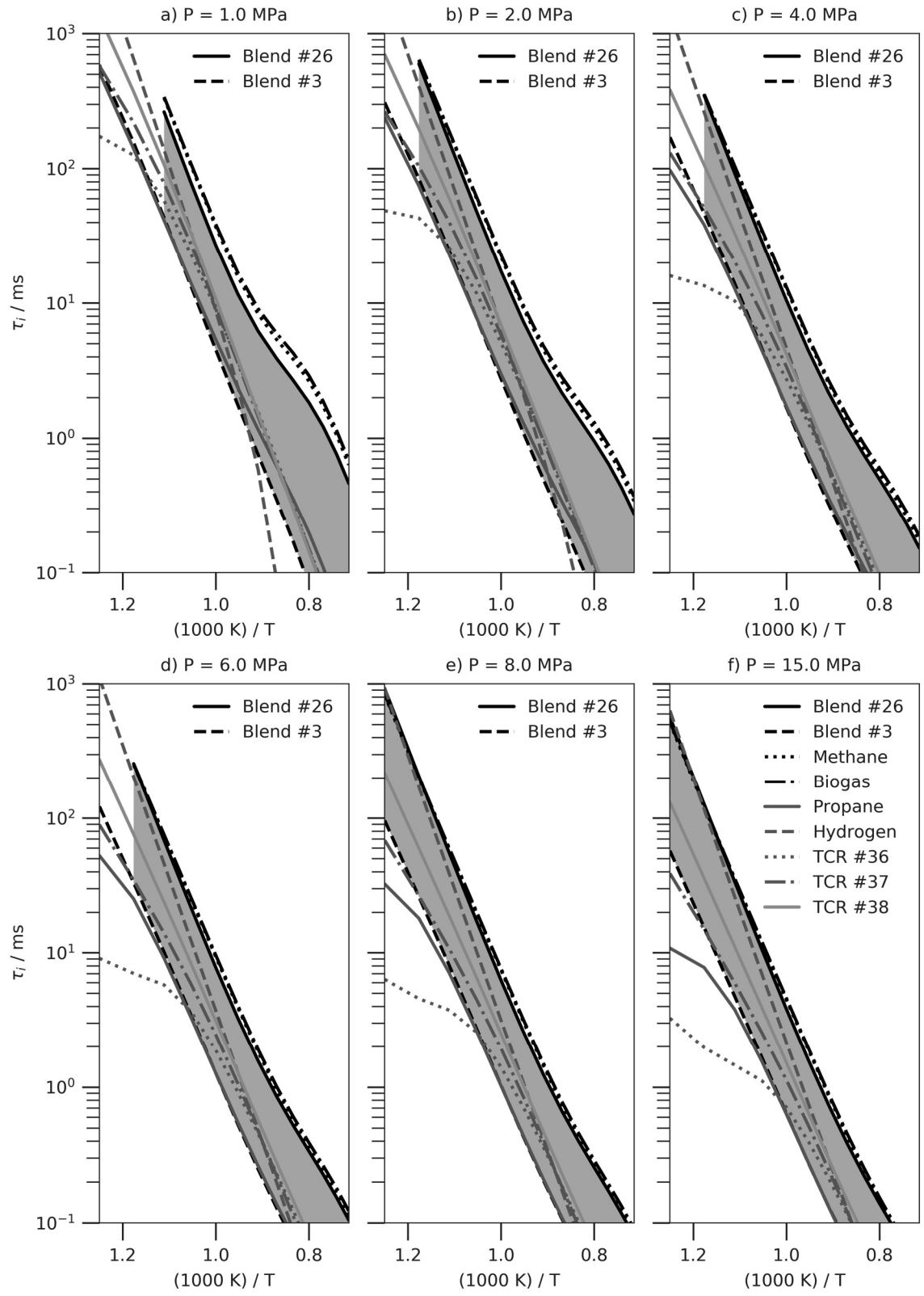

Figure 6-5: Ignition delay times at ϕ = 0.50

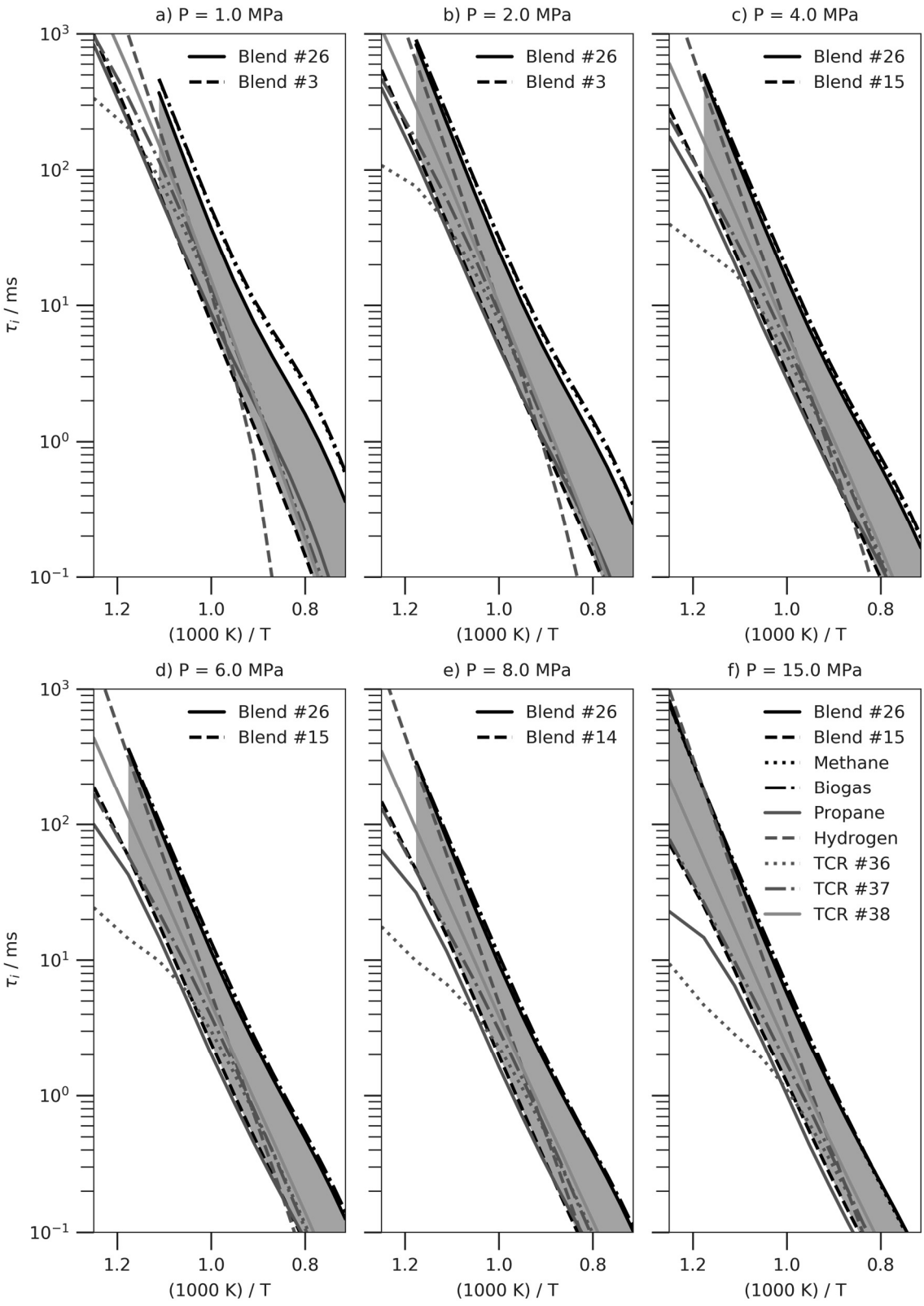

Figure 6-6: Ignition delay times at ϕ = 0.25

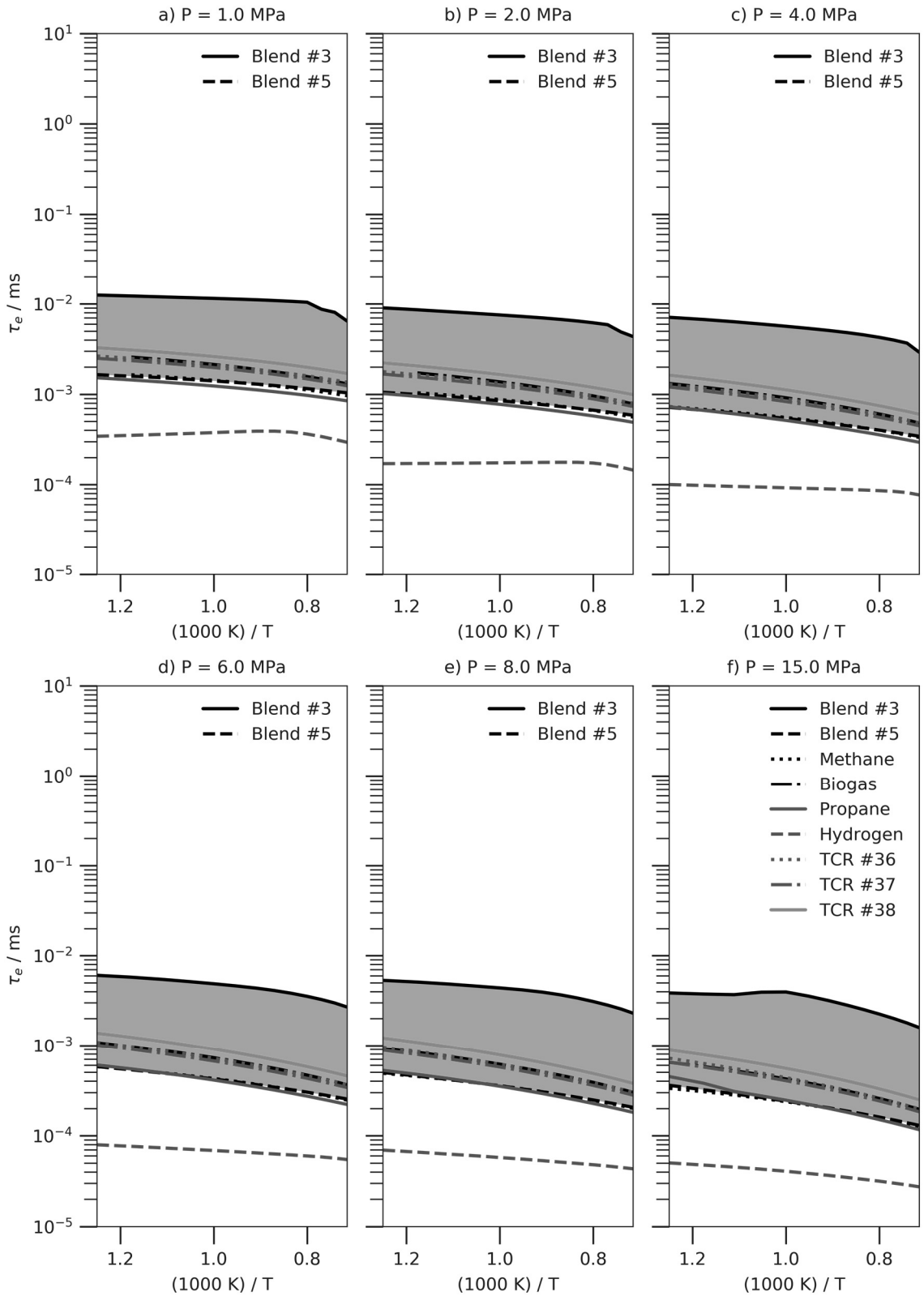

Figure 6-7: Excitation times at ϕ = 1.00

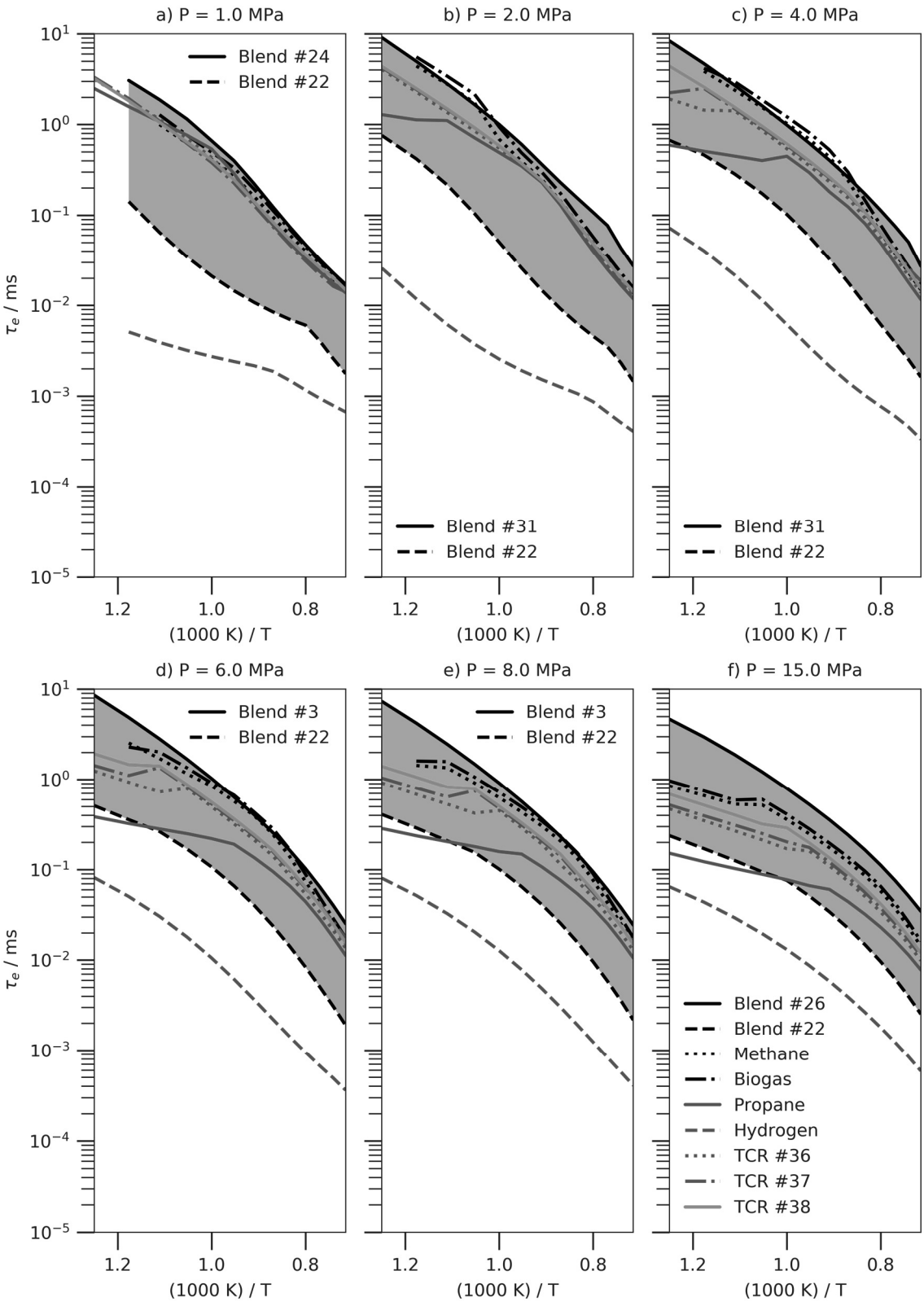

Figure 6-8: Excitation times at $\phi = 0.25$

Hydrogen features by far the lowest excitation times of all fuels throughout the whole investigated range of conditions, followed by fuel blend #5 at ϕ = 1.00 and fuel blend #22 at ϕ = 0.25. Blend #3 marks the upper limit at ϕ = 1.00, while at ϕ = 0.25 the upper limit is confined by fuel blends #3, #24, #26 or #31, depending on the particular pressure. When analysing the composition of these blends, it becomes obvious that the fuels with low excitation times generally feature low levels of dilution and/or high shares of hydrogen, while the fuels with large excitation times contain little to no hydrogen and feature higher levels of dilution in a CO_2 range from 40 to 50 vol%. The reference fuels as well as the TCR blends feature excitation times in the lower to medium range at ϕ = 1.00, while at ϕ = 0.25 the excitation times are in the middle to upper range compared to the other fuels.

The ignition behaviour of fuel blend #3 is contradictory at first glance. Its ignition delay times are among the shortest, while the excitation times are among the longest of all investigated fuel blends. This is due to its particular composition which reproduces a heavily diluted syngas consisting mainly of CO and CO_2 and a minor fraction of higher hydrocarbons, as occurs in some processes (cf. [125, 138]). It is known that small concentrations of hydrogen-containing materials appreciably catalyse the oxidation of CO which would otherwise be extremely difficult to ignite [68]. In this particular case, the higher hydrocarbons are represented by C_2H_4 which ignites and oxidises comparatively fast, forming water and other hydrogen containing species which catalyse the subsequent slower oxidation of CO. Thus, the ignition delay time is determined primarily by the small fraction of C_2H_4, while the excitation time is determined by the comparatively slow oxidation of the CO fraction which is responsible for most of the heat release.

Altogether, the results for the ignition delay times suggest that – compared to pure methane and biogas – most of the syngas and TCR gas blends are more reactive in terms of

auto-ignition propensity. The presence of higher hydrocarbons additionally enhances the reactivity and may also induce a negative temperature coefficient which has to be considered in the design of combustion systems. The ignition delay times are strongly dependent on temperature, while the effects of pressure and equivalence ratio are less pronounced. By contrast, the excitation times are influenced primarily by the heat release rate during oxidation of the fuel and are strongly dependent on the equivalence ratio, while the influence of pressure and temperature is less. This fundamentally different behaviour of the two characteristic parameters τ_i and τ_e implies that neither of them is a reliable indicator for assessing the reactivity and knock propensity of fuels when applied individually. Instead, they must be evaluated in a broader context. This can be accomplished by means of the ξ-ε diagram for fuels, as will be shown later.

6.6.2 Laminar flame speed

In Figure 6-9 and Figure 6-10 the laminar flame speeds of the investigated fuels are presented for stoichiometric (ϕ = 1.00) and lean equivalence ratios (ϕ = 0.50) for pressures from 1.0 MPa to 8.0 MPa respectively. The values were obtained from flame simulations with the POLIMI C1-C3 mechanism[11] and comprise the fuel blends #1 to #35. The TCR gas blends #36 to #37 were omitted due to the computational costs of flame simulations with the detailed kinetic mechanism for real fuels. These calculations should be the subject of future work with more computational resources or reduced kinetic schemes. It should be noted that in contrast to other investigations which focus on low temperature and pressure conditions, the flame simulations were carried out for temperatures and pressures up to 1 000 K and 8.0 MPa in an attempt to reproduce the conditions at the end of compression and during the beginning of combustion in modern turbocharged high speed gas engines.

[11] POLIMI C1-C3 high temperature mechanism version 1412, December 2014

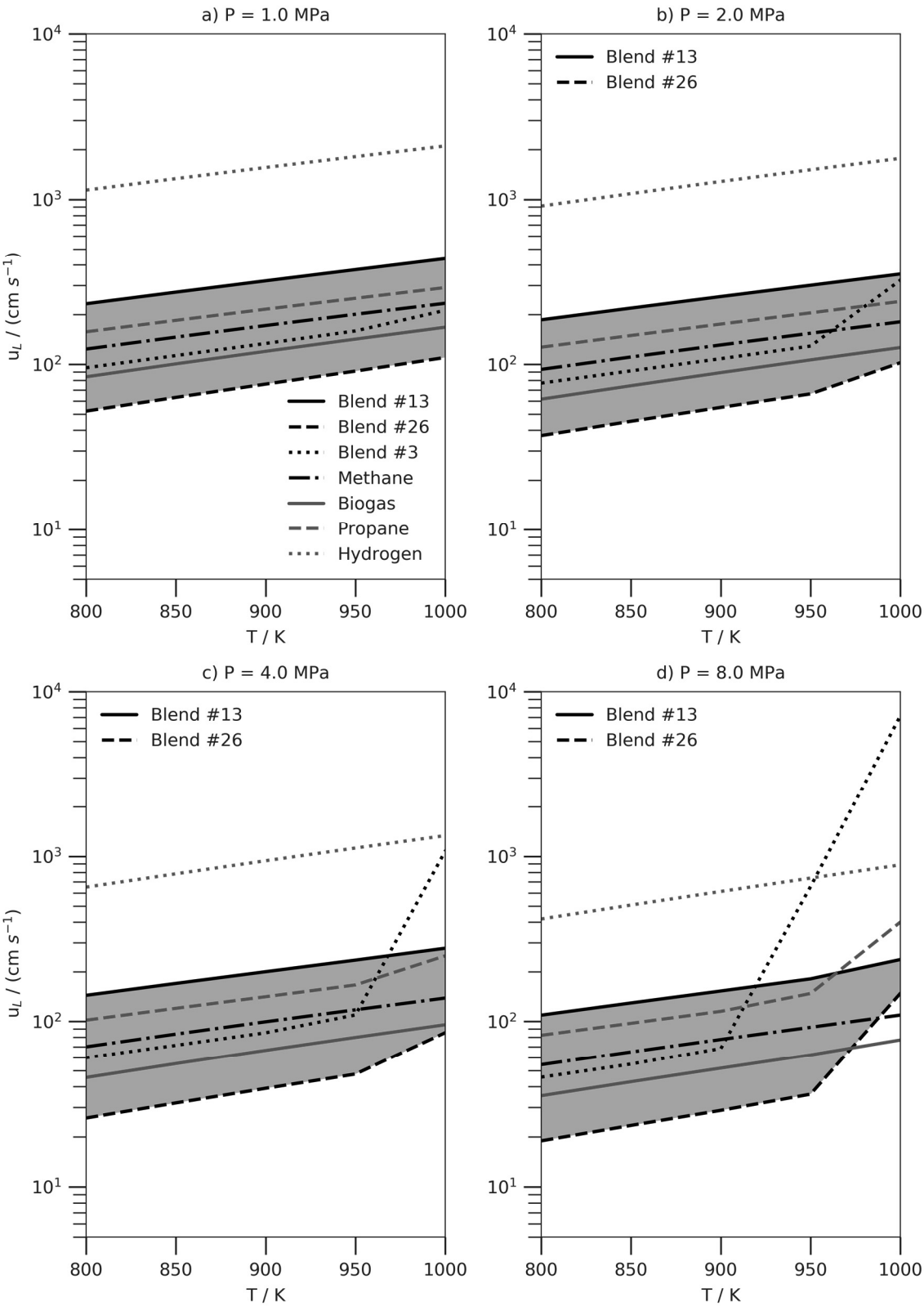

Figure 6-9: Laminar flame speeds at ϕ = 1.0

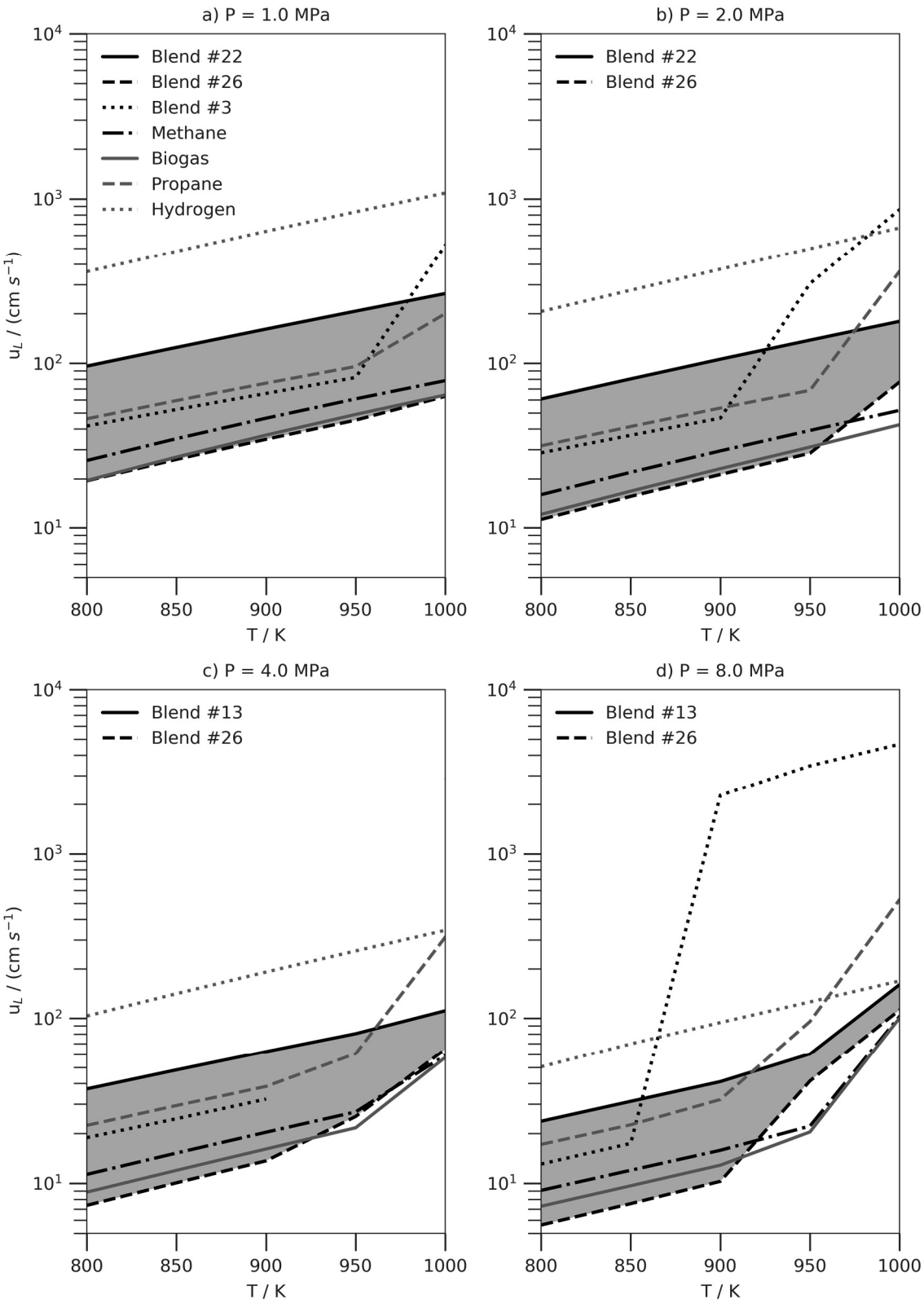

Figure 6-10: Laminar flame speeds at ϕ = 0.5

As can be seen from the plots, the laminar flame speed increases as the temperature rises and decreases as the pressure rises. This can be observed for all of the investigated fuels blends. At lean equivalence ratios (see Figure 6-10) the laminar flame speeds are generally lower than at stoichiometric conditions (see Figure 6-9) due to the dilution of the mixture.

In all cases the highest flame speeds were found for hydrogen, while fuel blend #26 exhibited the lowest flame speeds. The latter is also the blend for which the longest ignition delay times were observed, which indicates that it is generally the least reactive of the investigated fuel blends. This can be attributed to its comparatively inert composition of CO at 30 vol%, CH_4 at 11.25 vol%, CO_2 at 50 vol% and N_2 at 8.75 vol% without any fractions of hydrogen or higher hydrocarbons. Blends #13 and #22 feature the highest flame speeds of the investigated syngas blends. In both cases, this can be explained by the high share of 40 vol% hydrogen in the blend. At stoichiometric conditions, the flame speeds of the reference fuels methane and biogas are approximately in the medium to lower region covered by the syngas blends. Propane features slightly higher flame speeds in the middle to upper region of the syngas range. When moving to lean equivalence ratios, the flame speeds of the syngas fuels generally increase with regard to the reference fuels. This will require combustion control measures to compensate for the faster burning velocity when switching from standard to syngas fuels.

As shown by Hiltner [91] the calculated flame speed of a fuel can be directly related to the burn duration and combustion efficiency for a given engine design. Larger flame speeds will generally lead to higher combustion rates, resulting in higher peak temperatures and NO_x emissions but also in higher combustion efficiencies. At very low flame speeds, the burn duration becomes unacceptably long and engine operation becomes unstable. Hiltner observed that the laminar flame speed of syngas blends is generally higher than that of natural gas, which is also confirmed by the results of *this study*.

One measure to control the laminar flame speed is to dilute the mixture by decreasing the fuel-to-air equivalence ratio (cf. Figure 6-9 vs. Figure 6-10). It is known from engine experiments that the equivalence ratio at which a sample fuel attains the same laminar flame speed as a specified reference fuel corresponds to the required equivalence ratio for this fuel at full load operation for a given engine setup (cf. Schultze et al. [69]). The laminar flame speed of a fuel can thus be used as an indicator for the equivalence ratio which is required to operate a given engine with varying fuels keeping heat release and NO_x emissions approximately constant. The required equivalence ratio can be determined from a sweep of u_L over ϕ as illustrated in Figure 6-11: in order to switch an engine which was designed for methane at $\phi = 0.8$ to operation with fuel blend #13, the equivalence ratio needs to be lowered to $\phi \approx 0.58$. If the initial equivalence ratio for methane were $\phi = 0.65$, it would have to be lowered to $\phi \approx 0.48$ to run the engine with blend #13.

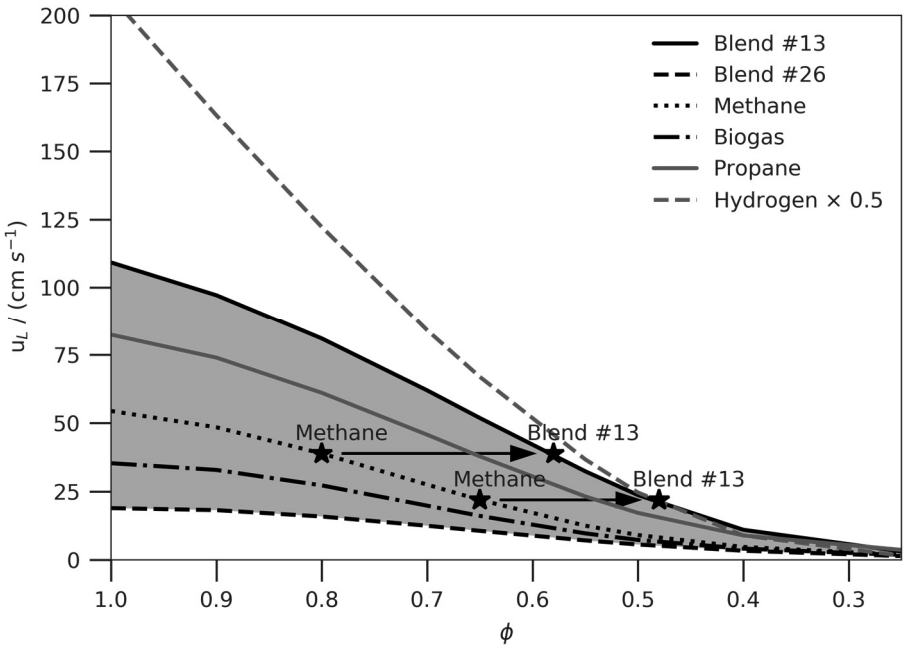

Figure 6-11: Laminar flame speed over ϕ at P = 8.0 MPa and T = 800 K

For some fuels the laminar flame speed shows a sudden and strong increase at high pressures and temperatures ≈ 900 to 950 K. This can be observed most prominently for syngas blend #3 and propane, but also for blend #26, methane and biogas. This effect is even more pronounced at lean equivalence ratios (cf. Figure 6-10). This behaviour is not very plausible, and rather than searching for a physical explanation one should consider that the kinetic mechanism is applied in an unsurveyed range here. The original POLIMI C1-C3 high temperature mechanism was developed from experimental flame speed data up to pressures of 60 atmospheres and temperatures of 470 K (cf. [65]). Although the mechanism performs well with mixtures of hydrocarbons and additions of hydrogen to hydrocarbons [65], it has not been experimentally verified with syngas mixtures comprising high shares of hydrogen, carbon monoxide, methane and higher hydrocarbons as investigated in the present study. In order to identify the most critical reactions with regard to the laminar flame speed, a sensitivity analysis was carried out for propane and fuel blend #3. The conditions were set to a temperature of 950 K, a low and a high pressure case of 1 MPa and 8 MPa, respectively, and stoichiometric and lean fuel-to-air equivalence ratios of 1.0 and 0.5. The results are displayed in Figure 6-12 (propane) and Figure 6-13 (syngas blend #3).

In the case of propane, the laminar flame speed is most sensitive to the rate constant of the chain branching step $H + O_2 \leftrightarrow O + OH$, which is part of the H_2-O_2 oxidation system. This holds true at low pressures for both stoichiometric and lean equivalence ratios. At higher pressures, reactions involving HO_2 and H_2O_2 become dominant, especially the recombination reaction $2\ HO_2 \leftrightarrow H_2O_2 + O_2$ and the decomposition reaction $2\ OH\ (+M) \leftrightarrow H_2O_2 + M$, which are part of an exothermic sequence in the H_2-O_2 system [68]. These reactions also play an important role in the oxidation of fuel blend #3. However, in the case of blend #3, the CO conversion reaction $CO + HO_2 \leftrightarrow CO_2 + OH$ is the most

influential at high pressures. This reaction is part of the so-called wet CO oxidation mechanism and is competitive to the reaction $CO + OH \leftrightarrow CO_2 + H$ which is the more dominant CO conversion route in most combustion situations [68], such as in the present case at low pressures. Another reaction which becomes highly influential for fuel blend #3 at high pressures is the abstraction reaction $C_2H_4 + OH \leftrightarrow C_2H_3 + H_2O$ which is part of the olefin oxidation system [68].

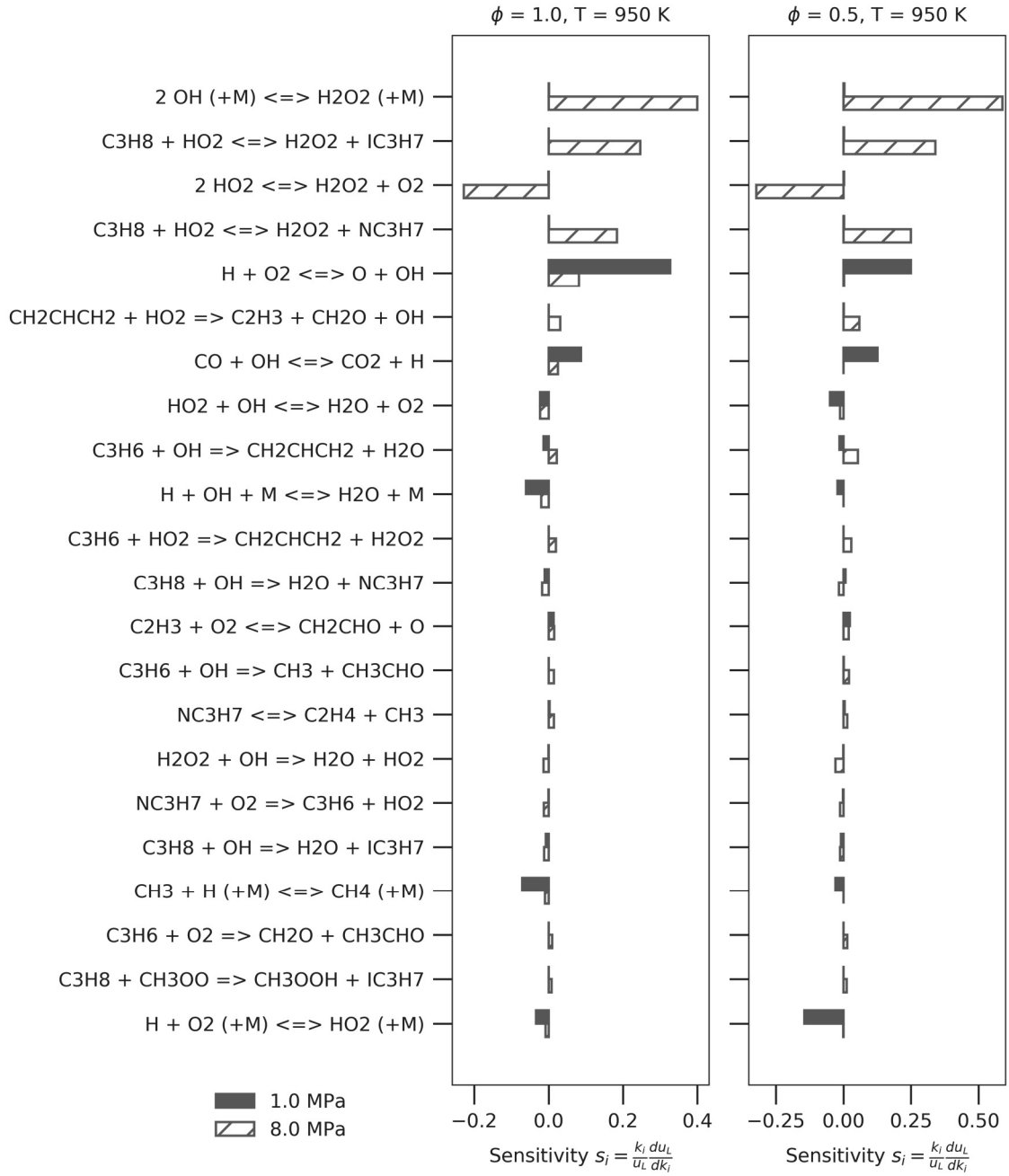

Figure 6-12: Laminar flame speed sensitivities for propane

In view of the results of the sensitivity analysis and the constituents of typical syngas blends, improvements of the mechanism should focus primarily on the H_2-O_2 and CO oxidation systems at high pressures considering especially three body and fall-off reactions, such as 2 OH (+M) ↔ H_2O_2 + M, for which the rate coefficients may change with pressure (cf. [68]). In addition, the abstraction reactions of higher hydrocarbons are often pressure sensitive and will have to be revised with regard to high pressure combustion systems.

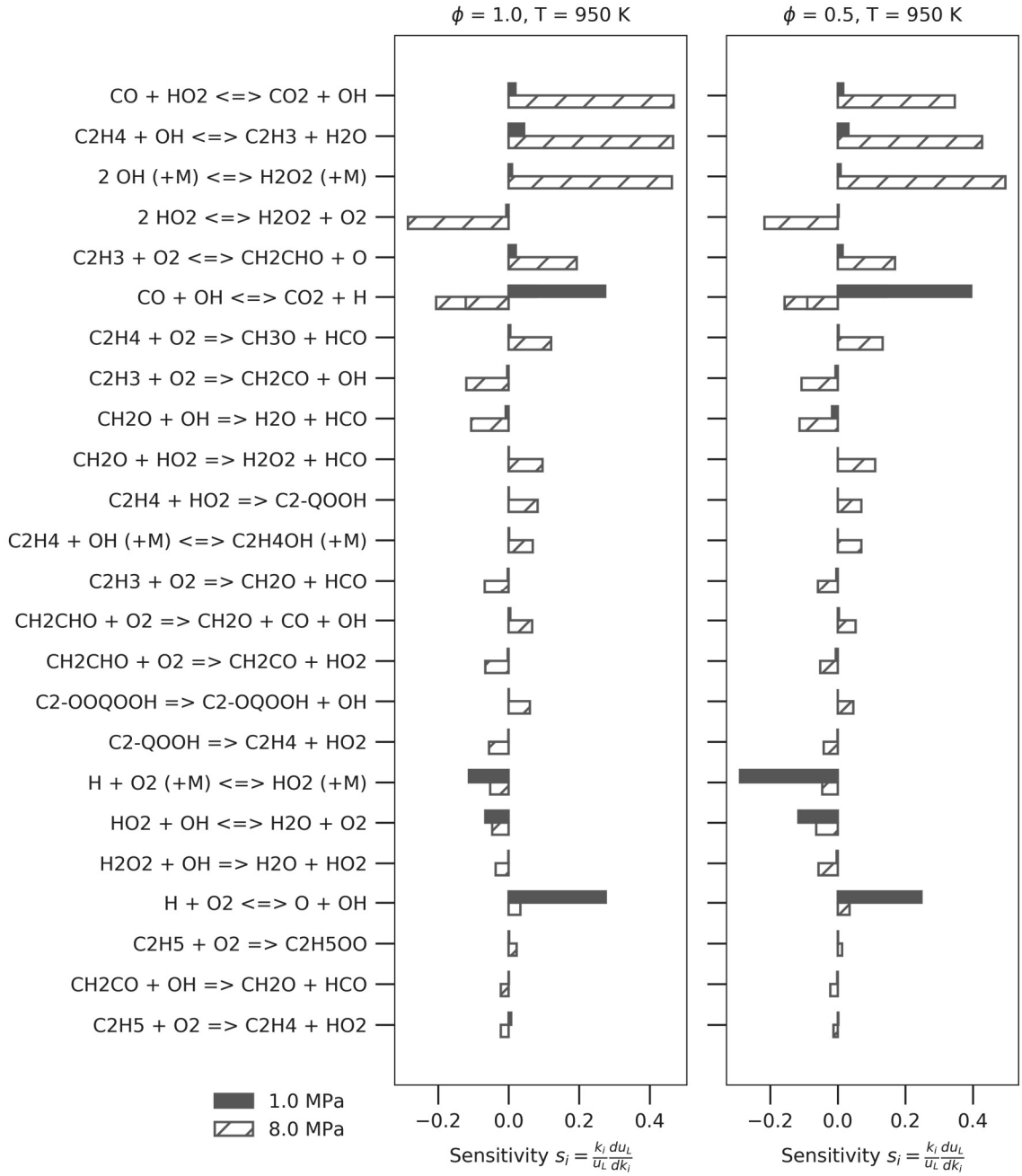

Figure 6-13: Laminar flame speed sensitivities for syngas blend #3

6.7 ξ-ε diagram and knock propensity

6.7.1 ξ-ε diagram for the investigated fuels at engine operating conditions

In Figure 6-14 to Figure 6-16 the ξ-ε diagrams for the investigated fuels are shown for stoichiometric and lean equivalence ratios (observe the different scalings of the ε-axis). The solid lines mark the detonation peninsula and the dashed lines mark the transition regime defined by Bates [71] as $-\bar{E}(\partial lnT/\partial\bar{r}) \approx 900\ldots6\,000$. The required values of τ_i and τ_e for calculating ε and ξ were determined by constant-volume reactor simulations with detailed chemical kinetics using the POLIMI mechanism. A hot spot radius of $r_0 = 5$ mm and a temperature gradient of $\partial T/\partial r = -2$ K/mm were assumed.

The empty circles represent the approximate state at the end of an isentropic compression of up to 8 MPa and 800 K in a turbocharged, high speed, SI gas engine with intercooler. The half-filled diamonds depict the state if this compression is continued to a pressure of 15 MPa at ≈ 950 K during combustion, assuming that the end gas core is adiabatic, that is, no heat is transferred from the flame to the unburned zone. Additionally, a state with identical pressure but at an elevated temperature of 1 100 K is displayed (half-filled triangles).

At stoichiometric conditions, a pressure of 8 MPa and a temperature of 800 K, all fuel blends are within the safe operating regime of deflagration or in the transition region to subsonic auto-ignition. When the pressure and temperature are increased to 15 MPa and 950 K, the fuel isentropes move towards the upper limit of the detonation peninsula into the transition regime where auto-ignition and deflagration can coexist. While auto-ignitions in the subsonic regime are not harmful for the engine (cf. [22, 24]), damaging knock may occur when the detonation peninsula is entered. The TCR blend #36 and propane are already in a regime where knock is to be expected. Finally, at the elevated temperature of 1 100 K, practically all fuels are well within the detonation peninsula approaching its lower bound at values of ξ close to unity which are associated with heavy knock and super-knock [23].

Altogether, methane and biogas show the highest resistance to knock, while propane and the TCR gas blends are generally more prone to knock. Hydrogen is not displayed in the ξ-ε diagram since it is located far to the right of the peninsula at values of $\varepsilon > 100$. Generally, values of $\varepsilon > 22$ (cf. propane and methane) exceed the limits for which the detonation peninsula is currently defined. Still, the values of ξ can be used to assess the knock propensity and the intensity of knock which is highest when ξ approaches unity.

Fuel blend #3 is marked individually in the detonation diagrams due to its special auto-ignition characteristics with low values of τ_i but large excitation times τ_e. This leads to comparatively low values of ξ, but also to low values of ε. Consequently, blend #3 remains well in the safe operating regime of subsonic auto-ignition at all investigated conditions, except at P = 15 MPa and T = 1 100 K. Thus, judging from the ξ-ε diagram, blend #3 is much less prone to knock than expected when evaluating only the ignition delay time.

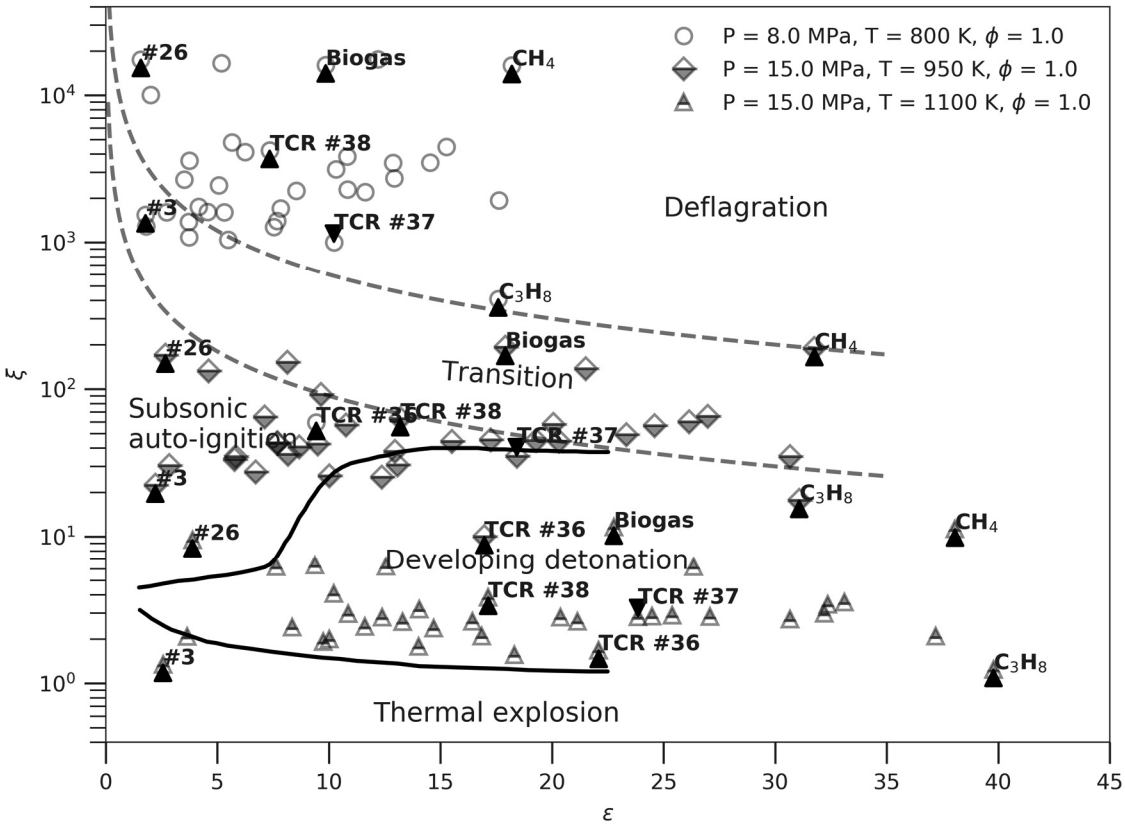

Figure 6-14: ξ-ε diagram at ϕ = 1.0

Fuel blend #26 is also highlighted in the diagram since it should be the least reactive of the investigated fuels according to its auto-ignition characteristics and laminar flame speed. In fact, this is confirmed in the ξ-ε diagrams, where blend #26 remains in a safe operating regime even at the most severe conditions of 15 MPa, 1 100 K and ϕ = 1.00 (cf. Figure 6-14).

Contrary to the results from the HCCI reactor simulation the TCR gas blends #36 to #38 now show the expected behaviour with regard to higher hydrocarbons. Blend #38 (no C5+ hydrocarbons) is the most knock-resistant and blend #36 (n-heptane added) is the most prone to knock. It is remarkable that even iso-octane (TCR blend #37), which is comparatively knock-resistant, increases the knock propensity considerably in comparison to the blend without C5+ hydrocarbons. This confirms the prominent role of higher hydrocarbons for the development of engine knock.

When shifting to lean equivalence ratios (Figure 6-15 and Figure 6-16), the values of ε for all fuels decrease considerably. Most fuels are now in the safe operating regime of deflagration or subsonic auto-ignition and only enter the detonation peninsula at the elevated temperature of 1 100 K. At this temperature the TCR fuel blends as well as propane are all within the narrow tip of the detonation peninsula, with TCR #36 and propane approaching its lower limit, indicating that heavy knock and super-knock are probable for this fuels.

At the ultra-lean equivalence ratio of $\phi = 0.5$, a pressure of 15 MPa and a temperature of 1 110 K, propane and the TCR blend #36 are slightly below the lower limit of the peninsula in the region of thermal explosion and most other syngas blends are on the left of the open narrow tip. Considering that this region is currently only loosely defined and may correspond to a regime where multiple modes of propagation may coexist [74], this should be simply interpreted as a condition where knock cannot be precluded.

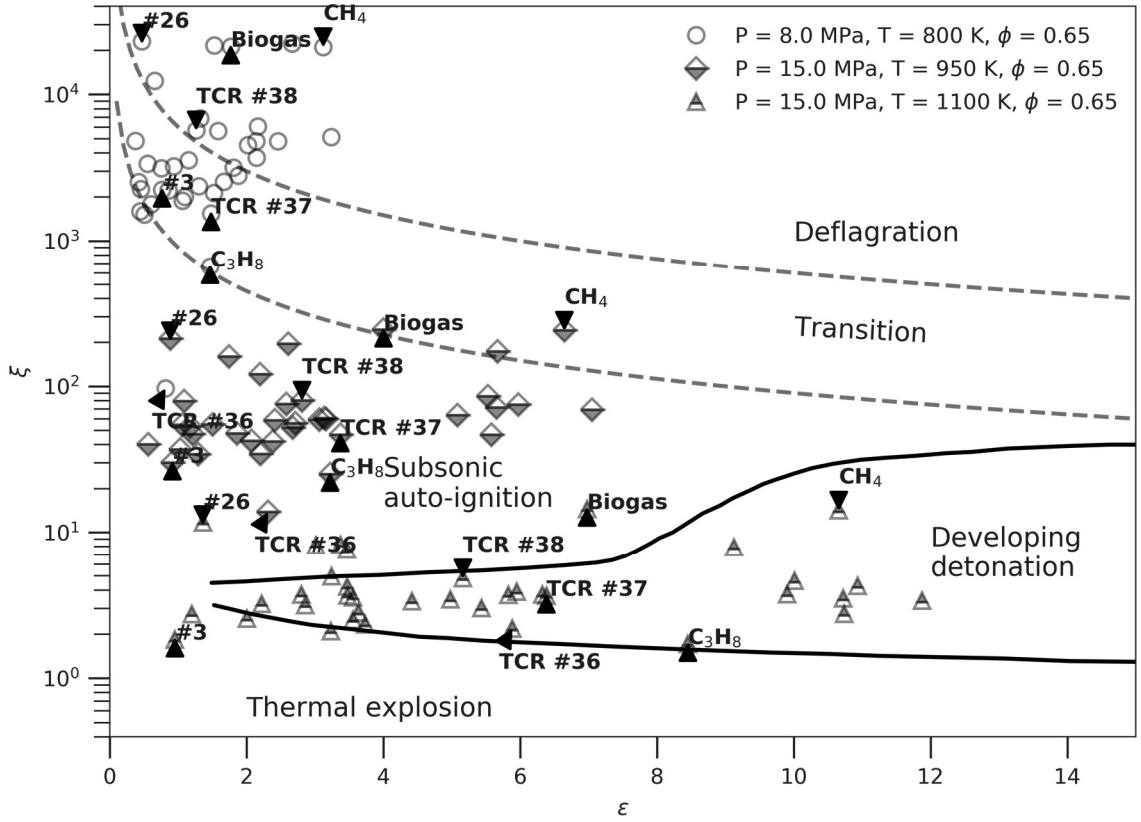

Figure 6-15: ξ-ε diagram at ϕ = 0.65

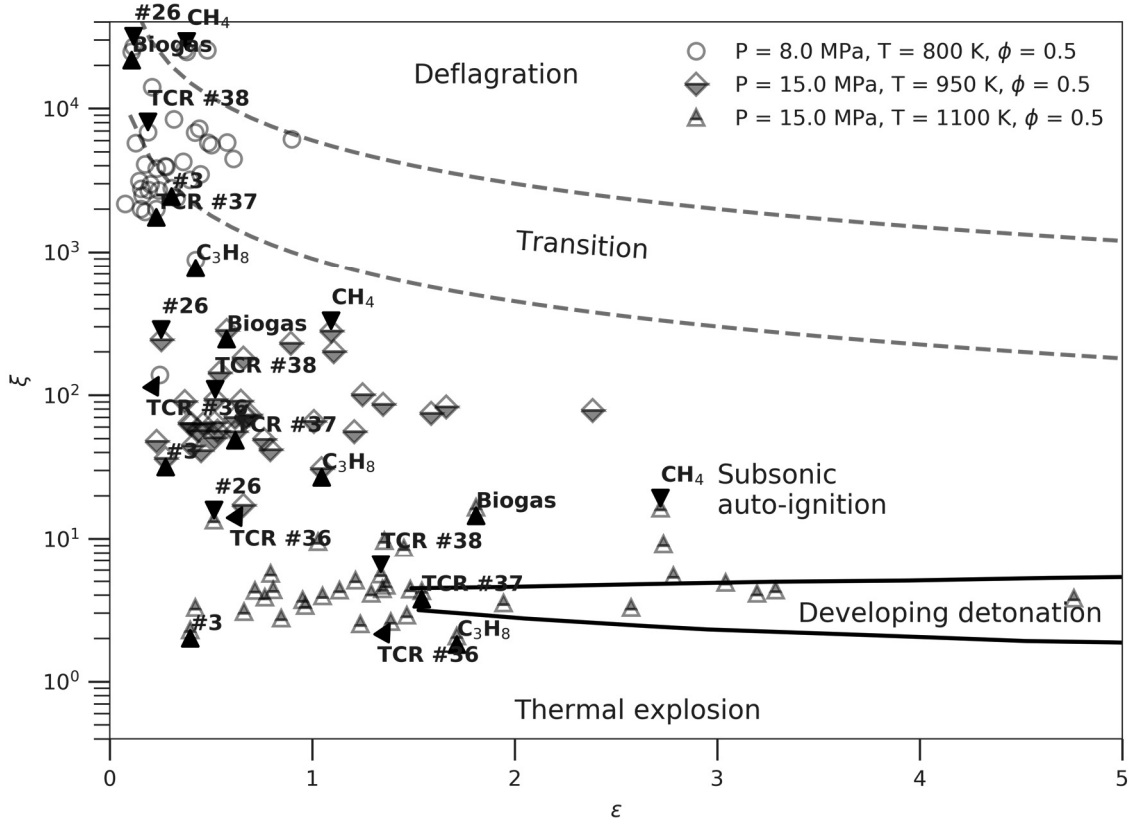

Figure 6-16: ξ-ε diagram at ϕ = 0.50

It is remarkable that at lean equivalence ratios, biogas does not enter the detonation peninsula at any conditions, not even at 15 MPa and 1 100 K. This confirms its excellent anti-knock characteristics. It is also noteworthy that practically all investigated syngas blends are less or at least not more prone to knock than pure propane, which is a commonly used engine fuel and constituent of liquefied petroleum gas. The application of syngas fuels should thus not present an unsolvable challenge for engine design and operation.

6.7.2 Effects of exhaust gas recirculation and water vapour fraction

effects of dilution with recirculated exhaust gas and water vapour on the combustion characteristics were investigated for two representative fuel gases. Methane (fuel #32) was chosen as the reference fuel and compared to the syngas blend #5 which consists of 40 vol% H_2, 25 vol% CO, 15 vol% CH_4, 10 vol% CO_2 and 5 vol% of C_2H_4 and C_3H_8. In both cases a stoichiometric base mixture was diluted with either H_2O from 0 to 40 vol% or recirculated exhaust gas (EGR) from 0 to 40 vol%. In the case of EGR both an equilibrium composition and a frozen state at 1 700 K were investigated. The recirculated exhaust gases were assumed to be dry. The constant-volume reactor model was used with the POLIMI mechanism for determining the ignition delay and excitation times. A hot spot radius of $r_0 = 5$ mm and a temperature gradient of $\partial T/\partial r = -2$ K/mm were applied for calculating the dimensionless parameters ε and ξ. A pressure of 15 MPa and a temperature of 950 K were set as initial conditions. The results are displayed in the ξ-ε diagrams Figure 6-17 and Table 6-7.

At the investigated conditions the non-diluted fuel blend #5 is initially in a regime at the upper boundary of the detonation peninsula where light knock is probable. By contrast, non-diluted methane is outside the detonation peninsula at these conditions and in the transition regime towards deflagration, where knock is not to be expected.

As can be seen from Figure 6-17, any dilution of the mixture either with residual gas or with water vapour decreases the values of ε, while the ξ values remain almost constant. By reducing ε, the operating regime shifts increasingly towards the safe region of subsonic auto-ignition above the narrow tip of the detonation peninsula. Considering equal volume fractions, water vapour has a much stronger effect than dry residual gas in this regard. In practice, the residual gas will usually not be dry but contain a certain amount of water vapour, depending on the type of EGR system used (cooled/condensing or non-cooled/non-condensing). This additionally enhances the anti-knock effect of exhaust gas recirculation.

In the case of methane, a dilution with EGR or water vapour has little benefits with regard to the knock-margin at the investigated pressure and temperature of 15 MPa and 950 K, since at these conditions the mixture is already in an operating regime in which knock is not very likely to occur. By contrast, in the case of the syngas blend #5, which is initially at the upper boundary of the detonation peninsula, the risk of knock can be reduced substantially by diluting the mixture. At EGR ratios of about 20 vol%, the operating regime is already well in the region of subsonic auto-ignition, which implies that safe operation with a reasonable knock-margin can be expected. If 20 vol% of water vapour instead of residual gas is added to the mixture, the operating regime moves even further to the left, far outside the boundaries of the detonation peninsula, which in practice should further increase the knock-margin.

Table 6-7: Ignition delay and excitation times for diluted mixtures

	EGR equilibrium				EGR frozen @1 700 K				Water vapour			
Dilution	τ_i	τ_e	ξ	ε	τ_i	τ_e	ξ	ε	τ_i	τ_e	ξ	ε
vol%	µs	µs			µs	µs			µs	µs		
0	8 090	0.259	202	31.76	8 090	0.259	202	31.76	8 090	0.259	202	31.76
10	8 838	0.451	219	18.26	7 749	0.451	192	18.26	8 202	0.625	205	12.93
20	9 749	0.877	240	9.43	8 029	0.876	198	9.44	8 497	1.709	215	4.65
30	10 887	1.970	266	4.21	8 452	1.967	207	4.22	8 990	5.457	230	1.43
40	12 359	5.444	299	1.53	9 010	5.432	218	1.53	9 716	97.768	251	0.08

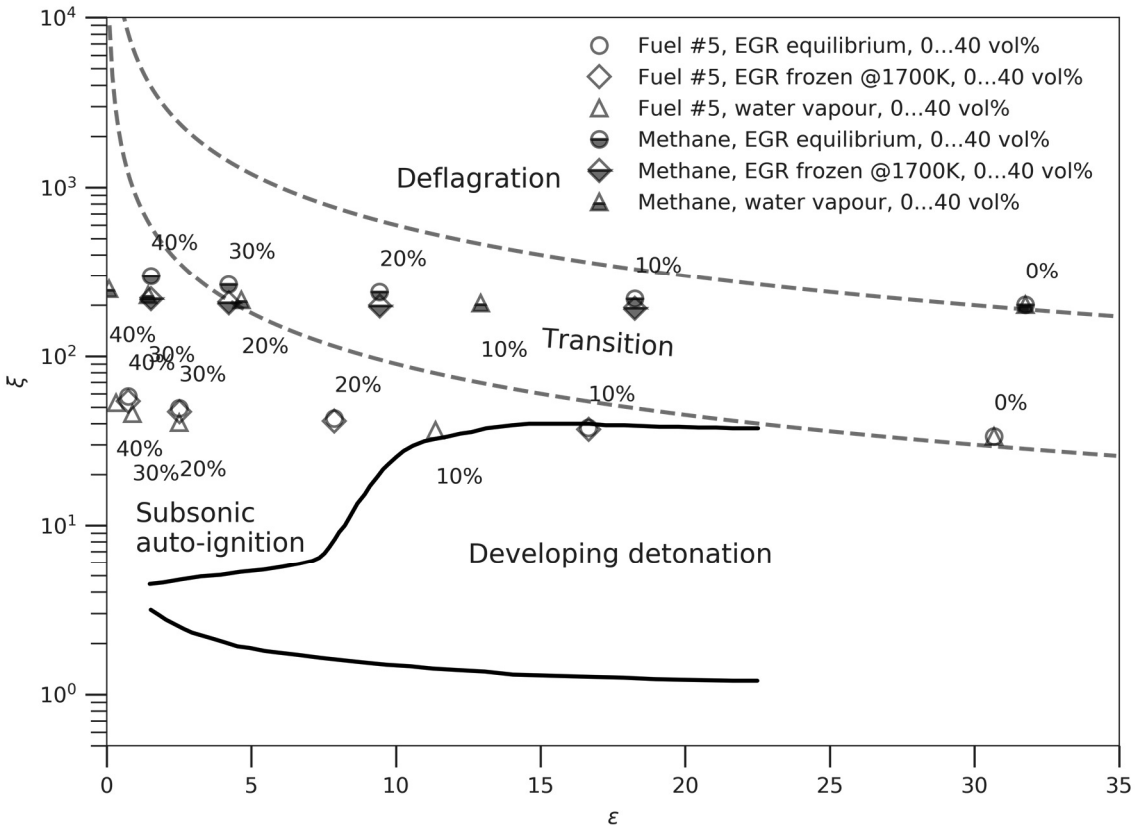

Figure 6-17: ξ-ε diagram for dilution with EGR and water vapour, P = 15 MPa, T = 950 K, ϕ = 1.0

The anti-knock effect of dilution with either residual gas or water vapour is associated with a reduction of the ε-values (cf. Figure 6-17 and Table 6-7). Considering the definition of ε (cf. Equation (4-102)) and assuming that the hot spot radius and the acoustic velocity are approximately constant, this reduction must be due to an increase of the excitation time τ_e of the diluted mixture, which is confirmed by the results presented in Table 6-7. According to the detonation theory, the increase of τ_e reduces the amount of energy that can be transferred into the acoustic front of a pressure wave travelling through a hot spot. Thus, harmful detonations which result in engine knock are less likely to happen.

Other than the ε-values, the ξ-values increase when diluting the mixture, which according to the definition in Equation (4-101) can be attributed to an increase of the ignition delay times τ_i. This is confirmed by the results in Table 6-7. However, the effect is of minor im-

portance and does not significantly contribute to shifting the operating regime into safe conditions, that is, away from the detonation peninsula. Thus, the anti-knock effect of dilution can be attributed primarily to the reduction of the ε-values caused by an increase of the excitation time τ_e, rather than to the increase of the ignition delay time τ_i.

As presented in sections 4.2.3 and 4.2.4, the composition of the residual gases can be assumed either to be in chemical equilibrium or to be frozen at a certain temperature. In comparison to the equilibrium composition the frozen composition is expected to exhibit a higher reactivity due to dissociated species and radicals present in the mixture. This should lead to a reduced ignition delay time τ_i and smaller values of ξ, which is confirmed by the results in Figure 6-17. By contrast, the values of ε are virtually not affected by the choice of the EGR model. Since the anti-knock effect of EGR is primarily determined by the ε-values, either model can be used and will deliver essentially the same results with regard to the probable auto-ignition regimes (cf. Figure 6-17).

In addition to the combustion kinetics effects presented here, thermodynamic effects – such as the increase of the heat capacity ratio of the cylinder charge by EGR – also play a role in controlling engine knock. However, the results of *this study* confirm that diluted mixtures with EGR or water vapour inherently exhibit less tendency to knock due to their auto-ignition characteristics.

6.7.3 Auto-ignition at the critical compression ratio in the ξ-ε diagram

According to the methodology presented in Chapter 4 (cf. Figure 4-1), the HCCI reactor simulation and the evaluation of the ξ-ε diagram are two independent methods and deliver different results which are not directly comparable. However, it would be interesting to investigate if any linkage between the two methods could be established in order to better understand the auto-ignition regime that is actually reproduced by the ideal HCCI reactor

simulation. Therefore, the individual temperature and pressure conditions which led to auto-ignition in the HCCI reactor simulations (cf. section 6.5) were evaluated and the according values of ξ and ε were calculated. Again, a hot spot radius of $r_0 = 5$ mm and a temperature gradient of $\partial T/\partial r = -2$ K/mm were assumed in order to be consistent with the calculations presented before. Figure 6-18 shows the resulting ξ-ε diagram. Stoichiometric ($\phi = 1.0$) and lean equivalence ratios ($\phi = 0.5$) are displayed accordingly.

The individual markers in the figure depict the values of ξ and ε for the state at which auto-ignition in the HCCI reactor first occurred. This state corresponds to the temperature and pressure conditions at the end of a compression with the critical compression ratio CR_c for the respective fuel blend.

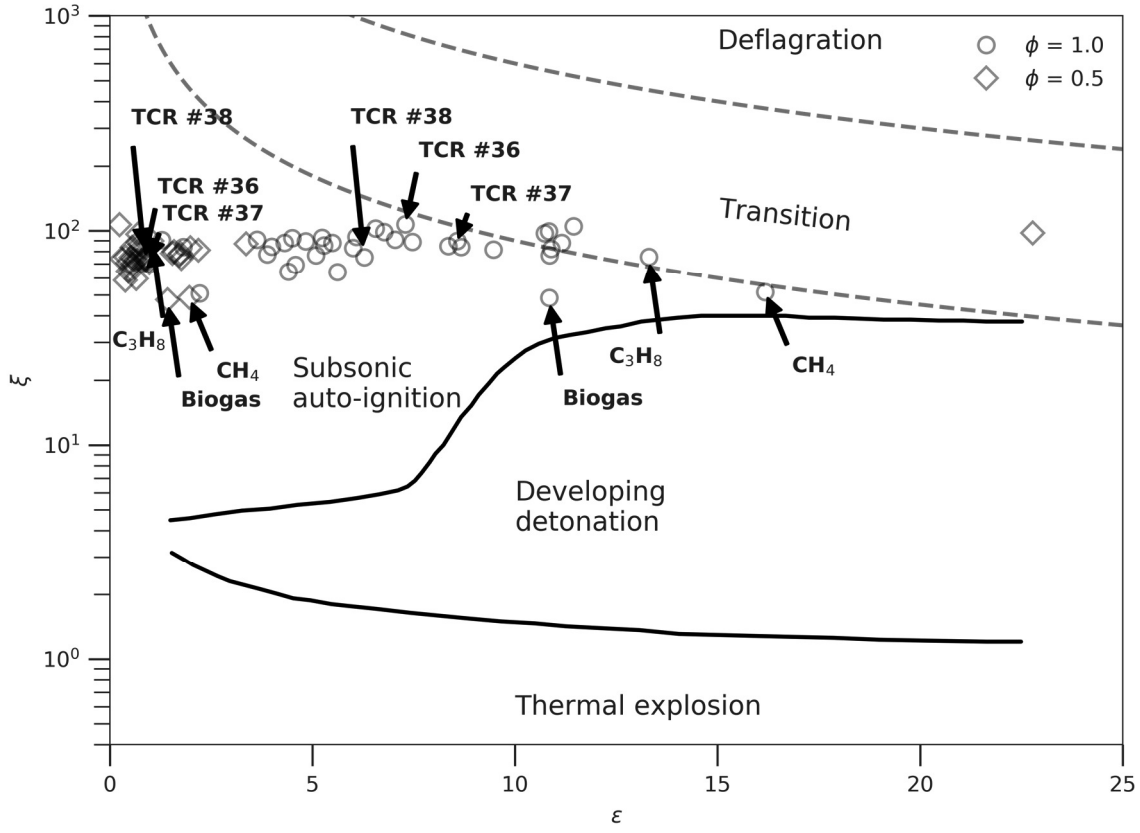

Figure 6-18: ξ-ε diagram at the critical compression ratio

The majority of identified operating points are situated in the regime of subsonic auto-ignition and some at the beginning of the transition to deflagration. None of the evaluated points is located inside the detonation peninsula. Interestingly, at the evaluated conditions all investigated fuels feature similar values of ξ which are all in a narrow range of approximately 50 to 110, regardless of the equivalence ratio. By contrast, the values of ε are spread over a wider range and the equivalence ratio has a strong effect, with the lean mixtures featuring much lower ε-values than the stoichiometric ones. This conforms well with the findings presented in sections 6.7.1 and 6.7.2, where dilution of the mixture was found to primarily decrease the values of ε while leaving ξ largely unaffected.

Based on experimental evidence from Netzer [22, 24] the regime of subsonic auto-ignition with values of ξ in the region of 10 to 100 corresponds to safe operating conditions, where harmful knock is unlikely to be expected. Practical HCCI engines operate in this regime, as data presented by Bates et al. [23] for a single cylinder engine suggests. The engine was operated in the regime of controlled subsonic auto-ignition free of knock with values of ξ between 30 and 50 and probably close to knock at values of $\xi < 10$ [23].

The identified operating regimes for the HCCI reactor auto-ignition conditions at the critical compression ratio confirm these findings surprisingly well, suggesting that the HCCI reactor simulation actually reproduces a homogenous, controlled subsonic auto-ignition rather than the conditions leading to knock in practical engine operation. Together with the shortcomings due to overlying thermodynamic effects (cf. section 6.5) these findings might explain the difficulties encountered also by other authors in using the critical compression ratio from HCCI reactor simulations as a rating method for the knock propensity of fuels (cf. [69, 96, 156]).

6.8 Evaluation of the Sankaran criterion

In order to assess the transition from auto-ignitive to deflagrative combustion the Sankaran criterion according to Mansfield et al. [102] was evaluated. Bates applied the data from Mansfield to determine a tentative general threshold of $-\bar{E}(\partial lnT/\partial\bar{r}) \approx 1\,500$ for the transition between the two regimes [23] and later extended the transition region to $-\bar{E}(\partial lnT/\partial\bar{r}) \approx 900\ldots6\,000$ [71]. Originally, the Sankaran criterion as presented by Mansfield is backed up by experimental data for syngas with a molar ratio of H_2:CO = 0.7 at equivalence ratios of ϕ = 0.1 and ϕ = 0.5, pressures from 0.3 to 1.5 MPa and temperatures up to 1 150 K [102]. In the present study the evaluation of the Sankaran criterion was now extended to the fuel matrix presented in Table 6-4 and to pressures from 1 to 8 MPa for stoichiometric and lean equivalence ratios of ϕ = 1.0 and ϕ = 0.5, respectively. The identified values of temperature and pressure at which the condition $\partial\tau_i/\partial T = (\partial T/\partial r\ u_L)^{-1}$ was met were applied to calculate the according values of $-\bar{E}(\partial lnT/\partial\bar{r})$. A hot spot radius of 5 mm and a temperature gradient of –2 K/mm were assumed in order to keep consistency with the parameters applied for constructing the ξ-ε diagram. The results are presented in Figure 6-19.

With the exception of hydrogen, the values of $-\bar{E}(\partial lnT/\partial\bar{r})$ obtained at ϕ = 0.5 are in good agreement with the transition region proposed by Bates, starting at $-\bar{E}(\partial lnT/\partial\bar{r}) \approx 900\ldots1\,300$ at 1 MPa and increasing up to $-\bar{E}(\partial lnT/\partial\bar{r}) \approx 2\,500\ldots5\,300$ at 8 MPa. By contrast, the resulting values at ϕ = 1.0 show a much wider spread at high pressures which increases to $-\bar{E}(\partial lnT/\partial\bar{r}) \approx 5\,000\ldots25\,000$ at 8 MPa. Interestingly, this now applies to the majority of the fuel blends and not only to hydrogen which shows high values of $-\bar{E}(\partial lnT/\partial\bar{r})$ already at the lean equivalence ratio. These observations indicate that the transition region of auto-ignition to deflagration might have to be extended towards higher values of $-\bar{E}(\partial lnT/\partial\bar{r})$ for stoichiometric mixtures of gaseous fuels at high pressures.

However, it has to remembered that the laminar flame speed data used for evaluation of the Sankaran criterion is not very reliable for high temperature and pressure conditions (cf. section 0). Moreover, the Sankaran criterion has not yet been backed up by experimental data for the investigated range of temperatures, pressures and fuel blends. These findings should thus be considered as preliminary and will have to be checked against extended simulations and experimental results in future studies.

Further investigations of the transition region could be worthwhile especially with regard to the evaluation of measurements in rapid compression machines, where high values of $-\bar{E}(\partial lnT/\partial \bar{r})$ might lead to erratic results for the ignition delay due to hot spot initiated auto-ignitions, from which a laminar flame propagates [71]. However, for practical engine operation the upper extent of the transition region is less relevant, since knock events are found to occur predominantly in operating regimes at low values of $-\bar{E}(\partial lnT/\partial \bar{r})$ and located within the detonation peninsula (cf. [22–24]).

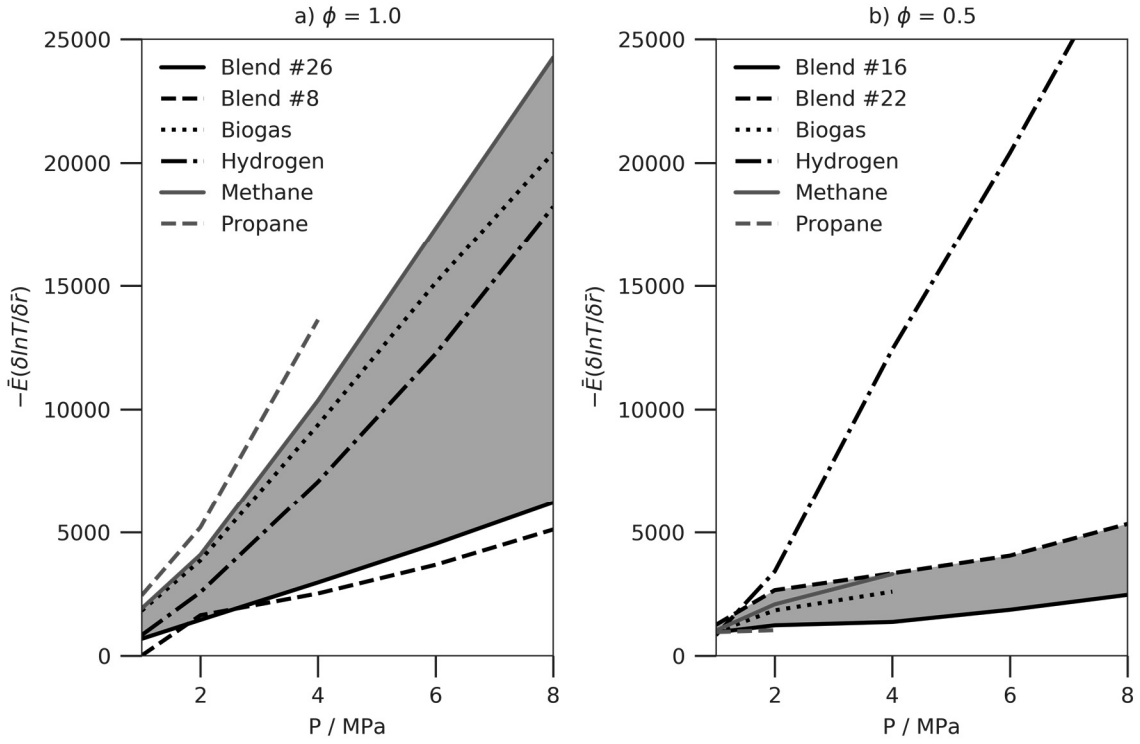

Figure 6-19: Evaluation of the Sankaran criterion

6.9 Summary

The combustion characteristics of 38 fuel gas blends were studied applying the methodology presented in Chapter 4 using the CoPa simulation toolbox introduced in Chapter 5. In order to cover a relevant range of fuel compositions, a fuel matrix was developed based on a statistical experimental plan and measured gas compositions from a TCR® 300 pilot plant. Methane, biogas from anaerobic digestion, hydrogen and propane were considered as reference fuels.

The differences in the energy content of the individual fuels were levelled out to a great extent by the according lower stoichiometric air requirement, resulting in fuel/air-mixtures whose heating values are all in a comparatively narrow range. This implies that engines operated with fuel gases from thermo-chemical conversion will essentially be able to deliver a similar power output as conventional biogas or natural gas engines if not limited by other constraints, such as engine knock.

The methane number of the investigated fuels was determined with different fuel rating methods. While the Cummins Westport Fuel Quality Calculator and the DNV Propane Knock Index calculator failed for practically all fuels except for pure methane, the MWM methane number was able to deliver confident results in about half of the cases. Additionally, the critical compression ratio was determined with an HCCI reactor simulation assuming the geometry and conditions of the MON test. The obtained values showed to be linearly correlated to the corresponding MWM methane numbers, although with considerable scatter which does not allow for an unambiguous assignment of the calculated CR_c to a specific value of MN. The HCCI reactor simulation showed overlying thermodynamic effects when rating lean mixtures due to the differences in heat capacity ratio which might lead to a lower critical compression ratio and thus to an apparently higher reactivity.

The results for the ignition delay times suggest that – compared to pure methane and biogas – most of the syngas and TCR gas blends are more reactive in terms of auto-ignition propensity. The presence of higher hydrocarbons additionally enhances the reactivity and may also induce a negative temperature coefficient, which has to be considered in the design of combustion systems. The ignition delay times are strongly dependent on temperature, while the effects of pressure and equivalence ratio are less pronounced. By contrast, the excitation times are strongly sensitive to the equivalence ratio, while the influence of pressure and temperature is less. This fundamentally different behaviour of the two characteristic parameters τ_i and τ_e implies that neither of them is a reliable indicator for assessing the reactivity and knock propensity of fuels when applied individually. Instead, they must be evaluated in a broader context.

The laminar flame speeds of the investigated fuels were found to increase as the temperature rises and decrease as the pressure rises. At lean equivalence ratios, the laminar flame speeds are generally lower than at stoichiometric conditions due to the dilution of the mixture. In all cases the highest overall flame speeds were found for pure hydrogen and for syngas blends containing high shares of hydrogen. With regard to the reference fuels methane and biogas, the investigated syngas blends mostly showed higher flame speeds, especially at lean equivalence ratios, which requires combustion control measures to compensate for the faster burning velocity when switching from standard to syngas fuels. Since the laminar flame speed can be directly related to the burn duration for a given engine design, this task can be accomplished, for example, by controlling the fuel-to-air equivalence ratio.

For some fuels the flame simulations yielded a sudden increase of the flame speeds at temperatures above ≈ 900 to 950 K and high pressures. This behaviour is not very plausible and it should be considered that the kinetic mechanism is applied in an unsurveyed range here. In order to identify the most critical reactions with regard to the laminar flame speed,

a sensitivity analysis was performed showing that at high pressures the reaction rates of the H_2-O_2 and CO oxidation systems become increasingly influential. Improvements of the mechanism should thus focus primarily on the H_2-O_2 and CO oxidation systems at high pressures, considering especially three body and fall-off reactions for which the rate coefficients may change with pressure. In addition, the abstraction routes of higher hydrocarbons are often pressure sensitive and will have to be revised with regard to high pressure combustion systems.

The ξ-ε diagram was used to assess the knock propensity of the investigated fuel blends at conditions corresponding to the end of compression and the beginning of combustion in modern high speed turbocharged gas engines. Methane and biogas showed the highest resistance to knock, while propane and the TCR gas blends were more prone to knock. Higher hydrocarbons were found to increase the knock propensity. Leaning of the mixture, exhaust gas recirculation and the addition of water vapour proved to be effective measures to reduce the risk of knock. Water vapour has a much stronger effect in this regard than dry EGR. The anti-knock effect of EGR and water vapour can be attributed primarily to an increase of the excitation times. This reduces the amount of energy that can be transferred into the acoustic front of an auto-ignition wave and leads to lower values of ε. By contrast, the ignition delay times where found to have only a minor influence by slightly increasing the values of ξ.

When introducing the conditions at which auto-ignition occurred in the HCCI reactor simulation (critical compression ratio) into the ξ-ε diagram, most of the values were found to be in the regime of subsonic auto-ignition, which suggests that the HCCI reactor simulation actually reproduces the conditions of a homogenous subsonic auto-ignition rather than the conditions leading to knock. This might explain some of the difficulties encountered when using the method for rating the knock propensity of fuels (cf. [69, 96, 156]).

The evaluation of the Sankaran criterion for the investigated fuels indicates that the transition region of auto-ignition to deflagration – which was proposed to be in a range of $-\bar{E}(\partial lnT/\partial \bar{r}) \approx 900\ldots6\,000$ by Bates [71] – would have to be extended to cover stoichiometric mixtures of gaseous fuels at high pressures. However, these findings suffer from the lack of reliable laminar flame speed data at high pressures and temperatures and have not yet been backed up by experimental data.

Chapter 7 Conclusions and future work

7.1 Conclusions

In *this study* the detonation theory and the Sankaran criterion were applied to predict stable operating regimes for biogenous fuel gas blends from thermo-chemical conversion at high pressures and temperatures. The main conclusions can be summarised as follows:

The composition of biogenous fuel gases from thermo-chemical conversion can vary considerably according to the feedstock and the process settings. Detailed data with regard to the combustion characteristics of these fuel gases at engine operating conditions for compositions occurring in practice is generally lacking. This applies particularly to gases from intermediate pyrolysis.

It was shown that the differences in the energy content of syngas fuels are levelled out to a great extent by their lower stoichiometric air requirement, resulting in fuel-air-mixtures which are in a range comparable to conventional gaseous fuels. This implies that in engine operation they will essentially be able to deliver a similar power output as conventional biogas or natural gas fuels. The remaining constraint for the applicability of syngas fuels is thus primarily engine knock.

Classical methods for assessing the knock propensity – such as the methane number – suffer from serious drawbacks when applied to these fuels. This applies especially for blends which feature high shares of H_2 and at the same time CO or contain higher hydrocarbons. Alternative methods, such as the propane knock index, showed to be not applicable to the syngas compositions occurring in practice.

Thus, HCCI reactor simulations were proposed in earlier studies as alternative tool for assessing the auto-ignition propensity of fuels. Indeed, it could be shown in the present study that the critical compression ratios obtained from HCCI simulations are correlated with the

corresponding methane numbers of the fuel, although with considerable scatter. Additionally, it has to be considered that the HCCI reactor simulations show overlying thermodynamic effects due to the change of heat capacity ratios occurring with different fuel mixtures. This may provoke misleading results, particularly when comparing mixtures with different equivalence ratios or different levels of dilution by exhaust gas recirculation or water vapour.

The ξ-ε diagram derived from the detonation theory was found to be more capable in this regard. This diagram defines possible regimes of subsonic auto-ignition, deflagration, detonation, thermal explosion as well as the transition between the modes and can be used to assess the knock propensity of fuels. The required values for the construction of the diagram are basically the ignition delay time τ_i and the excitation time τ_e, which can both be obtained from constant-volume chemical reaction kinetic simulations. In addition, the Sankaran criterion – which relates the laminar flame speed to the auto-ignitive propagation speed – can be used to further define the transition regime between subsonic auto-ignition and deflagration. Thus, the ξ-ε diagram combined with the Sankaran criterion has the potential to be used for the a priori characterisation of the auto-ignition propensity of fuels without the need for experimentation.

The ξ-ε diagram was applied to a range of practical fuel gas compositions from thermochemical conversion. Most fuel blends were found to be comparatively knock resistant at conditions corresponding to the end of compression in modern high speed turbocharged SI gas engines. When increasing the pressure and temperature, as would happen to the unburned end gas during combustion, practically all fuels moved into the detonation peninsula approaching its lower bound at values of ξ close to unity, which are associated with heavy knock and super-knock. Altogether, methane and biogas showed the highest resistance to knock, while the syngas blends were generally more prone to knock. This will have to be

considered when designing engines for multifuel systems, for example, by reducing the compression ratio. Higher hydrocarbons play an important role with regard to knock, and even relatively moderate fractions of C5+ hydrocarbons were found to substantially increase the knock propensity of gas blends.

Lean equivalence ratios, exhaust gas recirculation and the addition of water vapour proved to be very effective measures for mitigating the risk of knock. In terms of the ξ-ε diagram, the anti-knock effect can be primarily attributed to an increase in excitation times, which reduces the amount of energy that can be transferred into the acoustic front of an auto-ignition wave and leads to lower values of ε. By contrast, the increase of ignition delay times caused by the dilution of the mixture was found to have only a minor influence in this regard by slightly increasing the values of ξ.

The evaluation of the Sankaran criterion for the investigated fuels indicates that the transition region of auto-ignition to deflagration – which was proposed to be in a range of $-\bar{E}(\partial lnT/\partial\bar{r}) \approx 900\ldots6000$ by Bates [71] – would have to be extended to cover stoichiometric mixtures of gaseous fuels at high pressures. However, these findings suffer from the lack of reliable laminar flame speed data at high pressures and temperatures and have not yet been backed up by experimental data.

7.2 Suggestions for further work

The results of *this study* suggest that the presented methodology based on the detonation theory could indeed be a very suitable tool for a priori identifying stable operating regimes with syngas fuels. However, there are still numerous open questions which need to be addressed in future investigations.

First of all, the composition of fuel gases from intermediate pyrolysis should be investigated in more detail, particularly with regard to the fraction of higher hydrocarbons, which play an important role in the development of engine knock. In this regard it could also be interesting to explore the liquid fraction from intermediate pyrolysis which could serve as pilot fuel in dual fuel engines.

The methodology of the ξ-ε diagram depends on reliable excitation time data. Since the only method currently available to obtain such data is through numerical simulations [71] the methodology is very sensitive with regard to the applied chemical kinetic mechanism. Therefore, the existing chemical kinetic mechanisms will have to be thoroughly reviewed and possibly optimised with regard to their ability to adequately capture the excitation times. Additionally, the kinetic mechanism should be applicable for the calculation of laminar flame speeds at engine operating conditions in order to evaluate the Sankaran criterion.

In view of the computational costs, reduced kinetic mechanisms should be developed particularly for the computation of laminar flame speeds if the methodology is to be applied as part of an extensive research and development workflow. This could be, for example, the coupling of the detonation theory with CFD simulations as presented by Netzer et al. [24].

One drawback of the ξ-ε diagram in its current form is that it is not defined for fuels at conditions of $\varepsilon > 22$. This limits its applicability for gaseous fuels which feature very low excitation times, such as hydrogen. Additional work will thus be necessary to extend the current limits of the detonation peninsula towards larger values of ε. The same applies to the open narrow tip of the peninsula, which has to be further defined, particularly when considering ultra-lean or very diluted mixtures of syngas at high pressures and temperatures which exhibit very low values of ε and values of ξ being close to unity. In this regard it could also be of interest to further study the transition region between subsonic auto-ignition and deflagration based on the Sankaran criterion and the dimensionless parameter group proposed

by Bates [23]. In this context it will also be necessary to examine if such a transition regime actually exists at high pressures occurring in modern gas engines and if the Sankaran criterion is applicable at these conditions, since for syngas mixtures it is currently only confirmed up to 1.5 MPa by experimental data [102].

Another issue to be considered is that the ξ-ε diagram is, for the time being, restricted to laminar burning conditions [74]. This does not unduly limit its applicability, since turbulence time scales can be about three orders of magnitude larger than the auto-ignition times and the flame initiated from a hot spot will initially be laminar [23]. However, the significance of the ξ-ε diagram could be further increased by pairing it with the *U-K-diagram*, as suggested by Bates [25, 74], which takes into account the turbulent burning velocity and the Karlovitz stretch factor to enable a comprehensive assessment of auto-ignitive and turbulent burning regimes.

The work of Montoya et al. [156] as well as the results of *this study* suggest that – although not as straightforward as expected – it might be possible to establish a correlation between the critical compression ratio obtained by HCCI reactor simulations and classical fuel rating numbers, such as the methane number. Taking into account the findings of the present study, which show a correlation of the conditions at CR_c with the associated regime of subsonic auto-ignition in ξ-ε diagram, it could be of interest to investigate if a correlation with the methane number could be established by pairing the HCCI simulation with the ξ-ε diagram. This method could supplement the classical methods in cases where they fail, for example, in the case of fuels with high shares of hydrogen and at the same time carbon monoxide.

Finally, the findings of this study will have to be verified experimentally, either by detailed combustion studies, or, more straightforward, by matching the ξ-ε diagram with real engine operating points from syngas-fuelled gas engines.

References

1. Pant, K.K., Mohanty, P.: Biomass, Conversion Routes and Products - An Overview. In: Hornung, A. (ed.) Transformation of biomass. Theory to practice, pp. 1–30. Wiley, Chichester (2014)
2. Sansaniwal, S.K., Pal, K., Rosen, M.A., Tyagi, S.K.: Recent advances in the development of biomass gasification technology. A comprehensive review. Renewable and Sustainable Energy Reviews (2017). https://doi.org/10.1016/j.rser.2017.01.038
3. Lappas, A., Heracleous, E.: Production of biofuels via Fischer–Tropsch synthesis. In: Luque, R., Lin, C.S.K., Wilson, K., Clark, J. (eds.) Handbook of Biofuels Production, 2nd edn., pp. 549–593. Elsevier Science, s.l. (2016)
4. Neumann, J., Binder, S., Apfelbacher, A., Gasson, J.R., Ramírez García, P., Hornung, A.: Production and characterization of a new quality pyrolysis oil, char and syngas from digestate – Introducing the thermo-catalytic reforming process. Journal of Analytical and Applied Pyrolysis (2015). https://doi.org/10.1016/j.jaap.2014.11.022
5. Härtl, M., Pélerin, D., Dworschak, P., Maier, T., Stadler, A., Blochum, S., Gaukel, K., Jacob, E., Wachtmeister, G.: Potential of the sustainable C1 fuels OME, DMC, and MeFo for particle-free combustion in SI and CI engines. 5th International Engine Congress, Baden Baden (2018)
6. Bach, C.: Electro fuels as an alternative to electrification – an energetic and economic analysis. 5th International Engine Congress, Baden Baden (2018)
7. Hentschel, L., Michels, K., Garbe, T.: E-fuels - a central module for future engine design. 5th International Engine Congress, Baden Baden (2018)
8. Popp, T., Lechner, R., Becker, M., Hebauer, M., O'Connell, N., Brautsch, M.: Potentials of OME/diesel blends for stationary power production – Improving emission characteristics of a diesel CHP unit. Applied Thermal Engineering (2019). https://doi.org/10.1016/j.applthermaleng.2019.03.015
9. O'Connell, N., Röll, A., Lechner, R., Luo, T., Brautsch, M.: PODE-blend as pilot fuel in a biomethane dual fuel engine: Experimental analysis of performance, combustion and emissions characteristics. Renewable Energy (2019). https://doi.org/10.1016/j.renene.2019.04.127

10. Moreno-Benito, M., Agnolucci, P., Papageorgiou, L.G.: Towards a sustainable hydrogen economy. Optimisation-based framework for hydrogen infrastructure development. Computers & Chemical Engineering (2016). https://doi.org/10.1016/j.compchemeng.2016.08.005

11. Moliner, R., Lázaro, M.J., Suelves, I.: Analysis of the strategies for bridging the gap towards the Hydrogen Economy. International Journal of Hydrogen Energy (2016). https://doi.org/10.1016/j.ijhydene.2016.06.202

12. Hornung, A.: Bio-Hydrogen from Biomass. In: Hornung, A. (ed.) Transformation of biomass. Theory to practice, pp. 217–225. Wiley, Chichester (2014)

13. Karim, G.A.: Combustion in Gas-fueled Compression Ignition Engines of the Dual Fuel Type. In: Lackner, M., Winter, F., Agarwal, A.K. (eds.) Handbook of Combustion, vol. 3, pp. 213–235. WILEY-VCH, Weinheim (2010)

14. Eder, L., Kiesling, C., Pirker, G., Wimmer, A.: Development and Validation of a Reduced Reaction Mechanism for CFD Simulation of Diesel Ignited Gas Engines. In: Leipertz, A. (ed.) Engine Combustion Processes (XIII. Congress). Current Problems and Modern Techniques. Engine Combustion Processes, Ludwigsburg, 16.-17.03, pp. 299–312 (2017)

15. Brautsch, M., Lechner, R., Röll, A., O'Connell, N.: Experimental Investigation on Dual-Fuel Operation of CHP Engines with Biomethane and Various Pilot Fuels at Different Compression Ratios. Journal of Combustion Science and Technology (2019). https://doi.org/10.11715/rskxjs.R201805006

16. Lechner, R., O'Connell, N., Brautsch, M.: Identifikation von Einsatzmöglichkeiten und Potentialen der Zündstrahltechnologie zur Verbesserung der Anlageneffizienz und Wirtschaftlichkeit von BHKW-Anlagen mit experimenteller Überprüfung der Vorteile an einer Pilotanlage unter realen Bedingungen im Praxisbetrieb. [Abschlussbericht]. Forschungsinitiative Zukunft Bau F, vol. 2943. Fraunhofer IRB Verlag, Stuttgart (2015)

17. Heywood, J.B.: Internal combustion engine fundamentals. McGraw-Hill series in mechanical engineering. McGraw-Hill, New York (1988)

18. Auer, M., Wachtmeister, G.: Combustion modeling of lean-burning gas engines considering different fuel gases. In: WTZ Roßlau (ed.) Proceedings 6th Dessau Gas Engine Conference, Dessau, pp. 35–54, Dessau-Roßlau (2009)

19. Lämmle, C., Boulouchos, K., Bach, C.: Prediction and Interpretation of Combustion Processes in Natural Gas Engines. A comparative Overview of Simulation Methods for Practical Applications. In: WTZ Roßlau (ed.) Proceedings 4th Dessau Gas Engine Conference, Dessau, pp. 85–100, Dessau-Roßlau (2005)

20. Dimitrov, D., Chmela, F., Wimmer, A.: Eine Methode zur Vorausberechnung des Klopfverhaltens von Gasmotoren. In: WTZ Roßlau (ed.) Proceedings 4th Dessau Gas Engine Conference, Dessau, Dessau-Roßlau (2005)

21. Hann, S., Urban, L., Grill, M., Bargende, M.: Prediction of Burn Rate, Knocking and Cycle-to-Cycle Variations of Binary CNG Substitutes in Consideration of Reaction Kinetics Influences. In: Leipertz, A. (ed.) Engine Combustion Processes (XIII. Congress). Current Problems and Modern Techniques. Engine Combustion Processes, Ludwigsburg, 16.-17.03, pp. 63–77 (2017)

22. Netzer, C., Seidel, I., Pasternak, M., Mauss, F.: 3D CFD Engine Knock Predicition and Evaluation Based on Detailed Chemistry and Detonation Theory. In: Leipertz, A. (ed.) Engine Combustion Processes (XIII. Congress). Current Problems and Modern Techniques. Engine Combustion Processes, Ludwigsburg, 16.-17.03, pp. 185–196 (2017)

23. Bates, L., Bradley, D., Paczko, G., Peters, N.: Engine hot spots: Modes of auto-ignition and reaction propagation. Combustion and Flame (2016). https://doi.org/10.1016/j.combustflame.2016.01.002

24. Netzer, C., Seidel, L., Pasternak, M., Lehtiniemi, H., Perlman, C., Ravet, Frédéric, Mauss, Fabian: Three-dimensional computational fluid dynamics engine knock prediction and evaluation based on detailed chemistry and detonation theory. International Journal of Engine Research **19**, 33–44 (2018)

25. Bates, L., Bradley, D.: Deflagrative, auto-ignitive, and detonative propagation regimes in engines. Special Issue in Honor of Norbert Peters. Combustion and Flame (2017). https://doi.org/10.1016/j.combustflame.2016.05.023

26. Janbozorgi, M., Far, K.E., Metghalchi, H.: Combustion Fundamentals. In: Lackner, M., Winter, F., Agarwal, A.K. (eds.) Handbook of Combustion, vol. 1, pp. 1–51. WILEY-VCH, Weinheim (2010)

27. Zacharias, F.: Gasmotoren, 1st edn. Vogel-Fachbuch. Vogel, Würzburg (2001)

28. Lechner, R., O'Connell, N., Brautsch, M.: Survey of real-world carbon dioxide and methane emissions from gas engine powered CHP units. In: WTZ Roßlau (ed.) Proceedings 11th Dessau Gas Engine Conference, Dessau, pp. 184–195, Dessau-Roßlau (2019)

29. Grewe, F., Warketin, P., Rickert, M.: Turboaufgeladen - Miller - Lambda 1. Die neue 2G aura Baureihe. In: WTZ Roßlau (ed.) Proceedings 11th Dessau Gas Engine Conference, Dessau, pp. 76–89, Dessau-Roßlau (2019)

30. Andersson, Ö.: Diesel Combustion. In: Lackner, M., Winter, F., Agarwal, A.K. (eds.) Handbook of Combustion, vol. 3, pp. 415–440. WILEY-VCH, Weinheim (2010)

31. Kolaitis, D.I., Founti, M.A.: Cool Flames. In: Lackner, M., Winter, F., Agarwal, A.K. (eds.) Handbook of Combustion, vol. 1, pp. 265–294. WILEY-VCH, Weinheim (2010)

32. Beran, R., Baufeld, T., Ludu, A., Almer, W.: Entwicklung eines Micro-Pilot Gasmotors zur Erreichung höchster Wirkungsgrade auch bei kleineren Bohrungsgrößen. In: WTZ Roßlau (ed.) Proceedings 4th Dessau Gas Engine Conference, Dessau, pp. 9–24, Dessau-Roßlau (2005)

33. Unfug, F., Auer. M., Stiesch, G.: Analysis and Comparison of the Combustion of a lean natural gas/air Mixture in a Gas-Engine with scavenged Pre-Chamber and a Dual-Fuel Engine with Pilot Injection. In: Leipertz, A. (ed.) Engine Combustion Processes (XIII. Congress). Current Problems and Modern Techniques. Engine Combustion Processes, Ludwigsburg, 16.-17.03, pp. 105–118 (2017)

34. Merker, G.P., Schwarz, C.: Grundlagen Verbrennungsmotoren. Simulation der Gemischbildung, Verbrennung, Schadstoffbildung und Aufladung, 4th edn. Vieweg+Teubner Verlag / GWV Fachverlage GmbH, Wiesbaden, Wiesbaden (2009)

35. Pischinger, R., Klell, M., Sams, T.: Thermodynamik der Verbrennungskraftmaschine. Der Fahrzeugantrieb. Springer, Vienna (2002)

36. VIBE I. I.: Brennverlauf und Kreisprozess von Verbrennungsmotoren. VEB Verlag Technik, Berlin (1970)

37. Bonnevie-Svendsen, A., Boulouchos, K., Lämmle, C., Vlaskos, I.: Double-VIBE-Model for heat release in lean burn gas engines with prechamber ignition. In: WTZ Roßlau (ed.) Proceedings 6th Dessau Gas Engine Conference, Dessau, pp. 13–29, Dessau-Roßlau (2009)

38. Hiroyasu, H., Kadota, T.: Development and use of a spray combustion modeling to predict Diesel engine efficiency and pollutant emissions. Bull. JSME **26** (1983)

39. Auer, M.: Erstellung phänomenologischer Modelle zur Vorausberechnung des Brennverlaufes von Magerkonzept-Gasmotoren. Energietechnik (2010)

40. Walther, H.-P., Wachtmeister, G.: Phenomenological Combustion Model for Lean Burning Gas Engines with Pilot Injection. In: WTZ Roßlau (ed.) Proceedings 7th Dessau Gas Engine Conference, Dessau, pp. 255–274, Dessau-Roßlau (2011)

41. Frouzakis, C.E., Giannakopoulos, G.K., Wright, Y.M., Schmitt, M., Tomboulides, A.G.: Direct Numerical Simulations for Internal Combustion Premixed Gas Engines: First Steps, Challenges and Prospects. In: Leipertz, A. (ed.) Engine Combustion Processes (XIII. Congress). Current Problems and Modern Techniques. Engine Combustion Processes, Ludwigsburg, 16.-17.03, pp. 267–284 (2017)

42. Yokoo, N., Nakata, K., Iida, N. Ueda, T.: Research on the Improvement of the Knocking Prediction Accuracy by Considering the Effect of Negative Temperature Coefficient for High Compression Ratio Engines. In: Leipertz, A. (ed.) Engine Combustion Processes (XIII. Congress). Current Problems and Modern Techniques. Engine Combustion Processes, Ludwigsburg, 16.-17.03, pp. 173–184 (2017)

43. McBride, B.J., Zehe, M.J., Gordon, S.: NASA Glenn Coefficients for Calculating Thermodynamic Properties of Individual Species, NASA TP-2002-211556. NASA (2002)

44. Pachler, R.F., Ramalingam, A.K., Heufer, K.A., Winter, F.: Reduction and validation of a chemical kinetic mechanism including necessity analysis and investigation of CH4/C3H8 oxidation at pressures up to 120 bar using a rapid compression machine. Fuel (2016). https://doi.org/10.1016/j.fuel.2015.12.044

45. El Merhubi, H., Kéromnès, A., Catalano, G., Lefort, B., Le Moyne, L.: A high pressure experimental and numerical study of methane ignition. Fuel (2016). https://doi.org/10.1016/j.fuel.2016.03.016

46. Burke, S.M., Metcalfe, W., Herbinet, O., Battin-Leclerc, F., Haas, F.M., Santner, J., Dryer, F.L., Curran, H.J.: An experimental and modeling study of propene oxidation. Part 1. Speciation measurements in jet-stirred and flow reactors. Combustion and Flame (2014). https://doi.org/10.1016/j.combustflame.2014.05.010

47. Sung, C.-J., Curran, H.J.: Using rapid compression machines for chemical kinetics studies. Progress in Energy and Combustion Science (2014). https://doi.org/10.1016/j.pecs.2014.04.001

48. Golovitchev, V.I., Kärrholm, F.P.: Ignition: New Applications to Combustion Studies. In: Lackner, M., Winter, F., Agarwal, A.K. (eds.) Handbook of Combustion, vol. 1, pp. 85–106. WILEY-VCH, Weinheim (2010)

49. Lu, T., Law, C.K.: A directed relation graph method for mechanism reduction. Proceedings of the Combustion Institute (2005). https://doi.org/10.1016/j.proci.2004.08.145

50. Niemeyer, K.E., Sung, C.-J.: On the importance of graph search algorithms for DRGEP-based mechanism reduction methods. Combustion and Flame (2011). https://doi.org/10.1016/j.combustflame.2010.12.010

51. Niemeyer, K.E., Sung, C.-J., Raju, M.P.: Skeletal mechanism generation for surrogate fuels using directed relation graph with error propagation and sensitivity analysis. Combustion and Flame (2010). https://doi.org/10.1016/j.combustflame.2009.12.022

52. Stagni, A., Cuoci, A., Frassoldati, A., Faravelli, T., Ranzi, E.: Lumping and Reduction of Detailed Kinetic Schemes: an Effective Coupling. Ind. Eng. Chem. Res. (2014). https://doi.org/10.1021/ie403272f

53. Perini, F.: Optimally reduced reaction mechanisms for Internal Combustion Engines running on biofuels. PhD thesis, Università di Modena e Reggio Emilia (2011)

54. Smith, G.P., Golden, D.M., Frenklach, M., Moriarty, N.W., Eiteneer, B., Goldenberg, M., Bowman, T.C., Hanson, R.K., Song, S., Gardiner, W.C., JR., Lissianski, V.V., Qin, Z.: GRI-MECH 3.0. http://www.me.berkeley.edu/gri_mech/. Accessed 8 March 2017

55. Wang, H., You, X., Joshi, A.V., Davis, S.G., Laskin, A., Egolfopoulos, F.N., Law, C.K.: USC Mech Version II. High-Temperature Combustion Reaction Model of H2/CO/C1-C4 Compounds. http://ignis.usc.edu/Mechanisms/USCMech%20II/USC_Mech%20II.htm (2007)

56. Zhou, C.-W., Li, Y., Burke, U., Banyon, C., Somers, K.P., Ding, S., Khan, S., Hargis, J.W., Sikes, T., Mathieu, O., Petersen, E.L., AlAbbad, M., Farooq, A., Pan, Y., Zhang Yingjia, Huang, Z., Lopez, J., Loparo, Z., Vasu, S.S., Curran, H.J.: An experimental and chemical kinetic modeling study of 1,3-butadiene combustion: Ignition delay time and laminar flame speed measurements. Combustion and Flame (2018). https://doi.org/10.1016/j.combustflame.2018.08.006

57. Li, Y., Zhou, C.-W., Somers, K.P., Zhang, K., Curran, H.J.: The oxidation of 2-butene. A high pressure ignition delay, kinetic modeling study and reactivity comparison with isobutene and 1-butene. Proceedings of the Combustion Institute (2017). https://doi.org/10.1016/j.proci.2016.05.052

58. Kéromnès, A., Metcalfe, W.K., Heufer, K.A., Donohoe, N., Das, A.K., Sung, C.-J., Herzler, J., Naumann, C., Griebel, P., Mathieu, O., Krejci, M.C., Petersen, E.L., Pitz, W.J., Curran, H.J.: An experimental and detailed chemical kinetic modeling study of hydrogen and syngas mixture oxidation at elevated pressures. Combustion and Flame (2013). https://doi.org/10.1016/j.combustflame.2013.01.001

59. Metcalfe, W.K., Burke, S.M., Ahmed, S.S., Curran, H.J.: A Hierarchical and Comparative Kinetic Modeling Study of C 1 − C 2 Hydrocarbon and Oxygenated Fuels. Int. J. Chem. Kinet. (2013). https://doi.org/10.1002/kin.20802

60. Burke, S.M., Burke, U., Mc Donagh, R., Mathieu, O., Osorio, I., Keesee, C., Morones, A., Petersen, E.L., Wang, W., DeVerter, T.A., Oehlschlaeger, M.A., Rhodes, B., Hanson, R.K., Davidson, D.F., Weber, B.W., Sung, C.-J., Santner, J., Ju, Y., Haas, F.M., Dryer, F.L., Volkov, E.N., Nilsson, E.J.K., Konnov, A.A., Alrefae, M., Khaled, F., Farooq, A., Dirrenberger, P.,

Glaude, P.-A., Battin-Leclerc, F., Curran, H.J.: An experimental and modeling study of propene oxidation. Part 2. Ignition delay time and flame speed measurements. Combustion and Flame (2015). https://doi.org/10.1016/j.combustflame.2014.07.032

61. Zhou, C.-W., Li, Y., O'Connor, E., Somers, K.P., Thion, S., Keesee, C., Mathieu, O., Petersen, E.L., DeVerter, T.A., Oehlschlaeger, M.A., Kukkadapu, G., Sung, C.-J., Alrefae, M., Khaled, F., Farooq, A., Dirrenberger, P., Glaude, P.-A., Battin-Leclerc, F., Santner, J., Ju, Y., Held, T., Haas, F.M., Dryer, F.L., Curran, H.J.: A comprehensive experimental and modeling study of isobutene oxidation. Combustion and Flame (2016). https://doi.org/10.1016/j.combustflame.2016.01.021

62. Burke, U., Metcalfe, W.K., Burke, S.M., Heufer, K.A., Dagaut, P., Curran, H.J.: A detailed chemical kinetic modeling, ignition delay time and jet-stirred reactor study of methanol oxidation. Combustion and Flame (2016). https://doi.org/10.1016/j.combustflame.2015.11.004

63. Zhang, Y., Mathieu, O., Petersen, E.L., Bourque, G., Curran, H.J.: Assessing the predictions of a NOx kinetic mechanism on recent hydrogen and syngas experimental data. Combustion and Flame (2017). https://doi.org/10.1016/j.combustflame.2017.03.019

64. NUI Galway: AramcoMech 2.0. http://www.nuigalway.ie/combustionchemistrycentre/mechanismdownloads/aramcomech20/. Accessed 20 May 2019

65. Ranzi, E., Frassoldati, A., Grana, R., Cuoci, A., Faravelli, T., Kelley, A.P., Law, C.K.: Hierarchical and comparative kinetic modeling of laminar flame speeds of hydrocarbon and oxygenated fuels. Progress in Energy and Combustion Science (2012). https://doi.org/10.1016/j.pecs.2012.03.004

66. San Diego Mechanism web page: Chemical-Kinetic Mechanisms for Combustion Applications. http://combustion.ucsd.edu

67. Chmela, F., Krenn, M., Pirker, G., Schlick, H., Wimmer, A.: Heat Release Rate Simulation with Non-Natural Gases. In: WTZ Roßlau (ed.) Proceedings 8th Dessau Gas Engine Conference, Dessau, pp. 197–210, Dessau-Roßlau (2013)

68. Glassman, I., Yetter, R.A., Glumac, N.G.: Combustion, 5th edn. AP Academic Press/Elsevier, Amsterdam (2015)

69. Schultze, M., Drexel, C., Kollias-Pityrigkas, G.: Experimental and numerical investigation of gaseous hydrogenrich fuels in large gas engines. In: WTZ Roßlau (ed.) Proceedings 10th Dessau Gas Engine Conference, Dessau, pp. 307–318, Dessau-Roßlau (2017)

70. Hu, E., Li, X., Meng, X., Chen, Y., Cheng, Y., Xie, Y., Huang, Z.: Laminar flame speeds and ignition delay times of methane–air mixtures at elevated temperatures and pressures. Fuel (2015). https://doi.org/10.1016/j.fuel.2015.05.010

71. Bates, L., Bradley, D., Gorbatenko, I., Tomlin, A.S.: Computation of methane/air ignition delay and excitation times, using comprehensive and reduced chemical mechanisms and their relevance in engine autoignition. Combustion and Flame (2017). https://doi.org/10.1016/j.combustflame.2017.07.002

72. Burke, U., Somers, K.P., O'Toole, P., Zinner, C.M., Marquet, N., Bourque, G., Petersen, E.L., Metcalfe, W.K., Serinyel, Z., Curran, H.J.: An ignition delay and kinetic modeling study of methane, dimethyl ether, and their mixtures at high pressures. Combustion and Flame (2015). https://doi.org/10.1016/j.combustflame.2014.08.014

73. Zhang, Y., Jiang, X., Wei, L., Zhang, J., Tang, C., Huang, Z.: Experimental and modeling study on auto-ignition characteristics of methane/hydrogen blends under engine relevant pressure. International Journal of Hydrogen Energy (2012). https://doi.org/10.1016/j.ijhydene.2012.09.056

74. Bates, L.: Characterisation of reaction propagation from auto-ignition. PhD thesis, University of Leeds (2016)

75. Xu, H., Yao, A., Yao, C., Gao, J.: Investigation of energy transformation and damage effect under severe knock of engines. Applied Energy (2017). https://doi.org/10.1016/j.apenergy.2017.06.065

76. Ceschini, L., Morri, A., Balducci, E., Cavina, N., Rojo, N., Calogero, L., Poggio, L.: Experimental observations of engine piston damage induced by knocking combustion. Materials & Design (2017). https://doi.org/10.1016/j.matdes.2016.11.015

77. Wang, Z., Liu, H., Reitz, R.D.: Knocking combustion in spark-ignition engines. Progress in Energy and Combustion Science (2017). https://doi.org/10.1016/j.pecs.2017.03.004

78. Zhen, X., Wang, Y., Xu, S., Zhu, Y., Tao, C., Xu, T., Song, M.: The engine knock analysis – An overview. Applied Energy (2012). https://doi.org/10.1016/j.apenergy.2011.11.079

79. Kalghatgi, G.: Knock Onset, Knock Intensity, Super-knock and Pre-ignition in Spark Ignition (SI) Engines. In: Leipertz, A. (ed.) Engine Combustion Processes (XIII. Congress). Current Problems and Modern Techniques. Engine Combustion Processes, Ludwigsburg, 16.-17.03, pp. 133–149 (2017)

80. d'Adamo, A., Breda, S., Fontanesi, S., Irimescu, A., Merola, S.S., Tornatore, C.: A RANS knock model to predict the statistical occurrence of engine knock. Applied Energy (2017). https://doi.org/10.1016/j.apenergy.2017.01.101

81. Li, T., Yin, T., Wang, B.: A phenomenological model of knock intensity in spark-ignition engines. Energy Conversion and Management (2017). https://doi.org/10.1016/j.enconman.2017.06.078

82. Sotiropoulou, E., Harral, J., Tozzi, L.: A Method for Prediciting Knock in Gas Engines by means of Chemical Precursors from Detailed Chemistry CFD. In: WTZ Roßlau (ed.) Proceedings 8th Dessau Gas Engine Conference, Dessau, pp. 239–252, Dessau-Roßlau (2013)

83. Bougrine, S., Richard, S., Nicolle, A., Veynante, D.: Numerical study of laminar flame properties of diluted methane-hydrogen-air flames at high pressure and temperature using detailed chemistry. International Journal of Hydrogen Energy (2011). https://doi.org/10.1016/j.ijhydene.2011.06.053

84. Kumar, P., Kishan, P.A., Dhar, A.: Numerical investigation of pressure and temperature influence on flame speed in CH 4 H 2 premixed combustion. International Journal of Hydrogen Energy (2016). https://doi.org/10.1016/j.ijhydene.2016.04.036

85. Clean Combustion Research Center: Cloudflame. http://cloudflame.kaust.edu.sa/home. Accessed 25 May 2019

86. Pizzuti, L., Martins, C.A., Lacava, P.T.: Laminar burning velocity and flammability limits in biogas: A literature review. Renewable and Sustainable Energy Reviews (2016). https://doi.org/10.1016/j.rser.2016.05.011

87. Lee, H.C., Jiang, L.Y., Mohamad, A.A.: A review on the laminar flame speed and ignition delay time of Syngas mixtures. International Journal of Hydrogen Energy (2014). https://doi.org/10.1016/j.ijhydene.2013.10.068

88. Ouyang, L., Li, H., Sun, S., Wang, X., Lu, X.: Auto-ignition of biomass synthesis gas in shock tube at elevated temperature and pressure. Science Bulletin **2015**, 1935–1946 (22)

89. Liu, Z., Karim, G.A.: The Ignition Delay Period in Dual Fuel Engines. SAE transactions **1995**, 354–362

90. Hann, S., Urban, L., Grill, M., Bargende, M.: Prediction of burn rate, knocking and cycle-to-cycle variations of methane / hydrogen mixtures in stoichiometric and lean engine operation conditions. In: Proceedings 11th International MTZ Conference

91. Hiltner, J.: Combustion System Development and Simulation Tools for Engines Operating on Gasified Biomass Fuels. In: WTZ Roßlau (ed.) Proceedings 5th Dessau Gas Engine Conference, Dessau, pp. 250–263, Dessau-Roßlau (2007)

92. Beshouri, G., Jacobs, T.J., Choquette, G.: The Influence of Fuel Natural Gas Composition on Lean Burn Engines Using a Virtual Air/Fuel Ratio Sensor. In: WTZ Roßlau (ed.) Proceedings 11th Dessau Gas Engine Conference, Dessau, pp. 200–214, Dessau-Roßlau (2019)

93. Gülder, Ö.: Correlations of Laminar Combustion Data for Alternative S.I. Engine Fuels. SAE Technical Papers (1984)

94. Verhelst, S., T'Joen, C., Vancoillie, J., Demuynck, J.: A correlation for the laminar burning velocity for use in hydrogen spark ignition engine simulation. International Journal of Hydrogen Energy (2011). https://doi.org/10.1016/j.ijhydene.2010.10.020

95. Doosje, E., Salomons, A.G., Baert, R.S.G.: Influence of natural gas composition on SI engine operation, supported by burning velocity measurements. In: WTZ Roßlau (ed.) Proceedings 5th Dessau Gas Engine Conference, Dessau, pp. 4–26, Dessau-Roßlau (2007)

96. Wise, D.M.: Investigation into producer gas utilisation in high performance natural gas engines. PhD thesis, Colorado State University (2013)

97. Bradley, D., Head, R.A.: Engine autoignition: The relationship between octane numbers and autoignition delay times. Combustion and Flame (2006). https://doi.org/10.1016/j.combustflame.2006.09.001

98. Gu, X.J., Emerson, D.R., Bradley, D.: Modes of reaction front propagation from hot spots. Combustion and Flame (2003). https://doi.org/10.1016/S0010-2180(02)00541-2

99. Bradley, D., Kalghatgi, G.T.: Influence of autoignition delay time characteristics of different fuels on pressure waves and knock in reciprocating engines. Combustion and Flame (2009). https://doi.org/10.1016/j.combustflame.2009.08.003

100. Lutz, A.E., Kee, R.J., Miller, J.A., Dwyer, H.A., Oppenheim, A.K.: Dynamic effects of autoignition centers for hydrogen and C1,2-hydrocarbon fuels. Symposium (International) on Combustion (1989). https://doi.org/10.1016/S0082-0784(89)80181-X

101. Sankaran, R., Im, H.G., Hawkes, E.R., Chen, J.H.: The effects of non-uniform temperature distribution on the ignition of a lean homogeneous hydrogen–air mixture. Proceedings of the Combustion Institute (2005). https://doi.org/10.1016/j.proci.2004.08.176

102. Mansfield, A.B., Woolridge, Margaret, S.: High-pressure low-temperature ignition behavior of syngas mixtures. Combustion and Flame (2014). https://doi.org/10.1016/j.combustflame.2014.03.001

103. Kaltschmitt, M.: Biomass as Renewable Source of Energy: Possible Conversion Routes. In: Kaltschmitt, M. (ed.) Energy from Organic Materials (Biomass). A Volume in the Encyclopedia of Sustainability Science and Technology, Second Edition. Encyclopedia of Sustainability Science and Technology Series, pp. 353–389. Springer New York, New York, NY (2019)

104. Zhang, L., Xu, C., Champagne, P.: Overview of recent advances in thermo-chemical conversion of biomass. Energy Conversion and Management (2010). https://doi.org/10.1016/j.enconman.2009.11.038

105. Yuping, L., Chen, L., Wang, T., Ma, L., Ding, M., Zhang, X., Yin, X.: Demonstration of Pilot-scale Bio-dimethyl ether Synthesis Via Oxygen- and steam- enriched Gasification of Wood Chips. Energy Procedia (2015). https://doi.org/10.1016/j.egypro.2015.07.303

106. Rodero, R.M., Ángeles, R., Marín, D., Díaz, I., Colzi, A., Posadas, E., Lebrero, R., Muñoz, R.: Biogas Purification and Upgrading Technologies. In: Tabatabaei, M., Ghanavati, H. (eds.) Biogas. Fundamentals, Process, and Operation. Biofuel and Biorefinery Technologies, Volume 6, pp. 239–276. Springer, Cham (2018)

107. Valijanian, E., Tabatabaei, M., Aghbashlo, M., Sulaiman, A., Chisti, Y.: Biogas Production Systems. In: Tabatabaei, M., Ghanavati, H. (eds.) Biogas. Fundamentals, Process, and Operation. Biofuel and Biorefinery Technologies, Volume 6, pp. 95–116. Springer, Cham (2018)

108. Scholwin, F., Nelles, M., Grope, J.: Biogas for Energy Provision form Agricultural Feedstock: Hi-Tech Applications. In: Kaltschmitt, M. (ed.) Energy from Organic Materials (Biomass). A Volume in the Encyclopedia of Sustainability Science and Technology, Second Edition. Encyclopedia of Sustainability Science and Technology Series, pp. 809–821. Springer New York, New York, NY (2019)

109. Reil, S.: Zur Biomassevergasung in "stratified downdraft" Reaktoren und deren Prozessstabilisierung. PhD thesis, FAU Erlangen-Nürnberg (2019)

110. Schulzke, T.: Biomass gasification: conversion of forest residues into heat, electricity and base chemicals. Chemical Papers **73**, 1833–1852 (2019)

111. Patuzzi, F., Prando, D., Vakalis, S., Rizzo, A.M., Chiaramonti, D., Tirler, W., Mimmo, T., Gasparella, A., Baratieri, M.: Small-scale biomass gasification CHP systems: Comparative performance assessment and monitoring experiences in South Tyrol (Italy). Energy **112**, 285–293 (2016)

112. Di Marcello, M., Tsalidis, G.A., Spinelli, G., Jong, W. de, Kiel, J.H.A.: Pilot scale steam-oxygen CFB gasification of commercial torrefied wood pellets. The effect of torrefaction on the gasification performance. Biomass and Bioenergy (2017). https://doi.org/10.1016/j.biombioe.2017.08.005

113. Biagini, E., Barontini, F., Tognotti, L.: Gasification of agricultural residues in a demonstrative plant: corn cobs. Bioresource technology (2014). https://doi.org/10.1016/j.biortech.2014.09.086

114. Kurkela, E., Kurkela, M., Hiltunen, I.: Steam–oxygen gasification of forest residues and bark followed by hot gas filtration and catalytic reforming of tars: Results of an extended time test. Fuel Processing Technology (2016). https://doi.org/10.1016/j.fuproc.2015.06.005

115. Dahlquist, E., Naqvi, M., Thorin, E., Yan, J., Kyprianidis, K.: Comparison of Gas Quality from Black Liquor and Wood Pellet Gasification Using Modelica Simulation and Pilot Plant Results. Energy Procedia (2017). https://doi.org/10.1016/j.egypro.2017.03.437

116. Katsaros, G., Shankar Pandey, D., Horvat, A., Tassou, S.: Low temperature gasification of poultry litter in a lab-scale fluidized reactor. Energy Procedia (2019). https://doi.org/10.1016/j.egypro.2019.02.058

117. Bridgwater, A.V.: Review of fast pyrolysis of biomass and product upgrading. Biomass and Bioenergy (2012). https://doi.org/10.1016/j.biombioe.2011.01.048

118. Charusiri, W.: Fast Pyrolysis of Residues from Paper Mill Industry to Bio-oil and Value Chemicals: Optimization Studies. Energy Procedia (2015). https://doi.org/10.1016/j.egypro.2015.07.724

119. Jeong, Y.W., Choi, S.K., Choi, Y.S., Kim, S.J.: Production of biocrude-oil from swine manure by fast pyrolysis and analysis of its characteristics. Renewable Energy (2015). https://doi.org/10.1016/j.renene.2014.08.041

120. Torri, I.D.V., Paasikallio, V., Faccini, C.S., Huff, R., Caramão, E.B., Sacon, V., Oasmaa, A., Zini, C.A.: Bio-oil production of softwood and hardwood forest industry residues through fast and intermediate pyrolysis and its chromatographic characterization. Bioresource technology (2016). https://doi.org/10.1016/j.biortech.2015.10.086

121. Folgueras, M.B., Fernández, F.J., Ardila, C.R., Alonso, M., Lage, S.: Fast pyrolysis of Guadua angustifolia -Kunth. Energy Procedia (2017). https://doi.org/10.1016/j.egypro.2017.10.283

122. Erdogdu, A.E., Polat, R., Ozbay, G.: Pyrolysis of goat manure to produce bio-oil. Engineering Science and Technology, an International Journal (2019). https://doi.org/10.1016/j.jestch.2018.11.002

123. Mishra, R.K., Mohanty, K.: Thermal and catalytic pyrolysis of pine sawdust (Pinus ponderosa) and Gulmohar seed (Delonix regia) towards production of fuel and chemicals. Materials Science for Energy Technologies (2019). https://doi.org/10.1016/j.mset.2018.12.004

124. Boscagli, C., Tomasi Morgano, M., Raffelt, K., Leibold, H., Grunwaldt, J.-D.: Influence of feedstock, catalyst, pyrolysis and hydrotreatment temperature on the composition of upgraded oils from intermediate pyrolysis. Biomass and Bioenergy (2018). https://doi.org/10.1016/j.biombioe.2018.06.022

125. Ouadi, M., Brammer, J.G., Yang, Y., Hornung, A., Kay, M.: The intermediate pyrolysis of deinking sludge to produce a sustainable liquid fuel. Journal of Analytical and Applied Pyrolysis (2013). https://doi.org/10.1016/j.jaap.2013.04.007

126. Neumann, J., Jäger, N., Apfelbacher, A., Daschner, R., Binder, S., Hornung, A.: Upgraded biofuel from residue biomass by Thermo-Catalytic Reforming and hydrodeoxygenation. Biomass and Bioenergy (2016). https://doi.org/10.1016/j.biombioe.2016.03.002

127. Yang, Y., Brammer, J.G., Samanya, J., Hossain, A.K., Hornung, A.: Investigation into the performance and emissions of a stationary diesel engine fuelled by sewage sludge intermediate pyrolysis oil and biodiesel blends. Energy (2013). https://doi.org/10.1016/j.energy.2013.09.058

128. Ahmad, E., Jäger, N., Apfelbacher, A., Daschner, R., Hornung, A., Pant, K.K.: Integrated thermo-catalytic reforming of residual sugarcane bagasse in a laboratory scale reactor. Fuel Processing Technology (2018). https://doi.org/10.1016/j.fuproc.2017.11.020

129. Mohanty, P., Pant, K.K., Mittal, R.: Hydrogen generation from biomass materials. Challenges and opportunities. WIREs Energy Environ (2015). https://doi.org/10.1002/wene.111

130. Hiltner, J., Hoops, C., Wang, P.: Knock Prediction in Lean Burn Natural Gas Engines for Fuels with Significant Higher Hydrocarbon Content. In: WTZ Roßlau (ed.) Proceedings 8th Dessau Gas Engine Conference, Dessau, pp. 133–153, Dessau-Roßlau (2013)

131. Greenhalf, C.E., Nowakowski, D.J., Harms, A.B., Titiloye, J.O., Bridgwater, A.V.: A comparative study of straw, perennial grasses and hardwoods in terms of fast pyrolysis products. Fuel (2013). https://doi.org/10.1016/j.fuel.2013.01.075

132. Conti, R., Jäger, N., Neumann, J., Apfelbacher, A., Daschner, R., Hornung, A.: Thermocatalytic Reforming of Biomass Waste Streams. Energy Technol. (2017). https://doi.org/10.1002/ente.201600168

133. Neumann, J., Meyer, J., Ouadi, M., Apfelbacher, A., Binder, S., Hornung, A.: The conversion of anaerobic digestion waste into biofuels via a novel Thermo-Catalytic Reforming process. Waste management (New York, N.Y.) (2016). https://doi.org/10.1016/j.wasman.2015.07.001

134. Meyer, J., Neumann, J., Binder, S., Hornung, A.: Conversion of residual biomass in a thermocatalytic reforming plant experimental investigation of digestate. 22nd European Biomass Conference and Exhibition, 935–938 (2014)

135. Jäger, N., Conti, R., Neumann, J., Apfelbacher, A., Daschner, R., Binder, S., Hornung, A.: Thermo-Catalytic Reforming of Woody Biomass. Energy Fuels (2016). https://doi.org/10.1021/acs.energyfuels.6b00911

136. Mahmood, A.S.N., Brammer, J.G., Hornung, A., Steele, A., Poulston, S.: The intermediate pyrolysis and catalytic steam reforming of Brewers spent grain. Journal of Analytical and Applied Pyrolysis (2013). https://doi.org/10.1016/j.jaap.2012.09.009

137. Yang, Y., Brammer, J.G., Mahmood, A.S.N., Hornung, A.: Intermediate pyrolysis of biomass energy pellets for producing sustainable liquid, gaseous and solid fuels. Bioresource technology (2014). https://doi.org/10.1016/j.biortech.2014.07.044

138. Louwes, A.C., Basile, L., Yukananto, R., Bhagwandas, J.C., Bramer, E.A., Brem, G.: Torrefied biomass as feed for fast pyrolysis: An experimental study and chain analysis. Biomass and Bioenergy (2017). https://doi.org/10.1016/j.biombioe.2017.06.009

139. Wu, D., Xiao, L., Ba, Y., Wang, H., Zhang, A., Wu, X., Niu, M., Fang, K.: The Recovery of Energy, Nitrogen and Phosphorous from Three Agricultural Wastes by Pyrolysis. Energy Procedia (2017). https://doi.org/10.1016/j.egypro.2017.03.445

140. Verhelst, S., Wallner, T.: Hydrogen-fueled internal combustion engines. Progress in Energy and Combustion Science (2009). https://doi.org/10.1016/j.pecs.2009.08.001

141. Gieseking, B., Brown, A.S.: Novel algorithm for calculating the methane number of liquefied natural gas with defined uncertainty. Fuel (2016). https://doi.org/10.1016/j.fuel.2016.07.105

142. Andersen, P.: Algorithm for methane number determination for natural gases. Danish Gas Technology Centre a/s, Hørsholm (1999)

143. European Association of Internal Combustion Engine Manufacturers (EUROMOT): MWM MN calculation program. http://www.euromot.eu/publication-and-events/publications/ (2017)

144. The European Association of Internal Combustion Engine Manufacturers (Euromot). http://www.euromot.eu/ (2019). Accessed 5 June 2019

145. van essen, M., Gersen, S., H J Van Dijk, G, Levinsky, H.: Next generation knock characterization. In: International Gas Union Research Conference 2014, Copenhagen (2014)

146. Cummins Westport: Fuel Quality Calculator. http://www.cumminswestport.com/fuel-quality-calculator. Accessed 6 June 2019

147. Gersen, S., van essen, M., Levinsky, H., van Dijk, G.: Characterizing Gaseous Fuels for Their Knock Resistance based on the Chemical and Physical Properties of the Fuel. SAE International Journal of Fuels and Lubricants (2016). https://doi.org/10.4271/2015-01-9077

148. van essen, M., Gersen, S.: Ensure fitness for purpose for pipeline gas. Determine the quality of pipeline gas and secure safe and reliable use by calculating the Propane Knock Index (PKI) methane number. http://www.dnvgl.com/oilgas/natural-gas/fitness-for-purpose-for-pipeline-gas.html. Accessed 6 June 2019

149. Virnich, L., Geiger, J., Bergmann, D., Dhongde, A., Sankhla, H.: Predicition of knocking combustion in natural gas engines using detailed chemical reaction kinetics. In: WTZ Roßlau

(ed.) Proceedings 10th Dessau Gas Engine Conference, Dessau, pp. 151–162, Dessau-Roßlau (2017)

150. Goodwin, D.G., Speth, R.L., Moffat, H.K., Weber, B.W.: Cantera: An object-oriented software toolkit for chemical kinetics, thermodynamics, and Transport Processes. Zenodo (2018)

151. Saikaly, K., Rousseau, S., Rahmouni, C., Le Corre, O., Truffet, L.: Safe operating conditions determination for stationary SI gas engines. Fuel Processing Technology (2008). https://doi.org/10.1016/j.fuproc.2008.05.015

152. Saikaly, K., Le Corre, O., Rahmouni, C., Truffet, L.: Preventive knock protection technique for stationary SI engines fuelled by natural gas. Fuel Processing Technology (2010). https://doi.org/10.1016/j.fuproc.2010.01.011

153. Sarothi Roy, P., Ryu, C., Dong, S.K., Park, C.S.: Development of a natural gas Methane Number prediction model. Fuel (2019). https://doi.org/10.1016/j.fuel.2019.02.116

154. Malenshek, M., Olsen, D.B.: Methane number testing of alternative gaseous fuels. Fuel (2009). https://doi.org/10.1016/j.fuel.2008.08.020

155. Arunachalam, A., Olsen, D.B.: Experimental evaluation of knock characteristics of producer gas. Biomass and Bioenergy (2012). https://doi.org/10.1016/j.biombioe.2011.12.016

156. Gómez Montoya, J.P., Amell, A.A., Olsen, D.B.: Prediction and measurement of the critical compression ratio and methane number for blends of biogas with methane, propane and hydrogen. Fuel (2016). https://doi.org/10.1016/j.fuel.2016.08.064

157. van Essen, V.M., Gersen, S., van Dijk, G.H.J., Levinsky, H.B.: Next generation knock characterization. DNV GL Oil & Gas

158. McBride, B.J., Gordon, S., Reno, M.A.: Coefficients for Calculating Thermodynamic and Transport Properties of Individual Species. NASA-Report, TM-4513 (1993)

159. Kee, R.J., Rupley, F.M., Miller, J.A.: Chemkin-II: A Fortran chemical kinetics package for the analysis of gas-phase chemical kinetics. Technical Report SAND89-8009 (1989)

160. Kee, R.J., Coltrin, M.E., Glarborg, P., Zhu, H.: Chemically Reacting Flow. Wiley (2017)

161. Kee, R.J., Rupley, F.M., Meeks, E.: CHEMKIN-III: A Fortran Chemical Kinetics Package for the Analysis of Gas-Phase Chemical and Plasma Kinetics, SAND96-8216 (1996)

162. Kee, R.J., Dixon-Lewis, G., Warnatz, J., Coltrin, M.E., Miller, J.A., Moffat, H.K.: A Fortran Computer Code Package for the Evaluation of Gas-Phase, Multicomponent Transport Properties, SAND86-8264B (1998)

163. Gilbert, R.G., Luther, K., Troe, J.: Theory of Thermal Unimolecular Reactions in the Fall-off Range. II. Weak Collision Rate Constants. Berichte der Bunsengesellschaft für physikalische Chemie (1983). https://doi.org/10.1002/bbpc.19830870218

164. Chase, M.W.: NIST-JANAF thermochemical tables, 4th edn. American Institute of Physics, Woodbury, NY (1998)

165. Burcat, A.: Third millennium ideal gas and condensed phase thermochemical database for combustion. TAE, no. 867. Technion-Israel Institute of Technology, [Haifa, Israel] (2001)

166. Grill, M.: Objektorientierte Prozessrechnung von Verbrennungsmotoren. @Stuttgart, Univ., Diss., 2006. Univ, Stuttgart

167. Missen, R.W., Smith, W.R.: Chemical Reaction Stiochiometry (CRS): A Tutorial. http://www.chemical-stoichiometry.net (1998). Accessed 1 May 2019

168. The International Association for the Properties of Water and Steam: Revised Release on the IAPWS Industrial Formulation 1997 for the Thermodynamic Properties of Water and Steam, IAPWS R7-97(2012), Lucerne, Switzerland (2007)

169. Greenspan, L.: Functional Equations for the Enhancement Factors for CO2-Free Moist Air. Journal of Research of the National Bureau of Standards - A. Physics and Chemistry **Vol. 80A**, 41–44 (1976)

170. Sairanen, H.A., Heinonen, M.O.: Enhacement Factor for Water Vapor-Pressure Correction in Humid Methane. International Journal of Thermophysics **35**, 1280–1289 (2014)

171. Press, W.H., Teukolsky, S.A., Vetterling, W.T., Flannery, B.P.: Numerical recipes. The art of scientific computing, 3rd edn. Cambridge University Press, Cambridge (2007)

172. Benim, A.C., Syed, K.J.: Flashback Mechanisms in Lean Premixed Gas Turbine Combustion. Elsevier Science, Burlington (2014)

173. Burluka, A.A.: Combustion in a Spark Ignition Engine. In: Lackner, M., Winter, F., Agarwal, A.K. (eds.) Handbook of Combustion, Volume 3, pp. 389–414. WILEY-VCH, Weinheim (2010)

174. Mansfield, A.B., Wooldridge, M.S., Di, H., He, X.: Low-temperature ignition behavior of iso-octane. Fuel (2015). https://doi.org/10.1016/j.fuel.2014.08.019

175. Cantera: NumFOCUS Sponsored Project since 2018. http://numfocus.org/project/cantera. Accessed 18 May 2019

176. Cantera. http://cantera.org. Accessed 18 May 2019

177. McKinney, W.: Data Structures for Statistical Computing in Python. In: Proceedings of the 9th Python in Science Conference, pp. 51–56 (2010)

178. McKerns, M., Aivazis, M.A.G.: pathos: a framework for heterogeneous computing (2010)

179. McKerns, M.M., Strand, L., Sullivan, T., Fang, A., Aivazis, M.A.G.: Building a Framework for Predictive Science. In: Proceedings of the 10th Python in Science Conference (2011)

180. Hunter, J. d.: Matplotlib: A 2D Graphics Environment. Comput. Sci. Eng. (2007). https://doi.org/10.1109/MCSE.2007.55

181. Poinsot, T., Veynante, D. (eds.): Theoretical and Numerical Combustion, 3rd edn. (2012)

182. Lackner, M., Winter, F., Agarwal, A.K. (eds.): Handbook of Combustion. WILEY-VCH, Weinheim (2010)

183. Yu, G., Askari, O., Hadi, F., Wang, Z., Metgalchi, H., Kannaiyan, K., Sadr, R.: Theroretical Predicition of Laminar Burning Speed and Ignition Delay Time of Gas-to-Liquid Fuel. Journal of Energy Resources Technology **139** (2017)

184. Dobski, T., Rojewski, J., Wawrzyniak, J.: The analysis of the process of combustion of natural gases of high molar fraction nitrogen in reciprocating gas engines. In: WTZ Roßlau (ed.) Proceedings 7th Dessau Gas Engine Conference, Dessau, pp. 197–208, Dessau-Roßlau (2011)

185. Virnich, L., Hackelbörger, M., Geiger, J.: Reaction kinetic modeling of nitrogen oxide emissions of a lean burn large-bore natural gas engine. In: WTZ Roßlau (ed.) Proceedings 11th Dessau Gas Engine Conference, Dessau, pp. 304–317, Dessau-Roßlau (2019)

186. Xu, G., Hegde, R., Bardis, K., Kyrtatos, P., Wright, Y.M., Kotzagianni, M., Boulouchos, K.: Towards predictive numerical tools for the development of gas engines with prechambers. In: WTZ Roßlau (ed.) Proceedings 11th Dessau Gas Engine Conference, Dessau, pp. 92–107, Dessau-Roßlau (2019)

187. Kee, R.J., Grcar, J.F., Smooke, M.D., Miller, J.A., Meeks, E.: PREMIX: A Fortran Program for Modeling Steady Laminar One-Dimensional Premixed Flames. 85-8240. Sandia National Laboratories, Albuquerque (1985)

188. Ansys Chemkin-Pro. http://www.ansys.com/de-de/products/fluids/ansys-chemkin-pro. Accessed 18 May 2019

189. OpenSMOKE++. http://www.opensmokepp.polimi.it/. Accessed 18 May 2019

190. Cuoci, A., Frassoldati, A., Faravelli, T., Ranzi, E.: OpenSMOKE++ : An object-oriented framework for the numerical modeling of reactive systems with detailed kinetic mechanisms. Computer Physics Communications (2015). https://doi.org/10.1016/j.cpc.2015.02.014

191. Jones, E., Oliphant, T., Peterson Pearu, et.al.: SciPy: Open Source Scientific Tools for Python (2001)

Appendix A: Reaction kinetics software

With the release of CHEMKIN [159, 161] developed at *Sandia National Laboratories* in the 1980s, software for simulation of chemically reacting systems has been become readily available. CHEMKIN is now maintained and commercially distributed as Chemkin-Pro by ANSYS and features simplified models for the simulation of internal combustion engines with detailed chemical kinetics, such as a spark ignition model as well as a single and multi-zone HCCI engine models [188]. Additionally, it offers plug-in compatibility with other commercial engines simulation software suites, such as Gamma Technologies GT-Suite [188].

Cantera [150] is an open source object oriented software package for simulating chemically reacting flows, which was initially developed by Prof. David G. Goodwin at the *California Institute of Technology* and provides capabilities for modelling reactor networks and one-dimensional flames. It features conversion tools for importing chemical reaction mechanisms and fluid properties from the popular CHEMKIN format [159, 161], so that a wide range of reaction mechanisms from various research groups can be readily used. Cantera is applied for problems related to internal combustion engines (e.g., [21, 71, 90, 92, 149, 183–186]). Cantera features easy-to-use interfaces to Python and Matlab and can be used in applications written in C/C++ and Fortran 90. It is developed by volunteers and licensed under a permissive 3-Clause BSD license, ensuring that the software will remain open source and available for all to use [176].

A more recent alternative is OpenSMOKE++, a general framework developed by the *CRECK Modeling Lab* at the *Politecnico di Milano* for numerical simulations of reacting systems with detailed kinetic mechanisms [189, 190]. The framework is written entirely in object oriented C++ and designed to be easily extended and customised for user-specific

systems, for example, for the incorporation into multi-dimensional CFD codes [190] such as OpenFOAM through the OpenSMOKE++4OpenFOAM solvers [189]. The core functionality of OpenSMOKE++ is basically identical to Cantera, however with improved performance and stability as comparisons indicate [190]. OpenSMOKE++ is currently free for academic use [189].

The Cloudflame [85] platform of the Clean Combustion Research Center at King Abdullah University of Science and Technology offers a range of web-enabled tools for combustion research across academia and industry which are based on a Cantera and OpenSmoke backend.

A variety of other software programs for combustion kinetics intended for different purposes is available as either open source or commercial software. A comprehensive overview is presented by Glassman et al. [68].

Appendix B: Modules of the CoPa simulation toolbox

B.1 Gas module

The module *gas_module.py* is part of the CoPa core simulation package and is used to initialise the mixture of fuel, oxidiser and residual gas. The gas module builds upon the Cantera *Solution* class for chemically-reacting solutions and adds the processing for setting a defined mixture at a defined state including vapour control and the addition of residual gas with different compositions (wet/dry, equilibrium/frozen). For more details on the Cantera Solution class one can refer to the Cantera documentation [150] (https://cantera.org/).

In order to define the solution object one has to provide a chemical reaction mechanism, as well as thermodynamic and transport data in Cantera's .cti format. For converting CHEMKIN mechanism files into .cti format one can use the conversion tools provided with Cantera. The chemical mechanism file is specified in the simulation input file and must be available in the Cantera working directory. It is necessary that all species of the specified fuel and oxidiser are included in the mechanism file, otherwise an error will be thrown by Cantera.

The gas module defines three independent Solution objects (pure air, pure fuel, exhaust gas) which are then mixed according to the specified fuel/air equivalence ratio and residual gas fraction (exhaust gas recirculation). The respective methods are organised in a class *GasMix* (see Table B-1). For specifying the mixture an instance of the class is created, handling over the full parameter set which defines the mixture (fuel and oxidiser composition, equivalence ratio, temperature, pressure, ratio of exhaust gas recirculation,…) together with flags indicating how to compose the mixture (e.g., mole or mass fractions, dry or wet EGR, equilibrium or frozen state,…). The individual gas objects are then created by applying the respective methods to the instance of the class.

It should be noted that all species in the mixture are supposed to be ideal gases and condensed or solid phases are not considered. The only correction is applied for water vapour, which will be removed from the gas phase in case the saturation pressure is exceeded. The saturation temperature and pressure are determined following the IAPWS formulation [168] and the according methods are organised in a class *SteamProp* (Table B-2).

Table B-1: gas_module.py class GasMix

Method	Description	Input	Output
AF_stoic	Returns the stoichiometric air requirement of a given fuel	Cantera Solution object representing fuel mix (gas phase)	AF in mass and mole units
ftemp_adiabatic	Returns the adiabatic flame temperature of a given combustible mixture	Cantera final gas mixture object	Adiabatic flame temperature
fuel_heating value	Returns LHV and HHV of a given fuel	Cantera Solution object representing fuel mix (gas phase)	LHV and HHV in mass and volume units
mix_heating_value	Returns LHV and HHV of a combustible fuel-air-mixture	Cantera Solution object representing final mix (gas phase)	LHV and HHV in mass and volume units
set_fuel	Initialises fuel as gas phase object with specified composition.	Fuel composition, flag indicating mole or mass fractions	Cantera Solution object representing the fuel (gas phase)
set_unburned	Initialises unburned gas phase mixture of fuel and oxidiser at specified equivalence ratio.	Fuel object, composition of oxidizer, equivalence ratio, flag indicating mole or mass fractions	Cantera Solution object representing the unburned gas (gas phase)
set_burned	Initialises burned gas phase mixture in dry or wet chemical equilibrium or frozen composition at specified temperature.	Cantera unburned gas object, temperature and pressure, flag indicating equilibrium or frozen composition, freeze temperature, flag indicating wet or dry exhaust gas recirculation	Cantera Solution object representing the burned gas (gas phase)
set_mix	Initialises final gas phase mixture of unburned and burned gas according to specified ratio of exhaust gas recirculation at specified temperature and pressure.	Cantera unburned and burned gas objects, egr ratio, temperature and pressure flag indicating mole or mass fractions	Cantera Solution object representing final mix (gas phase)
_vapor_control	Checks if saturation pressure of mixture is exceeded at given temperature and pressure conditions.	Cantera Solution object representing final mix (gas phase)	Cantera Solution object representing final mix (gas phase) with water content according to saturation pressure

Table B-2: gas_module.py class SteamProp

Method	Description	Input	Output
sat_press	Returns saturation temperature according to IAPWS [168] at given pressure.	Pressure	Saturation temperature
sat_temp	Returns saturation pressure according to IAPWS [168] at given pressure.	Temperature	Saturation pressure

B.2 Simulation module

The module *sim_module.py* is the core module of the CoPa toolbox and contains all simulation functions (Table B-3), that is, functions that define and solve a chemically reacting system, such as a reactor or a flame. The Cantera software package is used as solver. The simulation module is essentially a high-level interface to Cantera providing pre-defined functions for simulation of auto-ignition and laminar flame speed. The implemented simulation functions are designed to work with the latest version 2.4.0 of Cantera. Additional general purpose solvers can be integrated using the *SciPy* open source tools for Python [191]. This is, for example, applied in the case of the *root_finding* function which uses Brent's method for scalar root finding from SciPy version 1.2.1 (https://www.scipy.org/).

All functions expect the mixture definition as a minimum input required to call the respective functions from the gas module and retrieve a Cantera Solution object, which is needed to set up the reactor and flame calculations. Additional input can be necessary, such as the reactor geometry in the case of the HCCI reactor simulation. All simulation functions return at least a history of the simulation run, that is, time series for reactors or spatial steady state distributions for flames, together with additional result values for the respective simulation.

The reactor functions use the Cantera *ReactorNet* class to define a reactor network consisting of two identical reactors, of which one is a chemically inert baseline reactor. The full species history is returned for both reactors. This is especially useful for the HCCI reactor, where the pressure and temperature profiles of the chemically inert reactor serve as baseline for detection of ignition. The flame simulation function *lam_flame* defines and computes a freely propagating flame using Cantera's composite domain *FreeFlame* class. For details on the Cantera classes one can refer to the documentation [150] (https://cantera.org/).

Table B-3: sim_module.py functions

Function	Description	Input	Output
equil_state	Equilibrates mixture while holding temperature and pressure constant. Uses Cantera's *equilibrate* method.	Mixture definition	Mole/mass fractions at chemical equilibrium
gasprop	Returns a set of gas properties, such as heating values and air-requirement by calling the respective functions of the gas_module	Mixture definition	Mixture properties
isochoric_reactor	Simulates combustion in an adiabatic constant-volume reactor. Uses Cantera's *Reactor* and *ReactorNet* class.	Mixture definition	Reactor history including baseline (time, volume, temperature, pressure, heat release, enthalpy, internal energy, species,…)
isobaric_reactor	Simulates combustion in an adiabatic constant-pressure reactor. Uses Cantera's *Reactor* and *ReactorNet* class.	Mixture definition	Reactor history including baseline (time, volume, temperature, pressure, heat release, enthalpy, internal energy, species,…)
hcci_reactor	Simulates combustion in an adiabatic piston reactor; a chemically inert reactor with same mixture is simulated as baseline. Uses Cantera's *Reactor* and *ReactorNet* class.	Mixture definition, geometry data of reactor (bore, stroke, compression ratio, rotational speed)	Reactor history including baseline (time, crank angle, piston speed, volume, temperature, pressure, heat release, enthalpy, internal energy, species,…)
root_finding	Finds the min. value of a target variable at which ignition occurs in a reactor. Uses SciPy Brent's method [191]	Target variable and reactor function to be applied	Identified target value and corresponding reactor history
lam_flame	Simulates one-dimensional, adiabatic, freely propagating flame. Uses Cantera's *FreeFlame* class.	Mixture definition, flag indicating transport mode mixture-averaged or multicomponent	Flame speed and flame history (grid, temperature, pressure, heat release, velocity, enthalpy, species,…),

B.3 Post processing module

The module *postproc_module.py* comprises the post-processing functions which are applied once the simulation results are available. The functions (see Table B-4) are usually called by the processing script after simulation and applied directly to the results DataFrame, but the post-processing module is designed to be independent from the actual simulation routines, so that it can be accessed individually at any time. This allows for adding additional post-processing routines if required, without having to repeat the whole simulation run.

Table B-4: postproc_module.py functions

Function	Description	Input	Output
act_temp	Calculates activation temperature by evaluating the gradient of the logarithmic ignition delay time over the inverse temperature (Arrhenius plot); applies a linear fit to the Arrhenius plot.	Reactor history	Activation temperature E/R
idx_extra	Calculates ignition delay with extrapolation method	Reactor history including baseline	Ignition delay
idx_thrsh	Calculates ignition delay with threshold method	Reactor history including baseline	Ignition delay
idx_diff	Calculates ignition delay with the differentiate method	Reactor history including baseline	Ignition delay
idx_max	Calculates ignition delay with the maximum method	Reactor history including baseline	Ignition delay
sankaran	Evaluates the Sankaran criterion	Values of ignition delay in the range to be investigated, hot spot radius and thermal gradient	Pressure and temperature conditions at which Sankaran criterion yields zero.
tau_e	Calculates excitation time; applies spline interpolations at lower bound of heat release curve.	Reactor history	Excitation time
xi-eps	Determines the dimensionless parameters ε and ξ.	Values of ignition delay, excitation time and sound speed in the range to be investigated, hot spot radius and thermal gradient	Dimensionless parameters ε and ξ

B.4 Experiment generation and processing

The modules of the simulation toolbox can be directly accessed from any Python script or shell such as an IPython console by importing the package into the namespace. However, for convenience pre-defined scripts for the generation of simulation input files and processing of the simulations were developed using the Pandas package [177]. Pandas offers a convenient way of organising and analysing scientific data in a spreadsheet style, where each row corresponds to a single simulation run and the according data is arranged in the columns. In the same manner, time-series can be handled very efficiently.

The simulation generation script *copa_generator.py* is used to generate a set of input parameters and store them in an input file for later processing. The input parameters are defined as dictionaries (pairs of keywords and the corresponding values) and stored in a Pandas DataFrame.

Processing of the simulations is performed by a separate script *copa_processor.py*, so that the generation of simulation input files and the actual processing can be accomplished on separate machines (e.g., desktop computer and workstation). The simulation processing script loads the simulation input file into a Pandas DataFrame and performs the pre-processing, main processing and post-processing steps. The main processing is handled by a multiprocessing pool using the pathos framework (version 0.2.3, https://pypi.org/project/pathos/ [178, 179]). The number of parallel processes is determined automatically depending on the CPU cores available on the respective workstation or can be set individually by the user. For large calculation sets the computation can be split into chunks.

The simulation results received from the multiprocessing pool are handled over to the post-processing step which calls the appropriate functions of the post-processing module. The simulation and post-processing results are then stored in a Pandas DataFrame for further processing.